2011-01-01

Monitoring Ecosystem Dynamics In An Arctic Tundra Ecosystem Using Hyperspectral Reflectance And A Robotic Tram System

Santonu Goswami
University of Texas at El Paso, santonu@gmail.com

MONITORING ECOSYSTEM DYNAMICS IN AN ARCTIC TUNDRA ECOSYSTEM USING HYPERSPECTRAL REFLECTANCE AND A ROBOTIC TRAM SYSTEM

SANTONU GOSWAMI

Environmental Science and Engineering Doctoral Program

APPROVED:

Craig E. Tweedie, Ph.D., Chair

John A. Gamon, Ph.D.

Ann Q. Gates, Ph.D.

Jose M. Hurtado, Ph.D.

Benjamin C. Flores, Ph.D.

Interim Dean of the Graduate School

Dedication

I dedicate this dissertation to my parents who taught me how to dream! I have walked a long walk and will continue this journey towards knowledge and enlightenment and I know that to the core of it all is my parents' blessings and encouragements that are helping me to go this long!!

MONITORING ECOSYSTEM DYNAMICS IN AN ARCTIC TUNDRA ECOSYSTEM USING HYPERSPECTRAL REFLECTANCE AND A ROBOTIC TRAM SYSTEM

by

SANTONU GOSWAMI, MS

DISSERTATION

Presented to the Faculty of the Graduate School of

The University of Texas at El Paso

in Partial Fulfillment

of the Requirements

for the Degree of

DOCTOR OF PHILOSOPHY

Environmental Science and Engineering Doctoral Program

THE UNIVERSITY OF TEXAS AT EL PASO

December 2011

Acknowledgements

I would like to acknowledge all the people who have helped me throughout my Ph.D student life in various ways. First of all, I would like to thank my dissertation committee for very helpful feedback and help on my research throughout my PhD years. My most sincere gratitude goes to my dissertation advisor Dr. Craig E. Tweedie for allowing me to work under his guidance and venture into this super exciting field of interdisciplinary environmental research. His guidance, help, encouragements throughout this process has really been wonderful. I can see how I have matured as an environmental researcher within these six years time. Coming from a completely different background into this brand new field of environmental research has not been easy, but the mentoring and guidance provided by Dr. Tweedie has really made it enjoyable. Thank you again for all these wonderful opportunities and introducing me to a whole new world of scientific research. I would also like to convey my sincere gratitude to Dr. John Gamon for his wonderful mentoring in my research. Under his mentoring, I was able to quickly learn the new remote sensing techniques for my research. I would also like to thank Dr. Gamon for introducing me to the SpecNet community, an association which has been tremendously helpful in my research. My sincere gratitude also goes to Dr. Ann Gates for her help and guidance in my cyberinfrastructure research through collaboration with the UTEP CyberSHARE center of Excellence. This collaboration opened up many opportunities for cyberinfrastructure research within the capacity of my dissertation, one of which is my collaboration with Irbis Gallegos. I would like to thank my friend and research partner Irbis for working together to build a piece of very important software for my research need. I would also like to convey my gratitude to Leonardo Salayndia and Paulo Pinheiro da Silva from the UTEP CyberSHARE

center for extending collaboration in my research. My sincere thanks also go to Dr. Jose Hurtado for willing to serve in my committee and also for helpful advice in various remote sensing methods and techniques.

My special thanks go to Barrow Arctic Science Consortium (BASC), our field logistics partner for all the help they provided in the field in Barrow, AK. It was a pleasure working with BASC without whom the fieldwork would have been lot more difficult. My special thanks go to Chico Perales from CH2MHill Polar Services for awesome help in the field and making my life so much easier. My thanks also go to all the colleagues from the Biocomplexity experiment.

I would also like to thank my colleague in the Systems Ecology Laboratory (SEL) for all the help throughout my PhD years. It was always good to have someone from the SEL family around in the field, especially when the weather conditions were harsh. Thank you all.

My sincerely thanks also go to Dr. Fred Huemmrich from NASA Goddard Space Flight Center for valuable advice and encouragements throughout all these years.

This study was funded via two National Science Foundation (NSF) grants (ASSP-0421588, HRD-0734825). My sincere thanks go to NSF for supporting this research. I would also like to thank Environmental Science and Engineering program for additional financial support during my PhD as Teaching Assistantship.

Lastly, but not the least I would like to thank everyone from my family for being so helpful and encouraging throughout the PhD process; especially, my fiancée Balaka, who has been very supportive towards the last stage of my PhD, which is probably the toughest. I do thank her for this amazing support and constant encouragement.

Abstract

Global change, which includes climate change and the impacts of human disturbance, is altering the provision and sustainability of ecosystem goods and services. These changes have the capacity to initiate cascading affects and complex feedbacks through physical, biological and human subsystems and interactions between them. Understanding the future state of the earth system requires improved knowledge of ecosystem dynamics and long term observations of how these are being impacted by global change. Improving remote sensing methods is essential for such advancement because satellite remote sensing is the only means by which landscape to continental-scale change can be observed.

The Arctic appears to be impacted by climate change more than any other region on Earth. Arctic terrestrial ecosystems comprise only 6% of the land surface area on Earth yet contain an estimated 25% of global soil organic carbon, most of which is stored in permafrost. If projected increases in plant productivity do not offset forecast losses of soil carbon to the atmosphere as greenhouse gases, regional to global greenhouse warming could be enhanced. Soil moisture is an important control of land-atmosphere carbon exchange in arctic terrestrial ecosystems. However, few studies to date have examined using remote sensing, or developed remote sensing methods for observing the complex interplay between soil moisture and plant phenology and productivity in arctic landscapes. This study was motivated by this knowledge gap and addressed the following questions as a contribution to a large scale, multi investigator flooding and draining experiment funded by the National Science Foundation near Barrow, Alaska (71°17’01” N, 156°35’48” W):

- How can optical remote sensing be used to monitor the surface hydrology of arctic landscapes?
- What are the spatio-temporal dynamics of land-surface phenology (NDVI) in the study area and do hydrological treatment has any effect on inter-annual patterns?
- Is NDVI a good predictor for aboveground biomass and leaf area index (LAI) for plant species that are common in an arctic landscape?
- How can cyberinfrastructure tools be developed to optimize ground-based remote sensing data collection, management and processing associated with a large scale experimental infrastructure?

The Biocomplexity project experimentally manipulated the water table (drained, flooded, and control treatments) of a vegetated thaw lake basin to investigate the effects of altered hydrology on land-atmosphere carbon balance. In each experimental treatment, hyperspectral reflectance data were collected in the visible and near IR range of the spectrum using a robotic tram system that operated along a 300m tramline during the snow free growing period between June and August 2005-09. Water table depths (WTD) and soil volumetric water content were also collected along these transects. During 2005-2007, measurements were made without experimental treatments. Experimental treatments were run in 2008 and 2009, which involved water table being raised (+10cm) and lowered (-10cm) in flooding and draining treatments respectively.

A new spectral index, the normalized difference surface water index (NDSWI) was developed and tested at multiple spatial and temporal scales. NDSWI uses the 460nm (blue) and 1000nm (IR) bands and was to capture surface hydrological dynamics in the study area using the

robotic tram system. When applied to high spatial resolution satellite imagery, NDSWI was also able to capture changes in surface hydrology at the landscape scale. Interannual patterns of land-surface phenology (measured with the normalized difference vegetation index - NDVI) unexpectedly lacked marked differences under experimental conditions. Measurement of NDVI was, however, compromised when WTD was above ground level. NDVI and NDSWI were negatively correlated when WTD was above ground level, which held when scaled to MODIS imagery collected from satellite, suggesting that published findings showing a 'greening of the Arctic' may be related to a 'drying of the Arctic' in landscapes dominated by vegetated landscapes where WTD is close to ground level.

For six key plant species, NDVI was strongly correlated with biomass ($R^2 = 0.83$) and LAI ($R^2 = 0.70$) but showed evidence of saturation above a biomass of 100 g/m^2 and an LAI of 2 m^2/m^2. Extrapolation of a biomass-plant cover model to a multi-decadal time series of plant cover observations suggested that *Carex aquatilis* and *Eriophorum angustifolium* decreased in biomass while *Arctophila fulva* and *Dupontia fisheri* increased 1972-2008.

New cyberinfrastructure were developed to enhance management and quality control of large volumes of hyperspectral data collected during the study in collaboration with UTEP's Cyber-ShARE Center of Excellence. Tools included Semantic Abstract Workflows and ontologies, software for data specification and verification, and an online vegetation spectral library.

This study has shown that ground and satellite remote sensing studies that utilize experimental and observational (time series) data, in combination with interdisciplinary collaboration can improve capacities needed for monitoring arctic change.

Table of Contents

Chapter 1: Introduction

Recent changes in the earth's atmosphere and climate are impacting the Earth System (Millennium Ecosystem Assessment 2005, IPCC 2007**).** Changes in terrestrial ecosystems have the capacity to further alter regional and global climate and other components of the Earth System through complex feedbacks between interacting physical, biological and human subsystems (ACIA 2005, Chapin et al. 2005, Hinzman et al. 2005). Loss of biodiversity (Millennium Ecosystem Assessment, 2005), land use and land cover change (Lepers et al. 2005), hydrological modification (Shaver et al. 2006, Hobbie et al. 1999), and altered biogeochemical cycles (McGuire et al. 2009, Hirsh et al. 2006, Schimel et al. 2001) have all been linked to climate change. However, it remains a challenge to understand deterministically, how ecological connectivity may drive other changes in the climate and other earth subsystems (Peters et al. 2008). Improving our understanding of the future state of the Earth System and how humans will need to adapt has become an urgent research priority in the environmental sciences. Fundamental to achieving this challenge has been the need for substantial investment in improving and/or building field, human and cyberinfrastructure, large scale scientific experimental manipulations, and scientific collection and dissemination networks (NEON 2009, AON 2008, Gamon et al. 2006b).

The Arctic appears to be responding to climate change more than any other region on Earth and these changes have the capacity to alter the future state of the Earth System (Schuur and Abbott 2011). This study aims to investigate the effects of variation in soil moisture on ecosystem dynamics in a large scale manipulation experiment in an arctic tundra landscape using hyperspectral reflectance data collected from a robotic tram system and a newly developed

cyberinfrastructure for data management and quality control. Findings from this project have the potential to improve understanding of the future state of the substantial arctic soil organic carbon pool and the design and management of science infrastructure needed to monitor global change impacts in the Arctic.

1.1 The Arctic and Global Change

The Arctic can be defined in several different ways. Based on insolation and the tilt of the earth's rotational axis, the Arctic is defined as the area north of the Arctic Circle or 66.5° N latitude, which experiences 24 hours of darkness and light in the winter and in summer respectively. Climatically, the Arctic is defined as a region where the maximum monthly average temperature is below 10° C (Koppen 1931). This boundary is also called the 10° C isotherm, and often aligns with the temperature-dependent distribution of trees (McGuire et al. 2006). While some define the Arctic by the southernmost boundary of discontinuous permafrost (McGuire et al. 2006), the most ecologically relevant, definition for terrestrial landscapes of the Arctic is the area north of the boreal forest treeline, also known as the tundra-taiga ecotone (Callaghan et al. 2002a). The area north of treeline is roughly 12 million square kilometers and is bounded to the north by the Arctic Ocean (Chapin et al. 2005). Each definition has an effective usage but none of them defines an exact boundary, except for the delineated Arctic Circle at 66.5° N. Although some of these definitions describe large, gradual transition zones, they do maintain a dynamic quality of spatial self-adjustment to changing climatic conditions. By addressing the Arctic as a regional set of ecosystems with specific

ecosystem functions, this document follows the ecological/ functional definition of Callaghan et al. (2002b).

Compared to other ecoregions on Earth, the Arctic appears to be experiencing the most pronounced impacts of climate change (IPCC 2007, ACIA 2005). Recent observations indicate that the Arctic has undergone numerous changes over the past century (Kaufman et al. 2009). Significant and concurrent changes include a general greening of the Arctic throughout the 1980s (Bhatt et al. 2010, Myneni et al. 1997), increased shrub dominance (Sturm et al. 2005), a rise in permafrost temperature (Osterkamp and Romanovsky 1999), and loss of arctic lake area (Smith et al. 2005). While this increasing multi-disciplinary knowledge regarding arctic ecosystem change has accumulated and been synthesized in more detail over recent years (Post et al. 2009, Hinzman et al. 2005, Serreze et al. 2000), uncertainty remains over the present and future structure and function of tundra ecosystems and the speed and direction in which they will respond to a changing climate (ACIA 2005). Definitive observational evidence of regional land cover change is likely the result of recent and sustained warming over decadal time scales (Tape, Sturm and Racine 2006, Sturm et al. 2005, Sturm et al. 2001), and these findings are largely corroborated by experimental warming manipulations (Walker et al. 2006, Wahren, Walker and Bret-Harte 2005). Many of the observed (Post et al. 2009, Hinzman et al. 2005, Smith et al. 2005) and modeled (McGuire et al. 2009, Sitch et al. 2007) climate change responses in arctic tundra ecosystems are related to altered surface hydrology. In the Arctic, the importance of surface hydrology on surface energy budgets (Euskirchen et al. 2007, Chapin et al. 2005), land-atmosphere carbon exchange (Merbold et al. 2009, Wolf et al. 2008), plant phenology (Walker et al. 2006, Arft et al. 1999), and geomorphic processes (McNamara and Kane 2009, Lawrence and

Slater 2005) are well recognized. Based on experimental evidence, observations and modeling, alteration of surface hydrology in arctic terrestrial ecosystems is likely to alter a range of interconnected ecosystem processes such as primary productivity (McGuire et al. 2009, Oberbauer et al. 2007, Illeris, Christensen and Mastepanov 2004), methanogenesis (Mazeas et a. 2009, Merbold et al. 2009, Petrescu et al. 2008), nutrient cycling (Arndal et al. 2009, McGuire et al. 2009, Jonasson, Castro and Michelson 2004), and land cover or plant community change (Walker et al. 2006, Smith et al. 2005, Callaghan et al. 2004).

Arctic ecosystems contain 25 percent of the world's soil organic carbon, much of which is contained in a greenhouse inert state within permafrost (IPCC 2007). The degree to which changes in land-atmosphere carbon exchange dynamics will interact with and offset the balance and stability of the substantial store of soil organic carbon in the Arctic (Tarnocai et al. 2009, Ping et al. 2008), is a primary concern (McGuire et al. 2009). If the increase in primary productivity predicted for the Arctic in response to warming does not balance net losses of CO_2 equivalent carbon to the atmosphere, a positive feedback to regional and potentially global warming will occur (Hudson and Henry 2009, Kimball et al. 2006). This positive feedback response to warming in the Arctic is likely to be controlled by soil moisture and surface hydrology (Huemmrich et al. 2010, McGuire et al. 2006). Subsequently, there is a need to monitor these parameters and determine how they are changing over time and space to better understand the future state of the Arctic system and the likely repercussions of change in this system. Substantial efforts before, during and now following the 2007-2009 International Polar Year have focused on improving environmental observing capacities in the Arctic, particularly the future fate and transport of the Arctic soil organic carbon store (National Academy of

Sciences 2006, ICARP-II report 2005, National Academy of Sciences 2004). Such efforts highlight the importance of observations that span plot to global scales. Because of the many advantages remote sensing offers to such scaling challenges and spatial extrapolation (Stow et al. 2004), the development of remote sensing approaches and technologies in an integrated arctic observing network is a key priority.

1.2 Importance of Remote Sensing to Global Change Science

Remote sensing has been used to measure and monitor important biophysical parameters such as vegetation biomass (Hudson et al. 2009), ecosystem productivity and Light Use Efficiency (LUE) (Huemmrich et al. 2010) in various studies in the Arctic studying recent changes. One of the key strengths of remote sensing is that it enables the capacity to study ecosystem processes and properties spanning multiple spatial and temporal dimensions from local to global scales (Stow et al. 2004, Donoghue 2002).

Remote sensing can be performed from platforms that are ground based, airborne, or satellite borne. Ground based remote sensing sensors and high spatial resolution imaging systems can be used to monitor select study sites to detect changes in vegetation composition or structure, and to determine the nature of changes identified from coarser resolution satellite sensors (Stow et al. 2004). Ground based sensors and low altitude aircraft borne high resolution imaging systems help improve the precision and specificity of measurement methods, while improving spatial resolution and accuracy. Satellite remote sensing data with high temporal resolution have been shown to be particularly valuable for tracking changes in vegetation production at regional, continental and global scales (Olthof et al. 2010, Hudson et al. 2009).

Spectral vegetation indices derived from remote sensing are commonly used for the study of ecosystem properties and processes (Hilker et al. 2010, Huemmrich et al. 1999, Gamon et al. 1997). The presence of different pigments in vegetation tissues gives characteristic spectral features (Fig. 1.1). Such vegetation spectral properties can be used for studying a range of plant and ecosystem structural and functional properties such as vegetation biomass (Boelman et al. 2003), leaf area index (Jia et al. 2009), plant productivity, vegetation stress (Gamon et al. 1997). During photosynthesis, chlorophyll molecules preferentially absorb light in the blue (0.45–0.52 μm) and red (0.63–0.69 μm) regions of the electromagnetic spectrum, which can include up to 90% of incident light in these wavelengths (Campbell 1996, Jensen 2000). For a typical healthy leaf, mesophyll cells may reflect as much as 76% of incident near infrared (NIR) energy (i.e., 0.9 μm) (Jensen, 2000). These characteristics of absorption and reflection in the blue-red to NIR wavelengths allow for the discrimination of inter and intra species differences, determination of plant stress, and the analysis of plant growth (Fig. 1.1). The characteristic shape of the spectral curve differs for different vegetation types because of certain plant physiological behavior in certain region of the spectrum and is exploited with the help of spectral vegetation indices as described below.

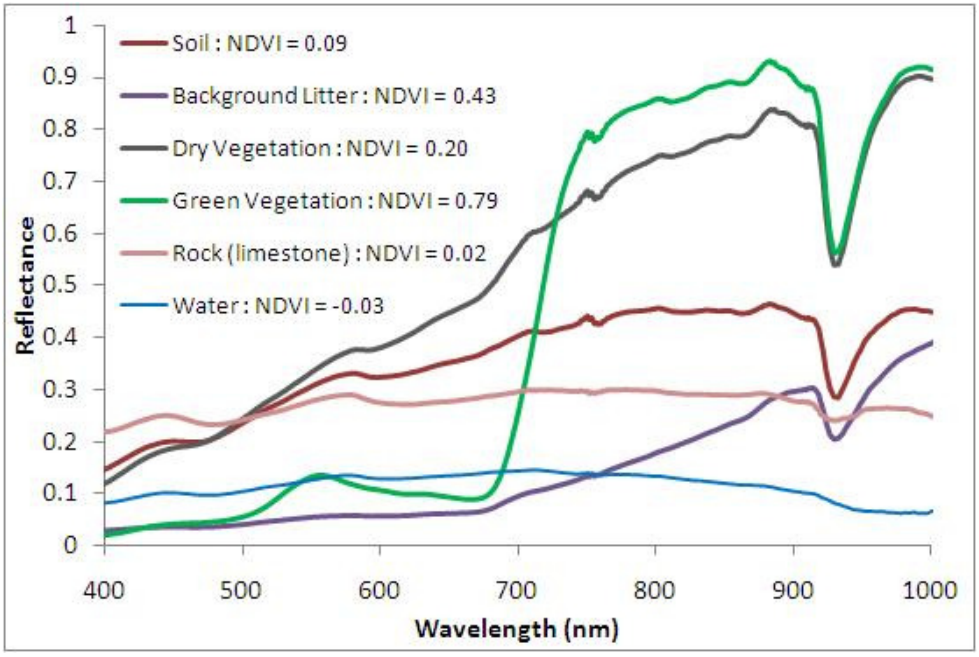

Figure 1.1. The above figure shows the characteristic spectral signatures for different vegetation and landcover types. NDVI values for different types show how presence of different pigments affects the NDVI values. The spectra used in creating this figure is taken from a web-based Vegetation Spectral Library (VSL, http://spectrallibrary.utep.edu) created as part of this study.

A vegetation index (VI) or a spectral vegetation index (SVI) is a quantitative predictor of plant biomass or vegetative vigor, usually formed from combinations of several spectral bands, whose values are added, divided, or multiplied in order to yield a single value that indicates the amount or vigor of vegetation (Jensen 2007). The simplest form of vegetation index is a ratio between reflectance in the near infrared and red spectra, called the simple ratio (SR) (Gamon et al. 2005). For healthy living vegetation, this ratio will be high due to the inverse relationship between vegetation reflectance in the red and infrared regions of the spectrum. Different vegetation indices using various combinations of different spectral bands have been developed to better investigate a variety of physiological states in vegetation (Gamon et al. 1997, Huete et al. 1997, Huete et al. 1988).

The most widely used vegetation index in the ecological and environmental science is NDVI (the normalized difference vegetation index) (Rouse et al. 1974), which is the normalized difference of the red and NIR region of the vegetation spectral curve. This relationship between the red and near infrared wavelengths provides the most information regarding vegetative properties such as health, stress level, green biomass and chlorophyll content (Laidler et al. 2003). Most of the vegetation indices that have been developed so far are mainly for the purpose of estimating above ground biomass (Boutton and Tieszen 1983) vegetation cover (Purevdorj et al. 1998, Richardson and Wiegand 1977), chlorophyll content (Tucker 1977), productivity (Box et al. 1989), net aboveground primary production (NPP) (Walker et al. 1995), and leaf area index (LAI) (Baret and Guyot 1991).

1.3 Overarching Challenges

Understanding how the Earth System is changing and how humans need to adapt to this change has catalyzed a rapid expansion of the environmental sciences. The urgency to better understand the implications of environmental change has driven paramount programmatic and operational changes in the ecological and environmental sciences. In recent times, environmental science has shifted towards becoming a more data-driven science, where researchers increasingly rely on the integrity of data collected by other researchers and multidisciplinary scientific networks (NSF Cyberinfrastructure vision for 21st century). There is also an increased utilization of advanced and standardized field based instrument technologies such as advanced instrument towers, sensor arrays, and autonomous vehicles. The need for optimizing data streams, automating quality checking procedures, managing, archiving and integrating large volumes of

data collected from field based and other instrument platforms (e.g. satellite) has increased in response to these developments.

Ecological field data are known to be notoriously difficult to assemble into usable databases (Michener and Brunt 2000). Near surface remote sensing data, which closely resembles the ecological field data also creates similar challenges. The present state of mechanisms to assess the adequacy of spectral instrumentation, calibration, and configuration are poorly developed as these measurements are generally performed manually. In addition to this, integrating spectral and other remotely sensed data are challenging because of the mismatch in measurements in spatial and temporal resolution. Discrepancies in ground-based spectral and other remotely sensed data occur because of the inability of current algorithms used in satellite measurements to adequately capture short-term variability resulting from disturbance and stress (Cheng et al. 2006, Running 2008) among other factors. Considering all these factors in combination with the large volume and complex nature of ground-based remote sensing datasets, the challenge of proper management and archiving of the collected data in a searchable format is substantial and likely to be limiting scientific discovery.

1.4 Goals and Objectives of this Study

Underpinned by the rationale presented above, this dissertation aims to monitor ecosystem dynamics in the study area using hyperspectral remote sensing and a robotic tram system within a large-scale hydrological manipulation experiment and examines how remote sensing and the development of cyberinfrastructure can be optimized to meet the needs of contemporary data driven environmental science. This dissertation research focuses on the following key research objectives and underlying questions:

- Research Objective 1: Develop an optical remote sensing method that can estimate surface water depth (SWD) and surface water cover (SWC) for arctic tundra.
    - Using optical remote sensing methods, how can surface water depth (SWD) and surface water cover (SWC) be estimated?
    - How can such a surface water index be scaled across multiple temporal and spatial domains?
    - Can the method be used to identify inter-annual variability in the hydrology of the study area?
- Research Objective 2: Characterize how the land-surface phenology of an arctic tundra landscape responds to experimental flooding and draining using hyperspectral reflectance.
    - What are the spatio-temporal dynamics of land-surface phenology (NDVI) in the study area and does altered soil moisture affect interannual dynamics of NDVI?
    - Can satellite scale observations detect seasonal and inter-annual variability in land-surface phenology?
- Research Objective 3: Investigate relationships between NDVI, Biomass, and Leaf Area Index (LAI) for six key plant species near Barrow, Alaska.
    - How do key plant species differ in biomass, LAI and spectral properties?
    - How can spectral indices be used to estimate biomass and LAI for key plant species?

- Research Objective 4: Develop and test cyberinfrastructure tools that enhance the collection and quality control associated with hyperspectral data collection and assessment.
    - How can cyberinfrastructure tools improve the efficiency of data acquisition, quality control and management associated with the robotic tram system?
    - How can semantic abstract workflows be used to identify be used to transfer and document knoweledge?

The research objectives outlined above demand interdisciplinary approaches that draw from knowledge in ecology, remote sensing, physics and computer science. As such, this study will endeavor to span multiple disciplines and stimulate collaborations with domain experts to achieve the research goals listed above.

1.5 Project description

1.5.1 Study Site and Period

Field data collection was conducted within the Biocomplexity flooding and draining experiment on the Barrow Environmental Observatory (BEO) near Barrow, Alaska , 71°17'01" N, 156°35'48" W, (Fig. 1.2). The BEO is situated on the Alaskan Arctic Coastal Plain and has a low relief and an average elevation of 4 meters (Aguirre et al. 2008). Seventy two percent of the landscape near Barrow contains oriented lakes, drained thaw lake basins and small ponds (Hinkel et al. 2003). The Biocomplexity experimental area is located in a series of three coalesced drained thaw lake basins that include moist and wet tundra vegetation dominated by graminoid tundra (Teh et al. 2009). The study site is underlain by continuous permafrost and

includes thermokarst terrain typical of the Alaskan Arctic Coastal Plain (Brown et al. 1980). This includes thaw lakes, high and low-centered polygons, shallow ponds and lakes, and a shallow active layer that is generally less than 50 centimeters in the experimental area (Shiklomanov et al. 2010). Soils of the area are described by (Bockheim et al. 1999) and include cryoturbated gelisols, specifically Typic Aquorthels with high soil moisture content, Histoturbels, and Aquaturbels. The upper layer of this soil consists of carbon rich peat (*ca.* 50 kg/C/m^3) (Bockheim et al. 1999). Soils are generally moisture rich due to shallow drainage gradients, relatively low rates of evapotranspiration, and impeded drainage caused by ice-rich continuous permafrost (Bockheim et al. 1999, Miller et al. 1998).

Winter is generally long, dry and cold and the summers are relatively short, moist and cool (Brown 1980). The sun is above the horizon continuously from May 10th to August 2nd, and below the horizon from Nov 18th to Jan 24th (Brown 1980). Air temperature remains below freezing for nine months of the year and can fall below freezing during any of the three summer months. A gradual warming trend begins in April and snow melt typically occurs in early June. Wind speed varies little during the year, averaging 5.3 m/sec, with the fall months being the windiest. Fog and low cloud persist throughout the summer and the relative humidity generally exceeds 80% from June through September. Mean June to August precipitation is 58.4 millimeters (Engstrom et al. 2008).

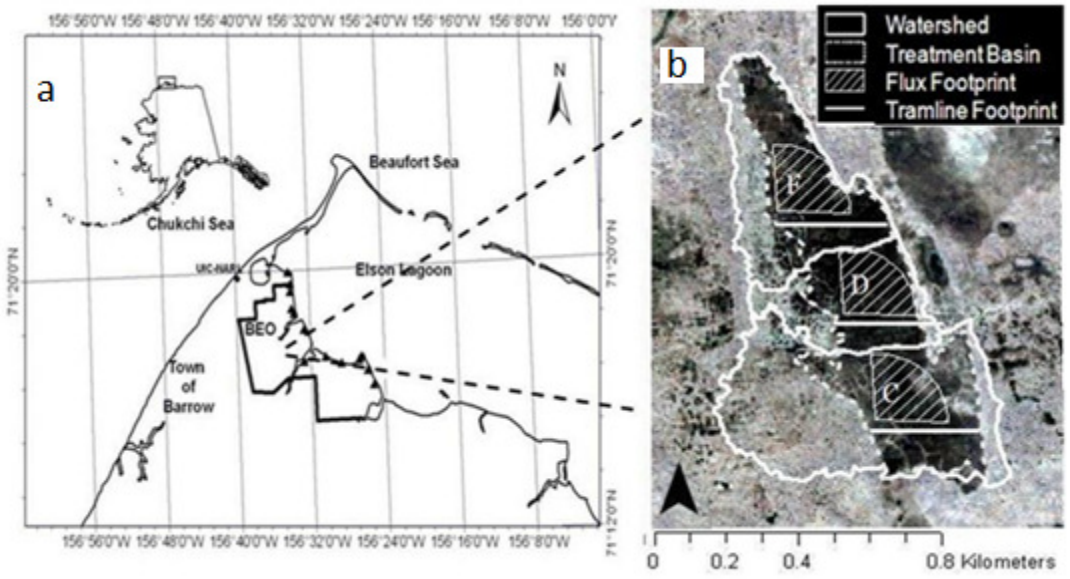

Figure 1.2. Location of the Barrow Environmental Observatory (BEO) near Barrow, Alaska (Fig. 1.2a). Figure 2b shows the location of the study area. The experimental design of the Biocomplexity Experiment includes experimentally flooded (north) and drained (central) treatments, and a control section (south) shown by the letters F, D and C respectively (Fig. 1.2b). Watersheds for each treatment and the inundated basin areas are highlighted (Fig. 1.2b). The straight lines indicate the three sampling transects ("tramlines"). The idealized footprints of the three flux tower footprints associated with the experiment are indicated by pie-shaped semi circles.

1.5.2 Experimental Infrastructure

As part of the Biocomplexity experiment, water tables were manipulated in a vegetated thaw-lake basin to investigate the impact of variation in soil moisture on land-atmosphere carbon, water and energy balance. In 2008 and 2009, following three years of baseline measurements (2005-2007), the lake basin was divided into three treatments, a flooded section (+10cm WTD), a drained section (-10cm WTD), and a control section where the water table was maintained relative to water levels outside the manipulation area (Fig. 1.2b). The experimental infrastructure established for this site includes a robotic tram system similar to that described by Gamon et al. (2006a) for a Californian Chaparral ecosystem. The tram system consists of three

300 meter-long transects ("tramlines") with one tramline located in each of the three treatment areas. Each tramline spanned the entire width of the lakebed and was oriented east–west to avoid midday shading of the south side (the sampling footprint of the tramline). An eddy covariance flux tower designed to measure trace gas flux for each of the treatment areas (Fig. 1.2b) was situated adjacent to each of the tramlines (Zona et al. 2009). The infrastructure established for the Biocomplexity experiment provided an ideal experimental research platform for this study as it established the capacity to repeatedly assess the surface spectral properties of the same land cover type and sampling footprint affected by contrasting surface hydrology regimes throughout the snow-free period.

1.5.3 Reflectance Measurements

Field reflectance data used in this study were collected during the annual 2005, 2006, 2007, 2008, and 2009 growing seasons, which span early June to late August. Spectral data were obtained using a dual-detector field portable spectrometer (Unispec DC, PP Systems, Amesbury, MA, USA), which collects radiance (radiation from the target) and irradiance (radiation from the sky) simultaneously, thereby permitting correction of surface reflectance under varying sky conditions (Gamon et al. 2006a). The two detectors were cross-calibrated using a white panel with 99% reflectance (Spectralon, Labsphere, North Sutton, NH, USA) at the beginning and at the end of each set of measurements along each tramline. Our Unispec-DC had a nominal range of operation between 303 and 1148 nm in 256 contiguous bands with a spectral resolution of approximately 3 nm and a full-width-half maximum of approximately 10 nm. The usable range of this detector (range with reasonable signal-to-noise) is approximately 400-1000 nm and was used in subsequent analyses accordingly.

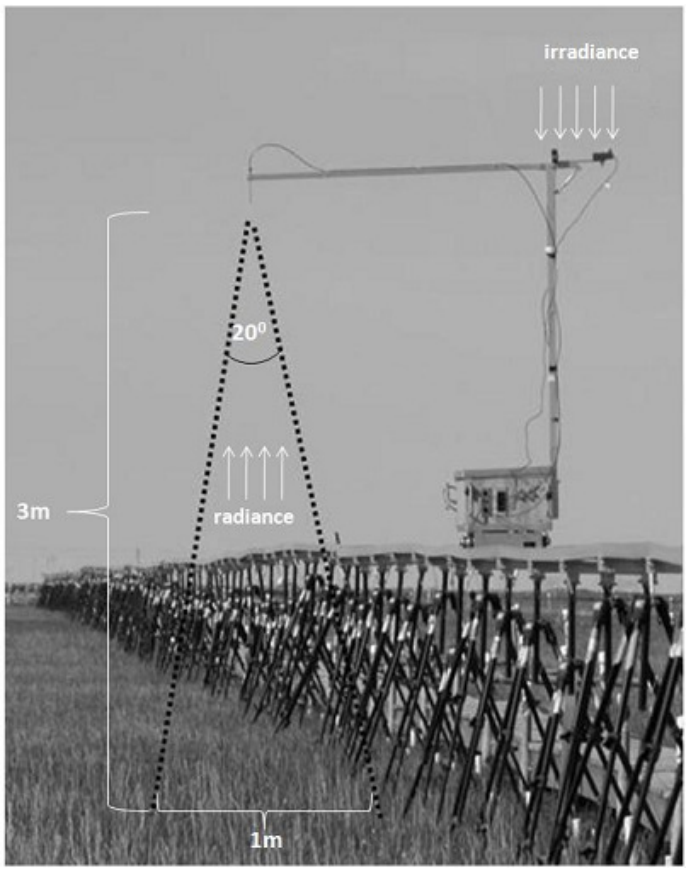

Figure 1.3. The robotic cart system used for collection of hyperspectral reflectance data at the Biocomplexity experiment in Barrow, Alaska. The figure illustrates the tram cart riding on an elevated 300-m long tramline. Radiance and irradiance are sampled each meter along the tramline. The field of view for radiance measurements on the south side of the tramline is illustrated by the dotted lines outlining the approximate spectrometer field-of-view at the foreoptic. The circular sampling footprint is approximately 1 m in diameter.

Along each tramline, reflectance data were collected by placing the field spectrometer on a semi-autonomous robotic cart (Gamon et al. 2006), which travelled along each of the 300 meter-long tramlines in a west-east direction (Fig. 1.3). The cart speed was set to approximately 1 meter every 5 seconds, allowing each 300 meter-long tramline to be sampled in approximately

25 minutes. A mechanical switch mounted on the base of the robotic cart was triggered when the cart passed over cross-bars situated at every meter along each tramline and activated the spectrometer to make a measurement. Each tramline was sampled up to three times per week if rain, mist, and extreme winds did not prevail. The downward looking foreoptic was positioned at approximately 3m above the ground and provided a field of view of approximately 20 degrees from the tip of the foreoptic. This equated to approximately a one square meter sampling footprint at ground level (Fig. 1.3). By repeating measurements throughout the snow free period, the tram system enabled us to obtain a spatially explicit seasonal and inter-annual time series of surface reflectance of the same land cover type under different surface hydrology regimes. Reflectance was calculated as the ratio of the irradiance and reflectance, corrected by the mean cross-calibration spectrum measured for each run of the cart along each tramline (see Gamon et al. 2006a for details). Reflectance data were processed using the software Multispec (Version 5.1, available at http://specnet.info), which calculated interpolated reflectance at one nanometer intervals between 303 and 1148 nm.

Surface reflectance data were collected along each tramline three to four times per week during the snow-free and shoulder seasons (approximately 10 to 14 weeks each year). Three hundred spectral measurements were made along each tramline every time the robotic cart was operated. Thus, 900 data files are collected every time data are collected in the lakebed for the three tramline areas each day of sampling. This generated approximately 55,000 spectral data files and 14,000,000 data points annually.

1.5.4 Other Measurements

Photos of each tramline footprint were acquired throughout the growing period using a digital camera (Nikon Coolpix 5400) that was mounted on the boom of the robotic cart and triggered manually using an electronic shutter cable. Water Table Depth (WTD) was measured manually every 10 meters along each tramline every time spectral measurements were made using a method similar to that described by Olivas et al. (2009). Four centimeter-wide perforated PVC tubing was placed in holes drilled in to the tundra, leaving approximately 20 centimeters of tubing above ground level. A ruler was used to measure the height of the water table relative to ground level. When the water level was below the surface WTD was considered negative and positive when the water table was above the surface. Hereon, negative WTD is termed 'below ground water' and positive WTD as 'standing surface water'. Soil moisture data were collected digitally using a time TDR300 soil moisture probe at every meter of the tramlines every time reflectance measurements were collected. Thaw depth data were collected at two week intervals at every meter of the tramlines during the growing season. The measurements were made following standard methods described in Nelson and Hinkle (2000). Meteorological measurements, which included air temperature, relative humidity, photosynthetically active radiation (PAR) and precipitation data were collected using a HOBO automated weather station (AWS) installed at the east end of the central tramline. Data were collected at one minute intervals throughout the growing season.

1.6 Structure of Dissertation

This chapter has illustrated the importance and need for climate change impact research in the Arctic to further understand how arctic terrestrial ecosystem structure and functions will respond. The important roles remote sensing can play in advancing this science have also been discussed. This dissertation contains four data-intensive chapters formatted for publication in international peer reviewed journals (Chapters 2-5). Chapter 2 discusses the development of a new spectral vegetation index developed for monitoring surface hydrological dynamics; Chapter 3 examines how land-surface phenology varied seasonally, between years and in response to the experimental manipulation of WTD; Chapter 4 investigates the relationship between NDVI and vegetation biomass and leaf area index for six key plant species common in the Barrow Environmental Observatory (BEO); and Chapter 5 describes several newly developed cyberinfrastructure tools that aided data management and quality control of the hyperspectral data collected during the study. Chapter 6 presents the general discussions and conclusions of the dissertation. The first of these data chapters (Chapter 2), titled "*Surface hydrology of an arctic ecosystem: multi-scale analysis of a flooding and draining experiment using spectral reflectance*" was published in the Journal of Geophysical Research (Goswami et al. 2011, Volume 116, G00107, 14PP, 2011). Another paper associated with a data specification and verification software presented in Chapter 5, titled "*Towards near-real time data property specification and verification for arctic hyperspectral sensor data"* has also been published, with my Cyber-ShARE research partner and computer science doctoral candidate Irbis Gallegos as lead author (Gallegos et al. NAFIPS, 2011). Each of these data chapters address one of the central research objectives outlined above.

Chapter 2: Surface hydrology of an arctic ecosystem: multi-scale analysis of a flooding and draining experiment using spectral reflectance

This chapter was published in the Journal of Geophysical Research in 2011.

Citation: Goswami, S., J. A. Gamon, and C. E. Tweedie (2011), Surface hydrology of an arctic ecosystem: Multiscale analysis of a flooding and draining experiment using spectral reflectance, *J. Geophys. Res.*, *116*, G00I07, doi:10.1029/2010JG001346.

2.1 Introduction

Climate change appears to be most pronounced at high northern latitudes (IPCC 2007, ACIA 2005). Many of the observed (Post et al. 2009, Hinzman et al. 2005; Smith et al. 2005) and modeled (McGuire et al. 2009, Sitch et al. 2007) climate change responses in arctic tundra ecosystems are related to altered surface hydrology. In the Arctic, the importance of surface hydrology on surface energy budgets (Euskircken et al. 2007, Chapin et al. 2005), land-atmosphere carbon exchange (Merbold et al. 2009, Wolf et al. 2008), plant phenology and response to warming (Walker et al. 2006, Arft et al. 1999), and geomorphic processes (McNamara and Kane 2009, Lawrence and Slater 2005) are well recognized. Based on experimental evidence, observations and modeling, alteration of surface hydrology in arctic terrestrial ecosystems is likely to alter a variety of interconnected ecosystem processes such as primary productivity (McGuire et al. 2007, Oberbauer et al. 2007, Illeris et al. 2004), methanogenesis (Mazeas et al. 2009, Merbold et al. 2009, Petrescu et al 2008), nutrient cycling (Arndal et al. 2009, McGuire et al. 2009, Jonasson et al. 2004) and land cover or plant community change (Callaghan et al. 2007, Walker et al. 2006, Smith et al. 2005).

The degree to which changes in land-atmosphere carbon exchange dynamics will interact with and offset the balance and stability of the substantial store of soil organic carbon in the Arctic (Tarnocai et al. 2009, Ping et al. 2008) is a primary concern (McGuire et al. 2009). If the

increased primary productivity predicted for the Arctic does not balance net loss of CO_2 equivalent carbon loss to the atmosphere, a positive feedback to regional and potentially the global climate system will occur (Hudson et al. 2009, Kimball et al. 2006). This positive feedback response to warming in the Arctic is likely to be controlled by soil moisture and surface hydrology (Huemmrich et al. 2010, McGuire et al. 2006), so there is a need to monitor these parameters and determine how they are changing over time and space to better understand the future state of the Arctic system. Substantial efforts before, during and now following the 2007-2009 International Polar Year have focused on improving environmental observing capacities in the Arctic, particularly the future fate and transport of the Arctic soil organic carbon store (National Academy of Sciences 2006, ICARP-II report 2005, National Academy of Sciences 2004). Such efforts highlight the importance of observations that span plot to global scales. Because of the many advantages remote sensing offers to such scaling challenges (Stow et al. 2004), the development of remote sensing approaches and technologies in an integrated arctic observing network is a key priority.

Several remote sensing methods have been developed for monitoring surface hydrology or soil moisture over large spatial scales. To assess the state of surface hydrology in terrestrial ecosystems, remote sensing has been used to monitor inundation area (Smith et al. 2005, Smith et al. 1997), snowpack (Green et al. 2006), and vegetation water content (Serrano et al. 2000, Ustin et al. 1998, Roberts et al. 1997). Radar remote sensing based on microwave has been used successfully for assessing soil moisture status in some arctic landscapes (Kasischke et al. 2009, Meade et al. 1999). While radar is useful for estimating inundation area, the return signal is easily confounded by wind or the presence of vegetation that can alter the backscatter properties

(Smith 1997). LiDAR remote sensing has also been used in habitat mapping (wedding et al. 2008), mapping coral reef structure (Storlazzi et al. 2003) and measuring coral reef rugosity (Brock et al. 2006, Brock et al. 2004) and also in mapping bathymetry of coastal regions (Irish and White 1998). Optical remote sensing methods (using visible or near-infrared wavelengths) can penetrate water bodies, and have been applied to studies of bathymetry (Brando et al. 2009), seagrass (Phinn et al. 2008) and coral reefs (Hochberg et al. 2003). Additionally, optical remote sensing has often been used to assess vegetation moisture content through reflectance indices based on water absorption bands (Sims and Gamon 2003). Examples of the latter include the Water Index (sometimes called the Water Band Index) based on reflectance at the 970 nm water band (Peñuelas et al. 1993), and the Normalized Difference Water Index (Gao 1996) based on the 1240 nm water band. Additionally, some methods apply a form of Beer's Law to fit the water absorption coefficient spectrum to a reflectance spectrum, yielding an "Equivalent Water Thickness" (EWT) (Green et al. 2006, Sims and Gamon 2003, Roberts et al. 1997, Gao and Goetz 1995). Based on the assumption of Beer's law, which states that reflected or transmitted light is related to the exponent of the amount of an absorbing compound, EWT offers a physically-based alternative to other index based methods for assessing water (Gao and Goetz 1995). To the extent that water bodies or vegetation behave according to Beer's Law, and to the extent that calculation of EWT is based on a full spectrum (multiple bands rather than two bands) it seems that EWT should offer a superior method of assessing moisture status, but not all studies have supported this conclusion (Sims and Gamon 2003, Serrano et al. 2000). Consequently, the "best" method for retrieving surface hydrology information with optical remote sensing remains an open question and a key challenge.

Most of the optical remote sensing methods for assessing surface moisture properties utilize one or more water absorption features present in reflectance spectra (Green et al. 2006). Because these methods employ water absorption bands, they readily saturate, are easily confounded by atmospheric water vapor, and the vapor absorption bands overlap with liquid water features (Green et al. 2006, Sims and Gamon 2003). These issues create practical problems for quantitative retrieval of surface moisture measurements, particularly in areas with high atmospheric moisture such as the Arctic (Stow et al. 2004). Additionally, instrument limitations (e.g. low signal-to-noise) and artifacts (e.g. "second-order" or "stray light" errors) in certain spectral regions (e.g. the 970 nm water band) often confound a clear interpretation of water signals, particularly with silicon photodiode detectors (Sanchez-Azofeifa et al. 2009).

To our knowledge, optical remote sensing has not been applied to directly assess surface water depth (SWD), a sensitive indicator of surface hydrology and soil moisture in the Arctic, especially on the coastal plain of northern Alaska. One goal of this study was to develop a spectral index from optical remote sensing that could be used to estimate surface water depth (SWD) and surface water cover (SWC), and to characterize changes in surface hydrological properties at multiple spatial and temporal scales. To maximize the extrapolation potential of such an index, we specifically sought an index that could not be confounded by atmospheric moisture, would be relatively free from instrument errors, and would be commonly available from ground-based, airborne or satellite-borne instruments. Another goal of this study was to evaluate treatment effects as part of the Biocomplexity experiment, as described below.

2.2 Methods

2.2.1 Study Area

The study was conducted within the Biocomplexity flooding and draining experiment on the Barrow Environmental Observatory (BEO) near Barrow, Alaska , 71°17'01" N, 156°35'48" W, (Fig. 1.2). The BEO is situated on the Alaskan Arctic Coastal Plain and has a low relief and an average elevation of 4 meters (Aguirre et al. 2008). Seventy two percent of the landscape near Barrow contains oriented lakes, drained thaw lake basins and small ponds (Hinkel et al. 2003). The Biocomplexity experimental area is located in a series of three coalesced drained thaw lake basins that include moist and wet tundra vegetation dominated by graminoid tundra (Tweedie et al. in prep.). The study site is underlain by continuous permafrost and includes thermokarst terrain typical of the Alaskan Arctic Coastal Plain (Brown et al. 1980) such as thaw lakes, high and low-centered polygons, shallow ponds and lakes, and a shallow active layer that is generally less than 50 centimeters in the experimental area (Shiklomanov et al. submitted). Soils of the area are described by Bockheim et al. (1999) and include cryoturbated gelisols, specifically Typic Aquorthels with high soil moisture content, Histoturbels, and Aquaturbels. The upper layer of this soil consists of carbon rich peat (ca. 50 kg/C/m^3) (Bockheim et al. 2001). Soils are generally moisture rich due to shallow drainage gradients, relatively low rates of evapotranspiration, and impeded drainage caused by ice-rich continuous permafrost (Bockheim et al. 1999, Miller et al. 1998).

Winter is generally long, dry and cold and the summers are relatively short, moist and cool (Brown 1980). The sun is above the horizon continuously from May 10th to August 2nd, and below the horizon from Nov 18th to Jan 24th (Brown 1980). Air temperature remains below

freezing for nine months of the year and can fall below freezing during any of the three summer months. A gradual warming trend begins in April and snow melt typically occurs in early June. Wind speed varies little during the year, averaging 5.3 m/sec, with the fall months being the windiest. Fog and low cloud persist throughout the summer and the relative humidity generally exceeds 80% from June through September. Mean June to August precipitation is 58.4 millimeters (Engstrom et al. 2008).

2.2.3 Experimental Infrastructure

As part of the Biocomplexity experiment, water tables were manipulated in a vegetated thaw-lake basin to investigate the impact of variation in soil moisture on land-atmosphere carbon, water and energy balance. In 2008 (the year of this study), following three years of baseline measurements (2005-2007), the lake basin was divided into three treatments, a flooded section (+10cm WTD), a drained section (-10cm WTD), and a control section where the water table was maintained relative to water levels outside the manipulation area (Fig. 1.2b). The experimental infrastructure established for this site includes a robotic tram system similar to that described by Gamon et al. (2006a). The tram system consists of three 300 meter-long transects ("tramlines") with one tramline located in each of the three treatment areas. Each tramline spanned the entire width of the lakebed and was oriented east–west to avoid midday shading of the south side (the sampling footprint of the tramline). An eddy covariance flux tower designed to measure trace gas flux for each of the treatment areas (Fig. 1.2b) was situated adjacent to each of the tramlines (Zona et al. 2009). A range of other collaborative studies were conducted throughout the experimental area, including several featured in this special issue (Olivas et al.

2010). The infrastructure established for the Biocomplexity experimental provided an ideal experimental research platform for this study as it established the capacity to repeatedly assess the surface spectral properties of the same land cover type affected by contrasting surface hydrology regimes throughout the snow-free period.

2.2.4 Reflectance Measurements

Field reflectance data used in this study were collected from early June 2008 to late August 2008. This period spanned the majority of the 2008 snow-free period for the study site. Spectral data were obtained using a dual-detector field portable spectrometer (Unispec DC, PP Systems, Amesbury, MA, USA), which collects radiance (radiation from the target) and irradiance (radiation from the sky) simultaneously, thereby permitting correction of surface reflectance under varying sky conditions (Gamon et al. 2006a). The two detectors were cross-calibrated using a white panel with 99% reflectance (Spectralon, Labsphere, North Sutton, NH, USA) at the beginning and at the end of each set of measurements along each tramline. Our Unispec-DC had a nominal range of operation between 303 and 1148 nm in 256 contiguous bands with a spectral resolution of approximately 3 nm and a full-width-half maximum of approximately 10 nm. The usable range of this detector (range with reasonable signal-to-noise) was approximately 400-1000 nm, so this was the spectral range used in subsequent analyses.

Along each tramline, reflectance data were collected by placing the field spectrometer on a semi-autonomous robotic cart (*sensu* Gamon et al. 2006a), which travelled along each of the 300 meter-long tramlines in a west-east direction (Fig. 1.3). The cart speed was set to approximately 1 meter every 5 seconds, allowing each 300 meter-long tramline to be sampled in

approximately 25 minutes. A mechanical switch mounted on the base of the robotic cart was triggered when the cart passed over cross-bars situated at every meter along each tramline, activating the spectrometer to make a measurement. Three hundred spectral measurements were made along each tramline every time the robotic cart was operated. Each tramline was sampled up to three times per week if rain and mist did not prevail. The downward looking foreoptic was positioned at approximately 3m above the ground and provided a field of view of approximately 20 degrees from the tip of the foreoptic. This equated to approximately a one square meter sampling footprint at ground level (Fig. 1.3). By repeating measurements throughout the snow free period, the tram system enabled us to obtain a spatially explicit time series of surface reflectance of the same land cover type under different surface hydrology regimes. Reflectance was calculated as the ratio of the two channels, corrected by the mean cross-calibration spectrum measured for each run of the cart along each tramline (see Gamon et al. 2006a for details). Reflectance data were processed using the software Multispec (Version 5.1, available on http://specnet.info), which calculated interpolated reflectance at one nanometer intervals between 303 and 1148 nm.

2.2.5 Surface Hydrology

WTD was measured manually every 10 meters along each tramline every time spectral measurements were made, using a method similar to that described by Olivas et al. (2010). Perforated PVC tubing with a diameter of four centimeters was placed in holes drilled in to the tundra, leaving approximately 20 centimeters of tubing above ground level. A ruler was used to measure the height of the water table relative to ground level. When the water level was below

the surface WTD was considered negative and positive when the water table was above the surface. In cases of below-ground water (negative WTD values), SWD was assigned a value of zero; consequently, SWD simply refers to positive WTD values (i.e. areas of visible standing water).

Percent water cover was determined through image analysis of digital color photographs. Photos of each tramline footprint (matching the optical sampling areas) were acquired on July 18, 2008, using a digital camera (Coolpix 5400, Nikon) that was mounted on the boom of the robotic cart and triggered manually using an electronic shutter cable. The photo locations were also adjacent to WTD measurements, allowing direct comparison to WTD and SWD. Supervised classification in image processing software (ENVI, Version 4.2, ITT Visual Information Solutions, Boulder, CO, USA) was used for each photo to estimate SWC.

2.2.6 Reflectance and surface water

The development of a spectral index suitable for characterizing surface hydrology (WTD, SWC and SWD) required the assessment of spectral sensitivity to surface water. Reflectance was measured at separate locations along the tramline in the control treatment area over multiple locations having different SWC, WTD, and SWD, which were quantified as described above. Additionally, reflectance at every ten nanometers from 400 to 1000 nm was correlated with SWC, WTD and SWD at every 10 meters along the tram line on July 18, 2008. Both linear and logarithmic regressions were run to determine the best fit for each regression. We also evaluated the correlation between NDSWI (both linear and log versions) and negative WTD values (i.e. areas of no standing water because the water table was below the surface).

We used the regressions from the analysis described immediately above to derive two versions of a surface water index, the "Normalized Difference Surface Water Index" (NDSWI). The first version of NDSWI calculates the normalized difference of reflectance at 460 nm and 1000 nm ("NDSWI-linear," Equation 2.1 below). The second version of NDSWI used a similar equation and the same reflectance bands but required reflectance to be log transformed ("NDSWI-log," Equation 2.2 below). The relative success of NDSWI-linear and NDSWI-log in modeling SWC and depth (SWD, WTD) is presented below and is compared to two additional spectral indices that have also been used to describe plant or surface water status – the Water Band Index (WBI – Equation 2.3 below, Peñuelas 1993) and the Equivalent Water Thickness index (EWT – Equation 2.4 below, Sims and Gamon 2003, Roberts et al. 1997). EWT was calculated, using a Beer's Law approximation (Sims and Gamon 2003, Roberts et al. 1997, Gao and Goetz 1995), where the impact of surface water on reflectance is determined as the negative slope of the linear regression between the water absorption coefficient spectrum (Green et al. 2006, Sims and Gamon 2003) and the natural log of the reflectance spectrum over a wavelength range of 900 to 1040 nm. The formulas for calculating NDSWI-linear, NDSWI-log, WBI and EWT are:

$$\text{NDSWI-linear} = (R460 - R1000)/(R460+R1000) \quad \text{(Equation 2.1)}$$

$$\text{NDSWI-log} = \{\ln(R1000) - \ln(R460)\}/\{\ln(R1000) + \ln(R460)\} \quad \text{(Equation 2.2)}$$

$$\text{WBI} = R900/R970 \text{ (Peñuelas et al. 1997)} \quad \text{(Equation 2.3)}$$

$$\text{EWT} = -\Delta(\ln R)/\Delta(a) \quad \text{(Equation 2.4)}$$

July 18 values of EWT, WBI, NDSWI-linear, and NDSWI-log were correlated with SWC estimated from digital image analysis as described above (n = 90). For testing WTD and SWD,

we used calibrations of these same indices derived from certain dates and locations, but tested against other dates and locations within the 2008 sampling year. For example, these indices (Equations 2.1- 2.4) measured for five days (July 18, July 23, July 28, Aug 4, and Aug 9 of 2008) were first calibrated against corresponding SWD measurements for those dates using regression analysis. The two spectral indices that most strongly correlated with SWC and SWD in the above analyses (Equations 2.1 and 2.2) were then applied to the entire growing season by using these calibrations to predict SWD and WTD throughout the 2008 sampling period. These predictions were then tested against independent SWD and WTD measurements and used to make plots illustrating the temporal and spatial dynamics of surface water for the treatment areas over the 2008 season. Note that since photographic estimates of percent water cover were only available for one date (July 18), SWC could not be independently tested in this way.

Particular attention was paid in assessing the accuracy of the model for estimating SWD. Data from alternate sampling dates during the peak of the growing season (July 18, July 23, July 28, Aug 4, and Aug 9 of 2008) were combined to derive the final model for seasonal analysis. Seasonal SWD trends for each tramline were then modeled and compared to measured WTD to determine if the model over or under-estimated WTD in each of the experimental treatments. Mosaic plots combining all treatment dates and positions were derived to assess the spatio-temporal behavior of the model along each tramline and throughout the sampling period. To assist in the interpretation of these plots, microtopographic variation along each tramline was also examined. Data for microtopography were acquired from a one-meter digital elevation model developed for the study area from air-borne LiDAR acquired in late August 2006 (Tweedie unpublished data).

2.2.7 Spectral Mixture Analysis

To further understand the effect of surface water on spectral reflectance, we also explored the effects of SWC on the reflectance-based indices (Equations 2.1- 2.4) using spectral mixture analysis (Adams and Gillespie 2006). To do this, we selected 'pure' sites along the tram lines that were either 100% water cover or 100% vegetation cover on July 18, 2008, and created synthetic spectra of various mixtures of the two spectral types, ranging from 0% surface water cover (100% vegetation cover) to 100% surface water cover (0% vegetation cover), assuming linear mixing. These synthetic mixtures were then compared to actual field spectra of plots having various SWC and SWD values.

2.2.8 Scaling Analysis

Two high-spatial resolution multispectral satellite images (QuickBird, Digital Globe, Longmont, Colorado, USA) acquired on August 2, 2002 and July 27, 2008, were used to calculate NDSWI for the entire treatment basis for both pre- (2002) and post- (2008) treatment years. Note that due to frequent cloud cover in this region (Hope et al. 2004), these were the only clear-sky high resolution Quickbird images we were able to obtain for the experimental period. QuickBird images for these dates were available with four spectral bands: blue (450-520 nm), green (520-600 nm), red (630-690 nm) and near-IR (760-900 nm) at 2.8m resolution. Using ArcGIS (ESRI, Redlands, California), NDSWI was derived using Equation 2.1 above for both the 2002 and 2008 Quickbird images where R460 and R1000 was substituted with the blue and IR bands of the Quickbird image respectfully. The linear version of the NDSWI equation was used to avoid any problem with band math calculations using the satellite bands. The

difference in NDSWI between images (2008 minus 2002) was calculated to visualize and quantify treatment effects for different regions of the basin (flooding, vs. drained and control regions; tramline regions vs. flux tower regions vs. the entire treatment basin). The tramline transects and idealized flux tower footprints (based on experimental layout), and the inundated basin of the experimental area were delineated for each treatment area. For the 2002 and 2008 images, the NDSWI pixel values for the tram and flux tower footprints and treatment basins were extracted for statistical analyses (Systat Software Inc., Chicago, Illinois). To assess differences between the 2002 and 2008 NDSWI coverages for a given sampling area and treatment, t-tests were run. A univariate Analysis Of Variance (ANOVA) was used to assess the difference between treatments for the same sampling area type within a given year. To determine the difference in the frequency distribution of NDSWI between sampling areas within a given treatment area and year, a 2-sample Kolmogorov-Smirnov test was performed. This non-parametric test assesses whether the tramline footprint area and flux tower footprint area, for example, have a similar NDSWI frequency distribution or whether they are significantly different from one another – an important consideration in testing the scalability of measurements taken in different areas of a particular treatment area.

2.3 Results

Spectral reflectance was clearly affected by varying SWC within the treatment basin (Fig. 2.1). The least change was observed in the blue spectral region (450-500nm), and the biggest difference was observed in the near-infrared (>700nm) with reflectance decreasing markedly with increasing surface water (WTD, SWD, and SWC). Synthetic mixtures behaved in a similar

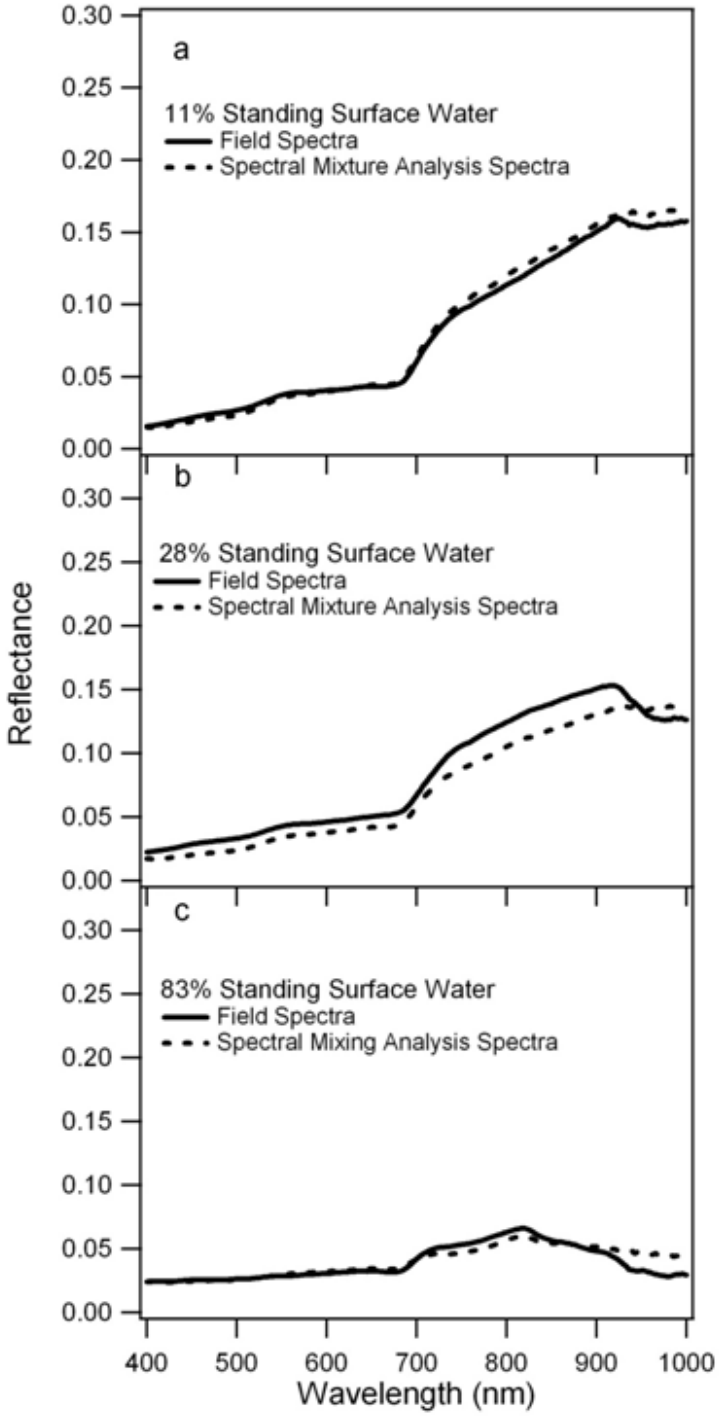

Figure 2.1. The effect of surface water (expressed as SWC) on reflectance spectra. Each field spectrum is compared to a modeled reflectance spectra using spectral mixture analysis for the same percent of standing surface water.

manner, and closely matched field spectra. This response to surface water coverage indicated that an index that accounted for the contrasting response to water between the blue and NIR bands could be used as an indicator of surface water (WTD, SWD, and SWC). To assess which wavelengths would be optimal for such an index, we correlated several metrics of surface water (WTD, SWD and SWC) with reflectance at every ten nanometers from 303 to 1148 nm for every location where reflectance, WTD, SWC were measured on July 18th 2008 (Fig. 2.2). Regardless of which water metric was used (WTD, SWD, or SWC), R^2 values were lowest in the blue (460 nm) and highest in the NIR (approximately 1000 nm), confirming that reflectance in the blue is poorly correlated with surface water, whereas reflectance in the NIR is strongly correlated with surface water. R^2 values between reflectance in the NIR and WTD and SWD were highest for a logarithmic model**.** R^2 values between reflectance and WTD were higher than those with SWD. R^2 values for SWC were nearly identical to those for SWD.

Of the indices tested, the best predictor of WTD was NDSWI-log, closely followed NDSWI-linear (Table 3.1). Both NDSWI versions (log and linear) exhibited identical R^2 values with SWC water cover (Table 3.2). All indices showed significant R^2 values with WTD and SWC although EWT had a stronger R^2 values with WTD than WBI and WBI had a stronger R^2 values with SWC than EWT (Tables 3.1 and 3.2). NDSWI-log showed a slightly higher R^2 values with WTD throughout most of the sampling period than NDSWI-linear (Fig. 2.3), although the overall differences were very small. Since independent SWC measurements were not made over the entire season (just July 18, 2008), we could not evaluate the seasonal dependence of the fits between these indices and SWC.

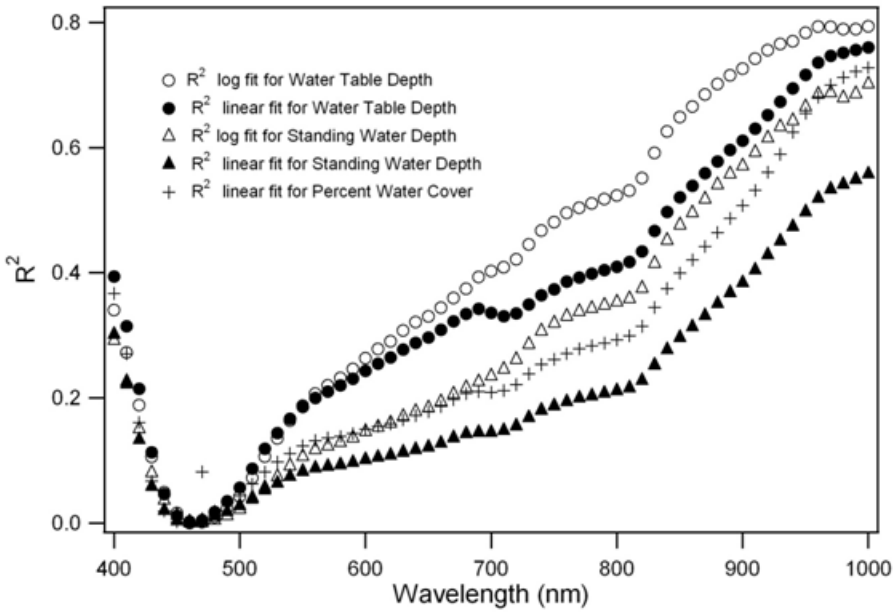

Figure 2.2. Correlation coefficients for wavelength vs. WTD, SWD and SWC. Data for this analysis was collected on July 18 2008.

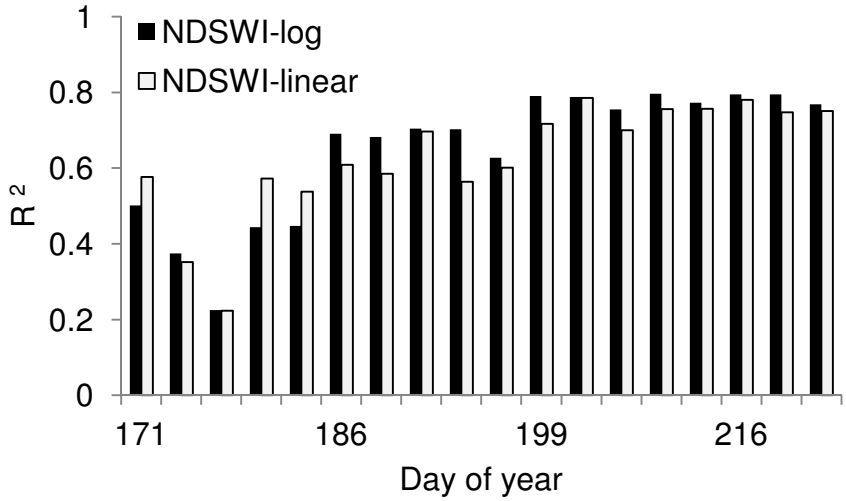

Figure 2.3. Correlation coefficients for the prediction of WTD from NDSWI for all tramlines comparing linear and log versions of the index for different dates in 2008.

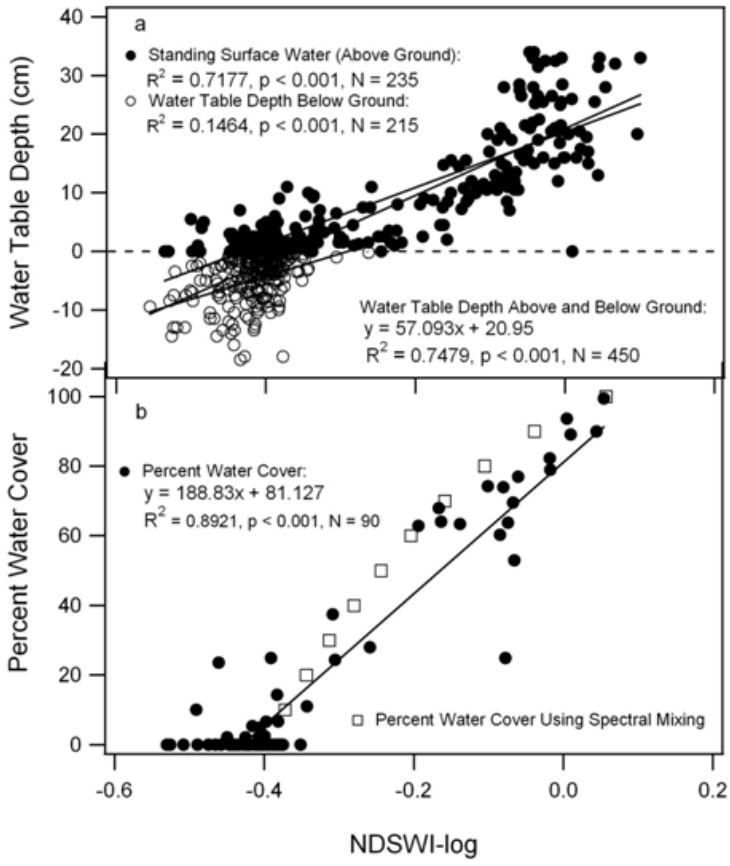

Figure 2.4. Model that predicts WTD (all points), SWD (solid circles), and below-ground water (open circles) (panel 6a) and SWC (solid circles, panel 6b) from NDSWI-log. This model was derived using data from July 18, 23, 28, August 4 and August 9, 2008. Modeled SWC using spectral mixture analysis are also shown (open circles, panel 6b).

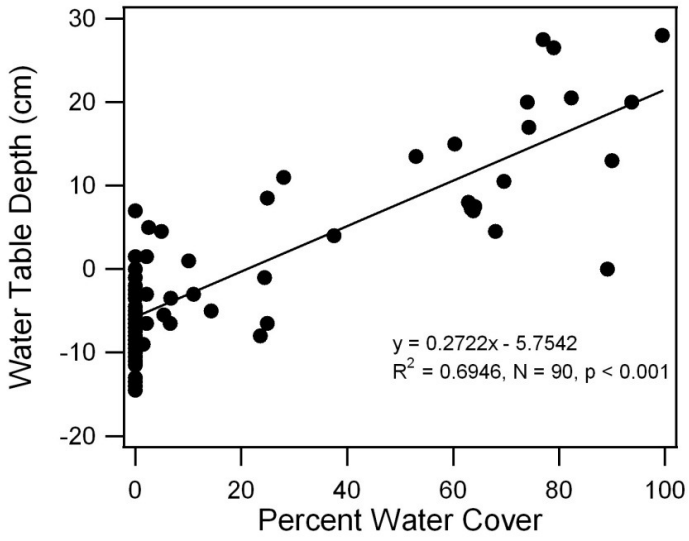

Figure 2.5. Correlation between SWC and WTD for July 18, 2008.

Table 3.1. Results of regressions between EWT, WBI, NDSWI-log, NDSWI-linear and WTD for July 18, 23, 28, August 4 and August 9, 2008. Y = WTD, x = index value.

Indices	Model Equation	R^2 - value	P - value	N - value
EWT	Y = 37.303x – 1.6882	0.55	< 0.001	450
WBI	Y = 19.271x – 18.854	0.50	< 0.001	450
NDSWI-linear	Y = 31.53x + 22.578	0.71	< 0.001	450
NDSWI-log	Y = 57.093x + 20.95	0.75	< 0.001	450

Table 3.2. Results of the regressions between EWT, WBI, NDSWI-log, NDSWI-linear and Percent Surface Water Cover (SWC) for July18, 2008. Y = Percent surface water cover, x = index value.

Indices	Model Equation	R^2 - value	P - value	N - value
EWT	Y = 133.15x + 6.5587	0.71	< 0.001	90
WBI	Y = 80.555x + 67.566	0.82	< 0.001	90
NDSWI-linear	Y = 108.67x + 88.562	0.89	< 0.001	90
NDSWI-log	Y = 188.83x + 81.127	0.89	< 0.001	90

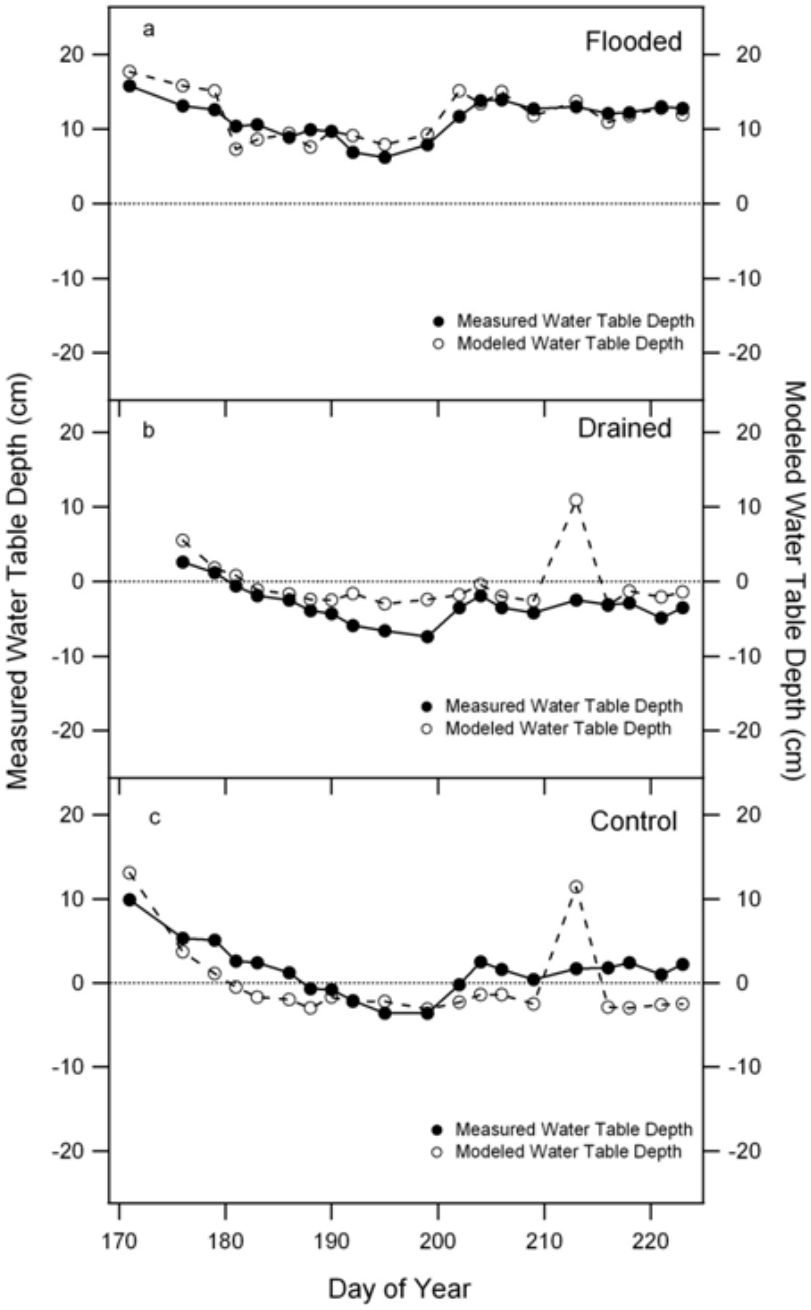

Figure 2.6. Seasonal patterns of mean measured WTD along the three tramlines and mean modeled WTD for each tramline. Panels 8a, 8b and 8c show flooded (north), drained (central) and control (south) treatments respectively. The peak in between day 210 and day 215 in the drained and control treatments indicate snow cover for that particular day.

The model for predicting WTD and SWC using NDSWI-log is given in figure 2.4. Linear models best described the relationship between NDSWI-log and WTD. However, when only SWD was included, a non-linear model improved the fit slightly (not shown), and NDSWI tended to saturate at larger WTD or SWD values. When below-ground values were examined separately (open circles, Fig. 2.4a) the R^2 value was greatly reduced, but still significant ($P < 0.001$, Fig. 2.4a). These results demonstrate that the NDSWI-based model's greatest predictive power was for SWD (i.e., positive WTD values). The R^2 value for linear regression between NDSWI-log and SWC was also highly significant (Fig. 2.4b). Modeled results from synthetic mixtures of water and vegetation (open circles, Fig. 2.4b) closely matched the results of the field measurements (closed circles, Fig. 2.4b), providing further support of a strong link between SWC and NDSWI-log for this landscape. SWC and SWD from July 18 (the date of photographic estimates of SWC) were strongly correlated (Fig. 2.5), suggesting that SWC, SWD, or some combination of the two could be driving this index.

In seasonal plots, modeled WTD closely followed measured WTD for all the tramlines but appeared to be more accurate for the north tramline, where WTD was higher compared to that of the other tramlines, which often had below ground water (Fig. 2.6). When the WTD values were most negative (e.g. between days 190 and 200 in the central and south treatment basins), the index tended to overestimate the below ground water (i.e., produce less negative WTD values, Fig. 2.6b and 2.6c). The index also had an abberant peak during a snowfall (day 213) in the central and south basins (Fig. 2.6b and 2.6c), but not in the flooded north basin (Fig. 2.6a), where SWD prevented snow from accumulating. Direct R^2 values between modeled and measured WTD for each tramline and for all treatments combined (Fig. 2.7) showed that

modeled WTD tended to over-predict WTD in the control treatment and under-predict WTD in the drained treatment. In the flooded treatment, where WTD values were positive, the model predicted WTD (i.e. SWD) most accurately.

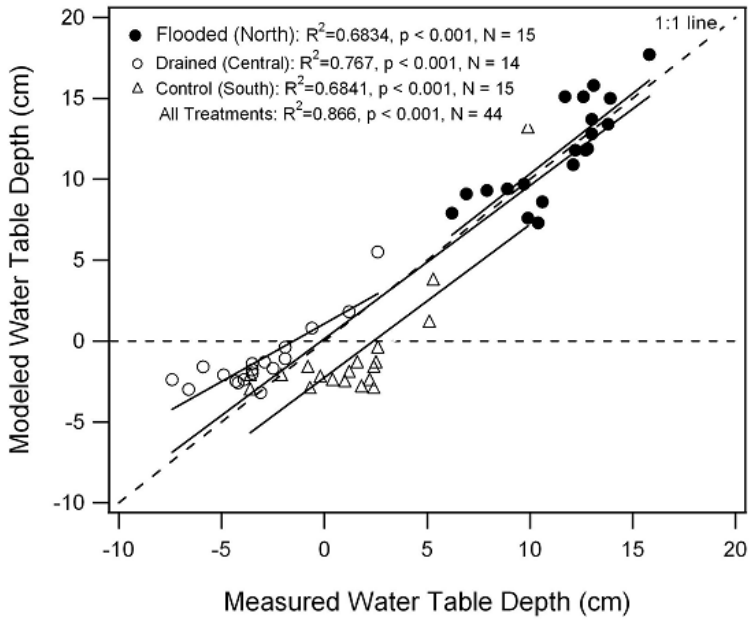

Figure 2.7. Modeled vs. measured mean WTD for all the three tramlines for the 2008 snow free period. Measured WTD data were collected from June 21 to August 11, 2008.

The model developed for WTD (Fig. 2.4a) also depicted the spatio-temporal dynamics of WTD along each tramline and throughout the sampling period (Fig. 2.8). Measured WTD and modeled WTD varied with substrate microtopography (Fig. 2.8, top panel). Locally high-elevation areas had the lowest WTD values, and low-elevation areas had the highest WTD values (green-yellow areas in the WTD image, Fig. 2.8). In early June soon after snow melt (ca. day 170), WTD was high. As the snow free period progressed, WTD decreased throughout each treatment. The horizontal banding in modeled WTD around day 210 for the central and south

tramlines was caused by snowfall, which was also prominent as an anomalous spike in these same treatments shown in figure 2.6b and 2.6c.

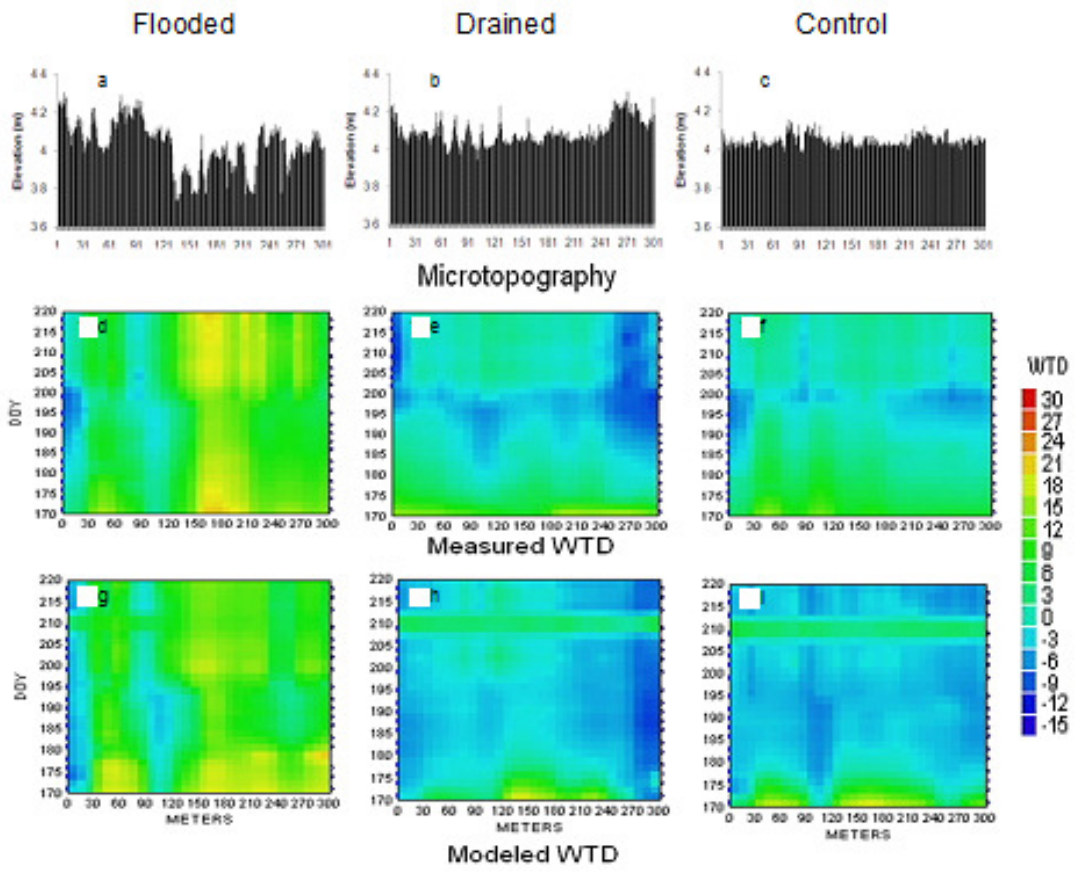

Figure 2.8. Modeled vs. measured mean WTD for all the three tramlines for the 2008 snow free period. Measured WTD data were collected from June 21 to August 11, 2008. The WTD values shown here are in centimeters.

NDWSI extrapolated across the experimental area using Quickbird satellite imagery from August 2nd 2002 (Fig. 2.9a, pre-treatment) July 27 2008 (Fig. 11b, post-treatment) showed spatial patterns and temporal changes in surface water. These changes were particularly evident for the northern basin (flooded treatment). In figure 2.9, three sampling areas – treatment basin, hypothetical flux footprint and tramline transects - are shown. The most conspicuous difference

between these NDSWI extrapolations is an increase in NDSWI (becoming wetter) in the flooded treatment area. Although significant differences between years were recorded in the drained and control treatment areas (asterisks, Fig. 2.10), these are relatively minor compared to the flooding treatment effect illustrated in figure 2.9 and further documented in figure 2.10.

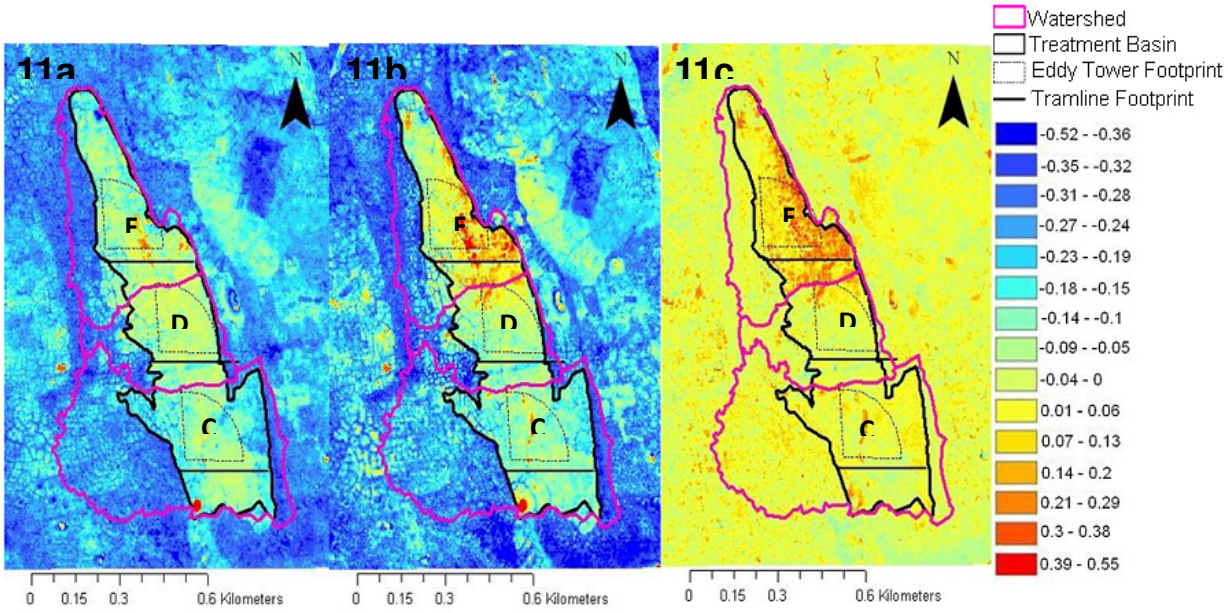

Figure 2.9. NDSWI-linear values extrapolated across the Biocomplexity experimental area using multispectral Quickbird images for 2002 (Fig. 11a, pre-treatment) and 2008 (Fig. 11b post-treatment). Figure 11c shows the difference of NDSWI-linear values for the two treatment years (2008-2002). The black lines show the outer boundary of the treatment basin areas: flooded (north) drained (central), and control (south). The letters F, D and C correspond to the flooded, drained and control treatment areas respectively and the color legend shows the NDSWI values. The sectors indicate hypothetical flux tower sampling footprints according to the original experimental design, with the vertices of the sectors indicating the locations of the flux towers.

Significant differences (t-test, $P < 0.05$) were noted between years for all sampling areas and treatments except for the tramline footprint in the drained treatment (see asterisks, Fig. 2.10). Univariate ANOVA showed no significant difference between the tramline footprints in the

control and drained treatments for both years (see letters, Fig. 2.10). The tramline footprint in the flooded treatment was significantly different from the tramline footprints in the drained and control treatments for both years (see letters, Fig. 2.10). Kolmogorov-Smirnov tests showed significant difference between tramline and flux footprints and treatment basins for all years and treatments except for the 2002 flooded treatment, where the tramline was similar to the flux tower footprint and treatment basin (Roman numerals, Fig. 2.10). These results generally highlight a successful flooding treatment in 2008, but revealed little apparent effect of the draining treatment, which yielded no impact detectable by NDSWI. These results also indicated substantial variability between sampling areas (tramline, flux footprint area, and treatment basin) in all three treatments (flooded, drained, and control) for both 2002 and 2008. Note that the surface hydrology of the control treatment varied between years for each sampling region, indicating interannual variability in surface hydrology independent of any experimental treatment effect.

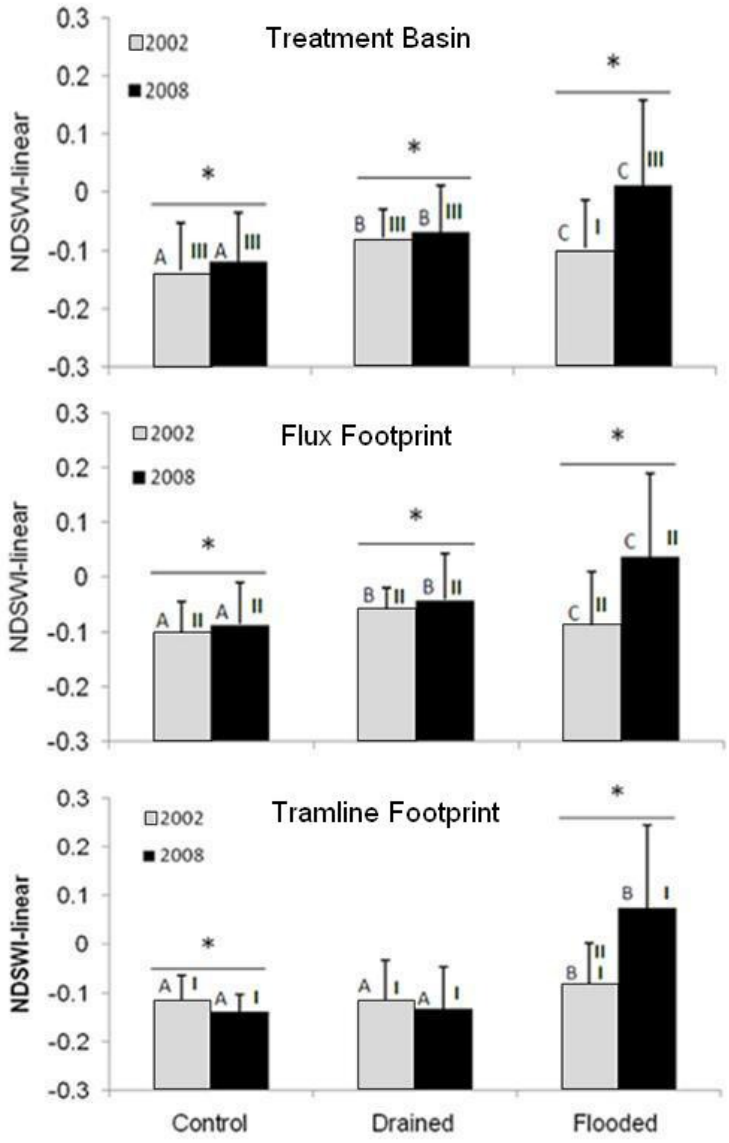

Figure 2.10. Comparison of average NDSWI-linear mapped to different sampling footprint areas using Quickbird 2002 and 2008 images. Error bars represent one standard deviation. '*' - Indicates significant difference ($P < 0.05$, T-Test) between years (2002 and 2008) for a given sampling area (tramline footprint, flux tower footprint, treatment basin) and treatment (flooded, drained, control). A/B/C - Indicates significant difference/similarity ($P < 0.05$, Univariate ANOVA) between treatments (flooded, drained, control) in a given year and type of sampling area. I/II/III – Indicates significant difference/similarity ($P < 0.05$, Kolomogorov-Smirnof test) between sampling areas (tramline footprint, flux tower footprint, treatment basin) within a given treatment and year.

2.4 Discussion

The Normalized Difference Surface Water Index (NDSWI) was able to accurately estimate SWC and SWD in an experimental flooding and draining experiment situated in a vegetated thaw lake basin on the Arctic Coastal Plain of northern Alaska. In the Arctic, soil moisture and surface hydrology are important in controlling plant community composition and ecosystem functional processes such as land-atmosphere carbon and water exchange and surface energy balance (Merbold et al. 2009, Walker et al. 2006, Chapin et al. 2005). Understanding how surface hydrology is changing with climate change could be key to understanding the future state of the Arctic. This study focused on developing a spectral index capable of estimating surface water status that would not be confounded by atmospheric moisture, would be relatively free from instrument errors, and would be commonly available from ground-based, airborne or satellite-borne instruments, and NDSWI appeared to meet this requirement.

Compared to EWT and WBI, two other spectral indices that have been widely used to estimate surface hydrological properties using remote sensing (Green et al. 2006, Sims and Gamon 2003, Roberts et al. 1997, Gao and Goetz 1995, Penuelas et al. 1993), NDSWI was a better predictor of SWD, SWC, and WTD within the study area. We initially expected that EWT could have captured these surface properties better than NDSWI because the calculation of EWT employs more wavebands, and more closely adheres to physical principles of Beer's law. However, both WBI and EWT used wavelengths within the 970 nm water absorption band, a region which is prone to instrument errors with the detector in our instrument (Sanchez-Azofeifa et al. 2009). It is likely that these factors contributed to the poorer fit with these indices. Additionally, the presence of more than one cover type (vegetation and water, having different

scattering properties), may have reduced the efficacy of EWT in this case, since Beer's Law assumes minimal scattering. Our instruments and sampling protocols were designed to correct for changing sky conditions (Gamon et al.2006a), but these corrections are often difficult under rapidly varying cloud conditions. Since the 970 nm water band can be affected by varying atmospheric moisture, the often cloudy and misty conditions of the site may have further contributed to the weaker fit with WBI and EWT. One reason why NDSWI may have performed better was that it uses wavelengths that are on the edge of (rather than near the middle of) the 970 nm water band. The slightly better prediction with the log version (versus the linear version) of NDSWI suggests that a Beer's law approximation may actually be a reasonable assumption for modeling SWD, since Beer's Law predicts an exponential extinction with depth, but this becomes problematic for wavelengths affected by varying atmospheric water vapor absorption (Sims and Gamon, 2003) and by poor instrument performance (low signal-to-noise and stray light errors).

Electromagnetic radiation in the optical region cannot penetrate deep into opaque surfaces (e.g. soil), which explains why negative WTD values were not modeled well with NDSWI (low R^2 values for open circles, Fig. 2.4a). When combined with positive WTD values (i.e. standing water above the surface), these negative values did not detract from the accuracy of the NDSWI-derived model. However, the low R^2 values between NDSWI and negative WTD values indicate that this model is not capable of accurately predicting below-ground water depth. This weakness explained the poorer fit in the control (south) and drained (central) treatment basins relative to the flooded (north) treatment, which was characterized by positive WTD values (i.e. SWD) for the seasonal sampling period (Figs. 2.6 & 2.7). Thus, we caution that the

detection of below ground water is not logically possible using the optical remote sensing techniques we have employed in this study, but note that they work well for visible surface water, whether expressed as SWC or as SWD (which were strongly correlated with each other**,** Fig. 2.5**).** Although this study shows a strong potential of NDSWI to be used as an index of SWD and SWC, we caution that further testing is required to determine the spatio-temporal scalability of NDSWI across multiple sensing platforms, and a broader range of land cover types, and regimes of surface hydrology.

For largely pragmatic reasons discussed above, we sought a spectral index that could not be overly confounded by atmospheric moisture and could be calculated from readily available ground-based, airborne or satellite-borne instruments. It appears that NDSWI meets this requirement. Further testing of NDSWI to assess its significance and extrapolation potential in the Arctic and elsewhere will need to address many remote sensing challenges. These include challenges specific to the Arctic (Stow et al. 2004), that span multiple spatial scales (Vanderbilt et al. 2007), address spectral variation between sensors - particularly optical and space borne sensors (Ganguly et al. 2008), and challenges that are specific to differing surface cover types and hydrological regimes. Remote sensing challenges inherent to the Arctic include but are not limited to characterization of diverse and fine scale landscape heterogeneity (Stoy et al. 2009, Williams et al. 2008), frequent cloud cover and high atmospheric moisture (Stow et al. 2004, Hope et al. 1993), and characterization of sometimes fine scale and often short-term biophysical phenomenon that are associated with ecosystem structure and function (Laidler et al. 2008, Vanderbilt et al. 2002). An example of the latter is the occurrence of a mid-summer snowfall (day 213 in Figs. 2.6b and 2.6c) documented in this study. At this time, snow accumulated in the

drained and control treatment areas but not in the flooded treatment area (Fig. 2.6a). The response of NDSWI to this event demonstrated a strong sensitivity to snow, which appears as an anomalously high NDSWI value (Figs. 2.6 and 2.8).

The capacity of NDSWI to characterize the surface hydrology of the study area enabled us to evaluate the performance of the experimental flooding and draining experiment. Like many other large-scale experimental manipulations in the ecological sciences, our flooding and draining experiment was unreplicated, was a logistic and operational challenge, and displayed a high degree of 'natural' variability in land cover and surface hydrology within and between treatment areas (Figs. 2.9 & 2.10). The integration of various sub-project or discipline-based sampling results from this long-term ecosystem experiment is just beginning to be determined and this study has facilitated this process by providing a tool for evaluating the surface hydrological properties of different treatment regions and periods. This study suggests that prior to experimental manipulation (i.e. in 2002), the basin of each experimental treatment had significantly different surface hydrology properties (Figs. 2.9, 2.10), as did the flux tower and tramline sampling regions (Fig. 2.10). There were significant differences between years, indicated by a difference in NDSWI for the control treatment (Figs. 2.9 & 2.10) and elsewhere throughout the study area outside of the experimental thaw lake basin (Fig.2.9). In 2008, flooding appeared to be more effective than draining throughout each treatment basin, and for the flux tower and tramline sampling footprints within these (Fig. 2.10). During the experimental manipulation, further draining of the "drained" basin by pumping water lower than the soil surface (WTD = 0) proved difficult, and this may help account for the lack of a clear result in the "drained" treatment. Additionally, we caution that our NDSWI-based model cannot

readily distinguish between WTD values of zero and negative values (below ground water), because optical remote sensing method cannot penetrate far below the soil surface, so a successful drainage treatment may not have been clearly detectable with this method.

A distinct advantage of NDSWI over the other spectral indices tested in this study is that it can be readily adapted to a range of available satellite remote sensing platforms. Considering the importance of surface hydrology on ecosystem processes and properties such as carbon dioxide and methane flux (Merbold et al. 2009, Wolf et al. 2008), surface energy balance (Euskircken et al. 2007, Chapin et al. 2005), plant phenology and response to warming (Walker et al. 2006, Arft et al. 1999), and geomorphic processes (McNamara and Kane 2009, Lawrence and Slater 2005), the potential for NDSWI to facilitate the advancement of modeling and spatial extrapolation of these processes seems promising. Similar to how satellite-derived NDVI is increasingly being used to model land atmosphere carbon flux, leaf area index, or plant biomass (Running et al 2004), we believe that, pending further testing and refinement, NDSWI could be applied in a similar manner to improve models of carbon dioxide or methane fluxes, which are highly dependent on surface hydrology (Merbold et al. 2009). If possible, this could facilitate the development of spatially explicit models that estimate net greenhouse warming potential through the combination of land-atmosphere carbon dioxide and methane flux models. Such development, including ground, air and satellite-based estimates of NDSWI, could be integrated within regional studies or observatories focused on carbon dynamics recommended recently called for by McGuire et al (2009).

2.5 Conclusions

This study has addressed a critical need in the Arctic terrestrial sciences – an improved capacity to detect and monitor surface hydrological properties that are associated with or regulate important ecological processes and phenomena. Our goal was to develop a spectral index from optical remote sensing tools that could be used to estimate SWD, and characterize changes in surface hydrology at multiple spatial and temporal scales. The Normalized Difference Surface Water Index (NDSWI) out-performed other spectral indices that have been used to estimate similar properties. This index appears to accurately estimate SWD and SWC for this landscape, and detected experimental treatment effects at multiple spatial and temporal scales in an experimental flooding and draining experiment. We caution that while our results describe a vegetated thaw lake basin on the Arctic Coastal Plain of northern Alaska, further work would be needed to extend this approach beyond the context of this particular experiment. We recommend further testing and refinement of NDSWI, and there may be substantial merit in evaluating its potential in the development of models that estimate ecological processes and phenomenon that are sensitive to surface hydrology such as land-atmosphere carbon dioxide, methane and water vapor exchange.

Chapter 3: Five years of land surface phenology in a large-scale flooding and draining manipulation

3.1 Introduction

Detecting the biotic responses of arctic terrestrial ecosystems to environmental change is essential for understanding the consequences of global change and the future state of the Arctic and Earth Systems (McGuire et al. 2009, Sitch et al. 2007, IPCC 2007, ACIA 2005). Many observed and modeled change climate change responses of arctic terrestrial ecosystems such as surface energy budgets (Chapin et al. 2005, Euskircken et al. 2007), land-atmosphere carbon exchange (Merbold et al. 2009, Wolf et al. 2008), geomorphic processes (Lawrence and Slater 2005, McNamara and Kane 2009), provision of ecosystem goods and services (Milennium Ecosystem Assessment, 2005), plant and landscape phenology (Bhatt et al. 2011, Jia et al. 2009, Walker et al. 2006), and response to warming (Arft et al. 1999, Walker et al. 2006) are related to surface hydrology. Of particular concern, is how the combined alteration of air and soil temperature, and altered surface hydrology will affect the structure and function of arctic terrestrial ecosystems, particularly ecosystem carbon balance (Post et al. 2009, Schuur et al. 2009). If the biomass increases forecast for most arctic terrestrial ecosystems (Euskirchen et al. 2010, Euskirchen et al. 2007) do not offset predicted losses of greenhouse gases to the atmosphere due to permafrost thaw and microbial decomposition of the substantial arctic soil carbon store (Tarnocai et al. 2009), greenhouse warming will be enhanced (Kimball et al. 2006).

Several key studies have shown that plants can serve as effective indicators of environmental change (Walker et al. 2006, Arft et al. 1999). At the leaf and plant level, plants can respond to change with an increase or decrease in green-leaf biomass (Riedel et al. 2005), pigments, and leaf water content (Hudson et al. 2010). At the plant community and ecosystem

level, plant responses to change include shifts in species composition and abundance and ecosystem processes such as nutrient cycling (Johnson et al. 2002) and surface energy balance (Euskirchen et al. 2007, Chapin et al. 2005). All of these multi-level plant responses to change can be observed and quantified using optical remote sensing techniques (Olthof et al. 2010, Puma et al. 2007). In the Arctic however, there has been a general paucity of ground based studies examining plant responses to change using remote sensing approaches (Boelman et al. 2003). As such, the transferability of algorithms developed for detecting these phenomenon in other ecosystems remain poorly tested and few studies have documented seasonal and interannual dynamics of land surface properties using these ground based methods. These methods have, however provided cost effective ground to satellite scaling (Ueyama et al. 2010) of leaf to landscape ecosystem properties and processes in other ecosystems (Hilker et al. 2008) and could help to overcome many of the deficiencies associated with satellite remote sensing in the Arctic (Stow et al. 2004).

Land surface phenology (LSP) is a measure of the seasonal variation in vegetated land surfaces that occurs in response to climate and can be observed using ground to satellite remote sensing approaches (Friedl et al. 2006). Using suitable vegetation spectral indices such as the NDVI (Normalized Difference Vegetation Index), which has been shown to be useful to estimate above ground green biomass and plant cover (Epstein et al. 2008, Boelman et al. 2003, Gamon et al. 1995), changes in the timing and extent of peak greenness (de Beurs et al. 2010), rates of green-up and senescence (Stow et al. 1993), differences between different landscape units, and change over time (Bhatt et al. 2010) can be quantified. NDVI is affected by various environmental factors (Nagol et al. 2009, Matsushita et al. 2007, Galvao et al. 2004).

Nonetheless, if executed correctly, landscape phenology can serve as an indicator of ecosystem state and change over time.

This study aims to improve our understanding of the spatial and temporal dynamics and variability in tundra land-surface phenology in a hydrological manipulation experiment. The study further aims to understand how land-surface phenology is affected by altered surface hydrology, and if such alterations can be documented with optical remote sensing at both the ground and satellite scales. Specifically, we examine interannual variability in landscape phenology and how changes in surface hydrology conducted in association with a large scale flooding and draining experiment affected seasonal dynamics of land-surface phenology. Building on a previous study that showed that Normalized Difference Surface Water Index (NDSWI) could be used to characterize surface water in the study area (Goswami et al. 2010), we also explore how NDVI dynamics relate to those of NDSWI and if these dynamics scale to the satellite scale using MODIS time series surface reflectance data obtained for the study site over the snow free growing period between 2000 and 2010.

3.2 Methods

3.2.1. Study Site and Experimental Design

This study was conducted within the Biocomplexity flooding and draining experiment located on Barrow Environmental Observatory (BEO) near Barrow, Alaska, 71°17'01" N, 156°35'48" W. This large-scale experimental infrastructure was designed to examine the role of altered water table on land - atmosphere carbon, water and energy balance. After three years of baseline data collection from 2005 – 2007 (2007 included a failed 2-week long experimental

manipulation at the beginning of the snowfree period), three experimental treatments were initiated and sustained through the 2008 and 2009 snow free periods. Treatments consisted of a control section that was unmanipulated and held relative to water tables outside the experimental area, and flooded and drained sections where the water table was raised and lowered by 10 cm relative to the control treatment respectively (Fig. 1.2b). This experimental design explicitly allowed for interannual variability to be incorporated, which in this unreplicated experiment was essential for assessing the integrity of the experiment by testing the hypothesis that during a wet year, ecosystem properties and processes in the control treatment would be similar to those of the wet treatment area in a dry year.

Vegetation within the Biocomplexity experimental area is predominantly moist and wet graminoid tundra (Teh et al. 2009). The study site is underlain by continuous ice and organic carbon-rich permafrost and the general landscape has characteristic thermokarst features common on the Arctic Coastal Plain including shallow ponds, high and low-centered polygons, polygon rims and troughs, and meadows (Brown et al. 1980). Active layer depth is typically less than 50 centimeters in the experimental area (Shiklomanov et al. 2010). Soils are generally moisture rich due to shallow drainage gradients and impermeable continuous permafrost, and are predominantly comprised of cryoturbated gelisols (Bockheim et al. 1999, Miller et al. 1998). Rates of evapotranspiration are relatively low (Liljedahl et al. 2011).

The study area has characteristic long and cold winters with a mean winter air temperature of -26.6°C in February. Summers are relatively cool and wet and mean maximum temperatures in July typically reach 4.7°C (Bockheim et al. 1999). During summer, 24 hour daylight prevails for 85 days between May 10 and August 2. The mean annual temperature for

Barrow is approximately -12.0°C (Oberbauer et al. 2007). Snowmelt occurs in early June when average daily air temperatures rise above 0°C, and snow typically begins to accumulate in mid to late September (Hobbie 1975).

3.2.2 Reflectance Measurements

A robotic tram system (Gamon et al. 2006a) was used to collect the field reflectance data used for this study. The tram system consisted of three 300 m long transects ("tramlines") with one tramline located in each of the three treatment areas and oriented in an east-west direction spanning the entire width of the lakebed. Each of the tramlines was 200 meters in length in 2005 and was extended by 100 meters in early spring of 2006. This required snow removal for the length of the extension (meter 201 – meter 300) for each of the tramlines. This infrastructure provided an ideal research platform for repeat measurement of surface spectral properties of the same study area affected by contrasting surface hydrology regimes throughout the snow-free period. A detailed description of the experimental infrastructure used for this study is given in (Goswami et al. 2011).

Reflectance data were collected at every meter along each tramline using a dual detector Unispec DC field spectrometer (PP Systems, Amesburry, MA, USA) housed within a robotic cart that was operated semi-autonomously (Gamon et al. 2006a). The cart travelled along the tramline at an average speed of 20cm/s, taking approximately 25 minutes to travel the full length of the 300m long tramline. The spectrometer was activated when a mechanical switch mounted on the base of the robotic cart was triggered as the cart passed over crossbars positioned every meter along each tramline. One run along the length of one tramline produced three hundred

spectral measurements every time the robotic cart was operated. A footprint area of approximately $1m^2$ was achieved by positioning the downward looking foreoptic (with a 20 degrees field of view) on a south-facing boom mounted to the cart approximately 3 m above ground level. The upward and downward looking detectors of the field spectrometer were cross-calibrated in the field using a white reflectance panel with 99% reflectance (Spectralon, labsphere, North Sutton, NH, USA) at the beginning and at the end of each run as described in Gamon et al (2006a). The Unispec DC had a nominal range of operation between 303 and 1148 nm in 256 contiguous bands with a spectral resolution of approximately 3 nm and a full width at half maximum of approximately 10 nm. Tram measurements were made three times every week during the field season if weather permitted (no extreme winds, fog, rain, or falling snow). Data used for the study documented in this paper was extracted from datasets that spanned the majority of the snow free growing period between mid June and mid August in all years between 2005 and 2009.

This study utilizes the Normalized difference vegetation index (NDVI) to document seasonal and interannual landscape phenological dynamics. NDVI values were calculated for each sampled meter of each tramline for every day measurements were made (n=300 measurements/tram/day) using the following equation (Gamon et al. 2006a):

$$NDVI = \frac{R(NIR) - R}{R(NIR) + R} \qquad \text{---------- Equation (3.1)}$$

Where R(Red) = 680nm and R(NIR) = 800nm

To visualize seasonal trends in NDVI, mean NDVI for each tramline and sample time was calculated for each of the five years of measurement (2005 – 2009).

Additionally, Normalized Difference Surface Water Index (NDSWI) (Goswami et al. 2011) was calculated to investigate the affect of surface water on reflectance spectra as follows:

$$NDSWI = \frac{Ln\ R\ (NIR) - Ln}{Ln\ R(NIR) + Ln\ R(Blue)} \quad \text{---------- Equation (3.2)}$$

Where R (Blue) = 460nm and R(NIR) = 100nm

3.2.3 Ancillary Measurements:

A range of ancillary measurements were made in addition to the reflectance measurements described above. Water table depth data were collected manually every 10 meters along each tramline within a day of the spectral measurements being acquired. Water table depth measurements were made relative to the ground surface using perforated PVC tubes inserted in holes drilled to below the active layer. Negative numbers indicate water levels below the ground surface whereas positive numbers indicate pooling of water above the ground surface.

Digital photos of each of the tramline footprints were taken several times during the 2006-2009 field seasons using a Nikon Coolpix 5400 camera mounted on the boom of the robotic tram looking downward. The camera was triggered manually every meter of the tramline using a remote trigger so that the footprint of the spectral measurements was captured. Oblique landscape photographs of each tramline area were also taken from the west end of each tramline once every week from early June to the end of August in 2009.

A HOBO automated weather station (AWS) was used to measure air temperature, relative humidity, precipitation and photosynthetic active radiation (PAR) between early June and late August at one minute intervals. The AWS was installed at the west end of the central tramline. Surface elevations at every meter of each tramline were measured using a survey grade Trimble differential GPS unit to document microtopographic variability along each of the tramlines.

3.2.4 Statistical Analysis

To determine the effect of experimental flooding and draining on seasonal LSP, a series of regression analyses were used. For pre-treatment years, regression models were built to predict mean NDVI values of the north and central tramlines from the measured NDVI at the southern tramline. During experimental years (2008-2009), to quantify treatment effects, measured NDVI from the north and central tramlines was subtracted from NDVI predicted with the use of the regression equations that modeled pre-treatment conditions The extent to which treatment effects could be determined for 2009 is limited by an interruption of water levels in the control treatment late in the growing season, which were experimentally altered by other investigators as part of a short-term experiment flooding experiment during the middle two weeks of August.

A gamut of interacting factors is known to affect both the vegetation signal and spectral measurement of NDVI in tundra landscapes (Stow et al. 2004, Jia et al. 2002, Hope and Stow 1995, Walker et al. 1995). To quantitatively explore the environmental controls of seasonal NDVI at the study site, regression tree analysis was performed using JPM 7.0 (SAS Institute,

Inc. Cary NC) statistical software where NDVI data for 2005 – 2009 averaged for each tramline was included as the y-response (dependent variable). X-response variables (independent variables) included day since snow melt (DSSM), mean daily air temperature, water table depth, and total daily PAR. Daily average temperature, water table depth and daily total PAR were calculated from AWS measurements. Regression tree analysis is a practical and informative (Khier et al. 2008) procedure useful for data exploration and several studies have used this approach to explore the presence of ecological thresholds (Khier et al. 2008, Michaelson et al. 2004, Franklin 1998, and Kandrika 2008).

NDSWI was developed to characterize the cover and depth of surface water from spectral bands common to a range of ground, aerial, and satellite optical remote sensing instruments, and increases with increasing water cover and depth (Goswami et al. 2011). For this study, NDWSI was calculated following Equation (3.2) for each year/tramline/measurement combination. Time series of mean NDSWI and NDVI values were plotted over the snow free period of the growing season for all five years of study (2005 – 2009) to explore how a change in NDVI correlated with a change in NDSWI (i.e. surface water) (Fig. 3.9). Differences in NDVI and NDSWI values between sampling times within a season were first calculated for a given measurement day by subtracting the NDVI and NDSWI value from the previous sampling day (e.g. “day 175” – “day 173”, “day 177” – “day 175”, “day 179” – “day 177” etc.) for all three treatment areas and treatment years (i.e. 2008 and 2009). Following this, linear regression models were developed between “the change in NDVI within a given sampling period” and “change in NDSWI within a given sampling period” for both the flooded (north), drained (central), and control (south) treatment areas. The drained and control sections of the study area had very little surface water

present compared to the flooded section during treatment years so regression models were developed separately for the flooded section.

To study how the relationships of NDSWI and NDVI held at the landscape level, 250m pixel size MODIS 8-day composite data were extracted from the Oak Ridge National Laboratory as a 2km by 2km study area using the study site as the center of the subset using data. NDVI values were created using Equation (3.1) and Band 1 (620-670nm ~ Red) and Band 2 (841-876nm ~ NIR). NDSWI values were calculated using Equation (3.2) and Band 3 (459-479nm ~ BLUE) and Band 5 (1230-1250nm ~ NIR). NDVI and NDSWI values were calculated for the average value of the entire subset swath at a given time period and also for individual pixels within the subset (n = 64 pixels). Regression models were developed between NDSWI and NDVI for the average values of the entire subset and for the individual pixels for the subset to investigate the effect of surface water on NDVI.

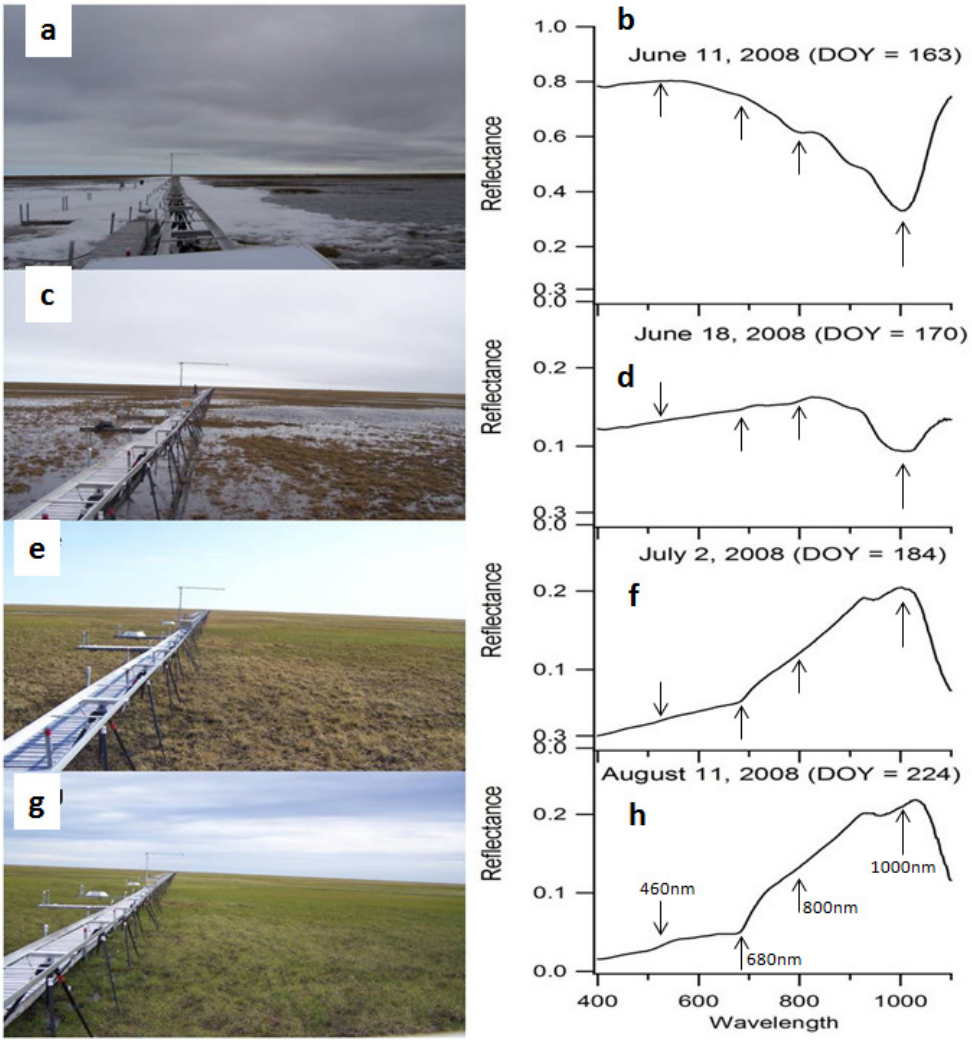

Figure 3.2. Seasonal changes in land-surface phenology visualized on the left with photographs and on the right with reflectance collected on the same day as the photographs and averaged over the 300m length of the south tramline. Surface spectral reflectance was able to capture the transition from snow melt to maximum greenness in the study area as shown above. The first photograph/plot pair shows the spectral characteristics of melting snow (1a,b), followed by the spectral characteristics of the experimental area immediately after snowmelt (1c,d), in the initial growth period (1e,f), and during the peak growing period (1g,h). The arrows pointing at 680nm and 800nm show the wavelengths used for calculating NDVI and the at 460nm and 100nm show the wavelengths used for calculating NDSWI.

3.3. Results

3.3.1 Seasonal and interannual variability in land-surface phenology

The transition of the tundra landscape near Barrow as it transitioned from snow-melt in late spring to peak greenness in late July to early August was effectively captured with photographs of site conditions acquired each time the tramlines were sampled. Surface reflectance spectra were also able to capture these transitional states of the landscape throughout the growing season (Fig. 3.1). The snow-melt state of the landscape (Fig. 3.1a), which typically occurs in early June, is represented by the spectrum given in figure 3.1b where the water absorption feature at approximately 970nm is clearly visible. Within the study area and following snow-melt, the landscape is generally flooded (Fig. 3.1c), which is represented by the rather flat reflectance spectra (Fig. 3.1d) and prominent water absorption feature. Following draining, infiltration, evapotranspiration and plant growth (Figs. 3.1e and 3.1g), the spectral signature of vegetation becomes more dominant and no longer includes a strong water absorption feature (Fig. 3.1f). This includes the development of the red edge, which is the rapid change in reflectance in the near infrared range (around 700nm) due to absorption by chlorophyll and a subtle water absorption feature in the 900 nm band through July. Peak growing season typically occurs in early to mid August (Fig. 3.1g) (Puma et al. 2007). NDVI derived from reflectance spectra given in figure 3.1 (Fig. 3.2), show strong seasonality associated with snow melt and greenup during the typical snow free period in the study area.

Seasonal plots of mean NDVI values for each tramline and year of study showed subtle seasonal differences but no striking differences interannually (Figs. 3.3a, 3.3b, and 3.3c). 2006 showed an early snowmelt compared to other years and may in part be related to snow removal

associated with the extension of each of the tramlines. The south tramline area had an early snowmelt in 2007. North tramline NDVI values for the 2008 season showed a sudden drop around day 200 that was followed by an increase in NDVI at the next measurement day, after which NDVI decreased again around day 210 and remained steady at a low value for the rest of the measurements made during that snow free period. Similar sudden drops in NDVI values were observed for the central and south tramlines, around day 210 for 2008. This sudden drop in NDVI values for the central and the south tramlines did not follow the patterns observed at the north tramline. NDVI values at the south and central tramlines increased after the sudden drop and followed the same seasonal pattern as described for the north tramline. The short-term variability in NDVI values are investigated in greater detail in figures 3.6 and 3.7 below. Between 2005 – 2009, seasonal peak values of NDVI always occurred earlier for the north tramlines compared to the south and central tramlines. Seasonal peak greening at the North tramline was five days earlier than the central and south tramlines in 2005, ten days earlier in 2006, two days earlier in 2007, and twelve days earlier in 2008, and ten to twelve days earlier in 2009 (Fig. 3.3d).

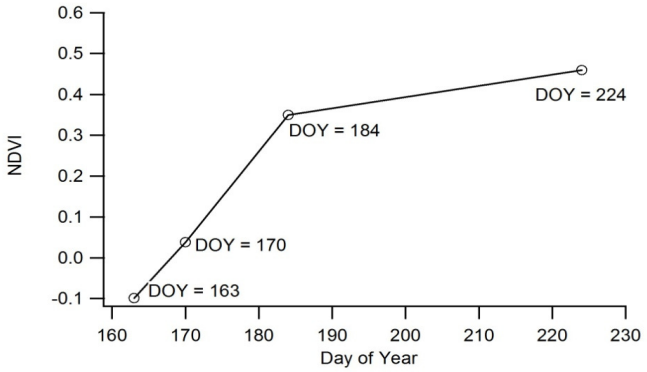

Figure 3.3. Change in land-surface phenology (NDVI) at different days of the year (DOY) over the course of the 2008 snow free period for the same dates shown in figure 3.1.

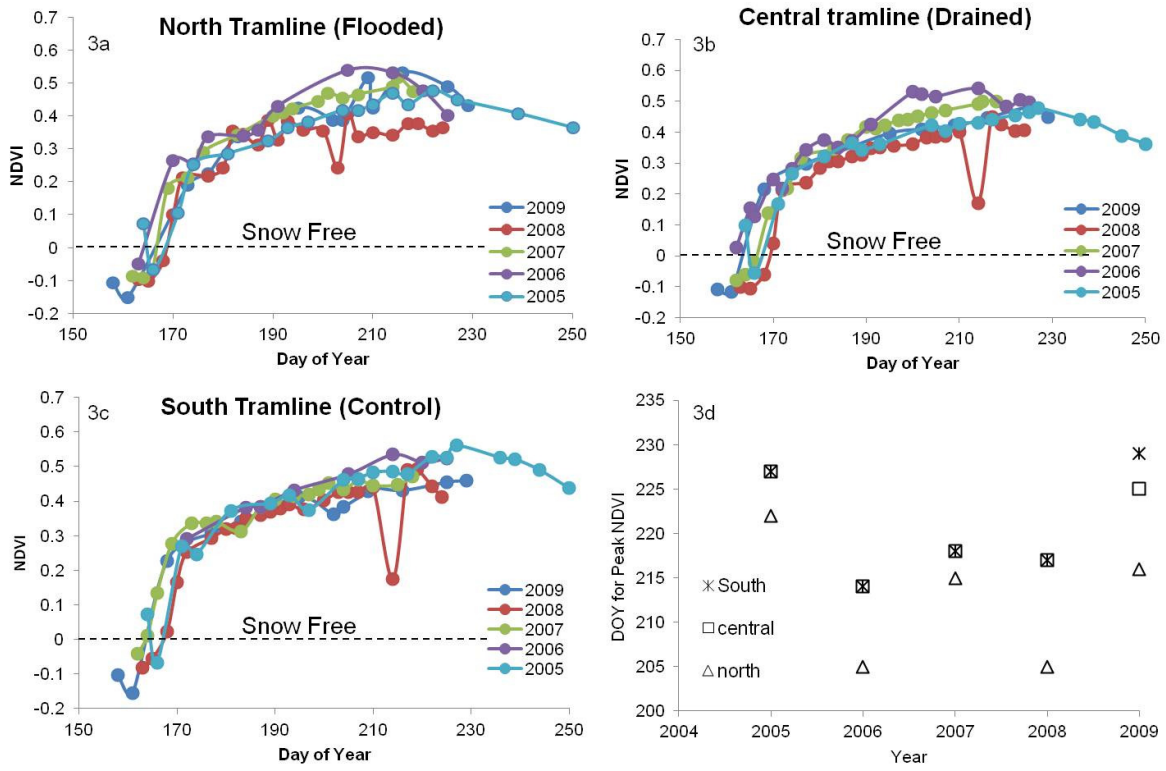

Figure 3.3. Seasonal and inter-annual patterns of land-surface phenology (mean NDVI for all measurements along each tramline) for each of the treatment areas for pre-treatment (2005, 2006, 2007) and treatment (2008, 2009) years. Initiation of greening was dependent on snow melt and a moderate level of variability in NDVI was noted for most treatments and years. The DOY corresponding to peak season NDVI is shown in 3d. The standard deviations for snow-free periods for all the tramlines for all the years were ≤ 0.1.

3.3.3 Treatment effects on interannual land-surface phenology

Correlations between south tramline NDVI values for 2005 – 2007 and NDVI values for this same period at the central and north tramlines showed strong relationships ($R^2 = 0.89$, $P < 0.001$ for south vs. central tramlines figure 3.4a; and $R^2 = 0.88$ $P < 0.001$ for south vs. north tramlines Fig. 3.4b). Similarly, regressions between WTD values for 2007 for south vs. central

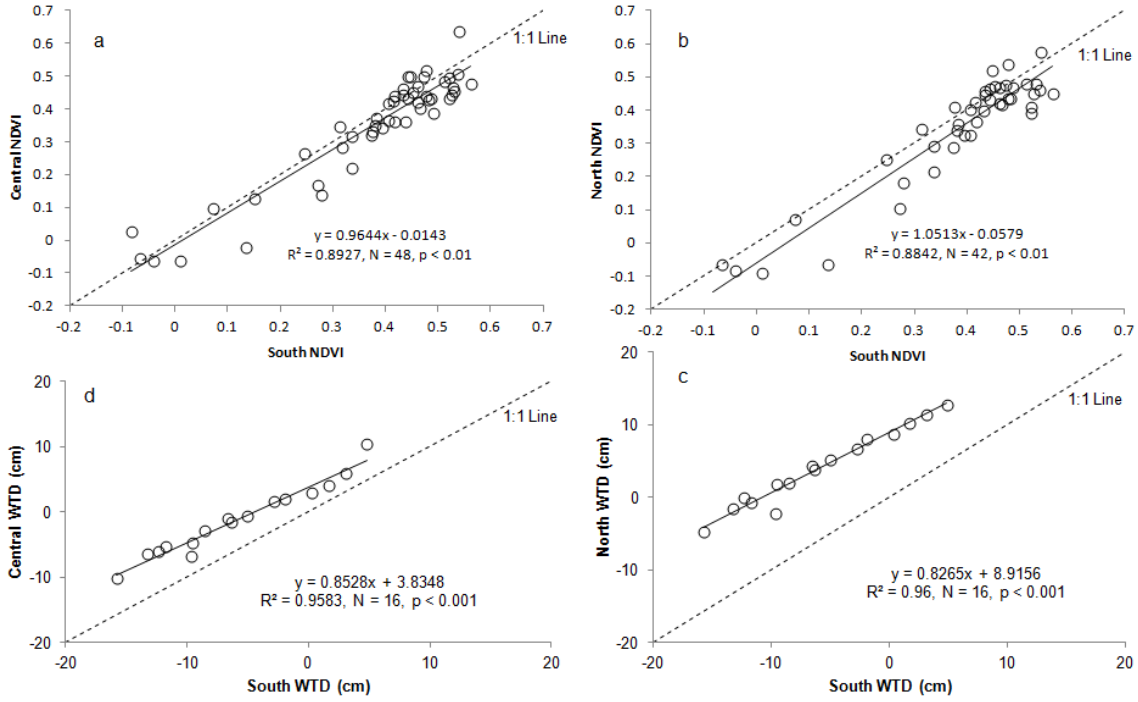

Figure 3.4. Figures 4a and 4b show the linear regression models developed from data in pre-treatment years to predict NDVI at the northern and central tramlines using measured NDVI in the southern control treatment area. Figures 4c and 4d show similar models developed for WTD using data from 2007 (pre-treatment year).

and south vs. north tramlines showed strong linear relationships ($R^2 = 0.96$, $P < 0.001$ for south vs. central, Fig. 3.4c; and $R^2 = 0.96$, $P< 0.001$ for south vs. north Fig. 3.4d). These strong relationships allowed for the experimental effects on WTD and NDVI to be quantified by calculating the difference between modeled values and measured values for WTD and NDVI during 2008 and 2009.

At the north tramline, measured vs. modeled WTD showed that measured WTD was consistently higher than modeled WTD for the majority of the 2009 growing season (Fig. 3.5a), while the measured WTD was only consistently higher than the modeled values towards the later part of the season starting around day 205 in 2008 (Fig. 3.5c). For both 2008 and 2009, measured

WTD was consistently lower than the modeled values for the central tramline (Fig. 3.5b, 3.5d). These suggest that the flooding treatment was most successful during 2009 and that a successful draining treatment was established in both 2008 and 2009.

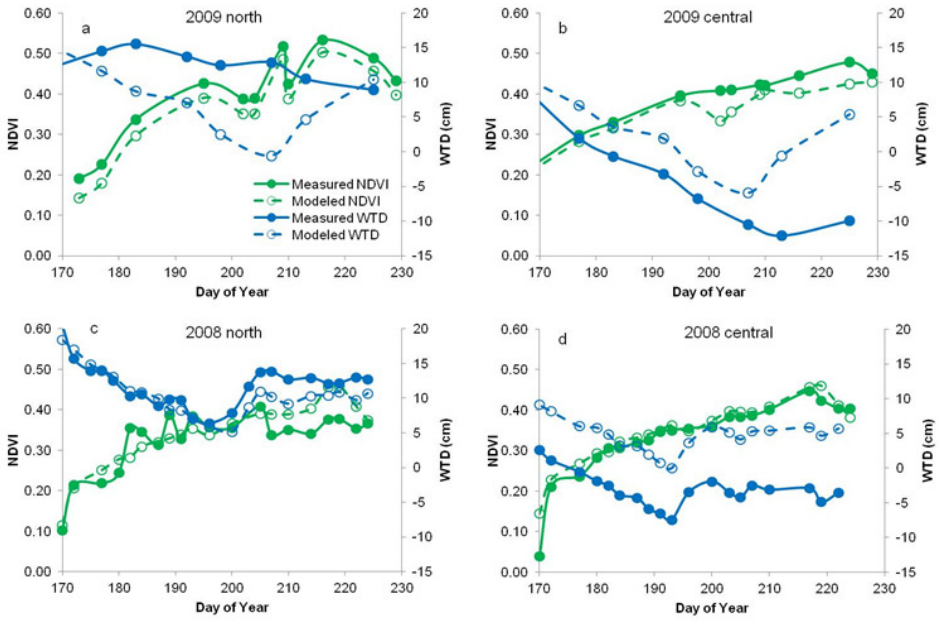

Figure 3.5. Comparison of modeled (no treatment) vs. measured NDVI and WTD (treatment) time series for the north and control treatments in 2008 and 2009. NDVI and WTD were calculated using the models developed given in figure 4 above for the snow free growing seasons of 2008 and 2009.

At the north tramline, measured vs. modeled NDVI showed that measured NDVI was consistently but only slightly higher than modeled NDVI throughout the growing season in 2009 (Fig. 3.5a) while the measured NDVI was slightly lower than the modeled values towards the later part of the season starting around day 205 for 2008 (Fig. 3.5c). For the central tramline, measured NDVI values varied considerably throughout the growing season in both 2008 and

2009 (Fig. 3.5c). Little difference between modeled and measured NDVI was observed in 2008 (Fig. 3.5d) but NDVI was higher than modeled values in 2009 after DOY 195 (Fig. 3.5b).

3.3.4 Relationship between land-surface phenology, microtopography and water table depth

To investigate phenomenon associated with the sudden drop in NDVI values observed in 2008, spatially detailed plots of NDVI, microtopography, and WTD were constructed for the north and south tramlines for measurements made on July 21 and August 6 in both 2007 and 2008. These periods varied considerably in WTD and the response of NDVI between experimental treatments, and thus were used to further investigate the relationship between NDVI and surface hydrology. Intercomparison of these plots (Fig. 3.6) showed that average WTD for the north tramline was approximately 15 cm higher in 2008 than in 2007 and approximately 12 cm above ground level. This meant that areas of lower topography along the north tramline were flooded in 2008 whereas the water table was below ground level on the same day in 2007. Corresponding with this, NDVI values for areas of lower elevation along the north tramline were lower in 2008 than in 2007. The same intercomparison for the south tramline (control) showed that NDVI values were not substantially different between the two years, despite similar absolute differences in mean WTD, which remained below ground level. Mean WTD increased by approximately 5 cm between July 18th and July 21st in 2008 at the north tramline due to flooding treatment. This resulted in a similar response in NDVI to the interannual differences described above between 2007 and 2008 and NDVI decreased markedly in the low lying areas (Fig. 3.7). Mean WTD for the south tramline also increased by approximately 5 cm (from -5cm to 0cm, i.e. below ground level) over this same time period but this did not result in a

change in NDVI. These investigations suggest that the presence of water above ground level interferes with NDVI signatures over short to long term periods, which is investigated in greater detail in Section 3.6 below.

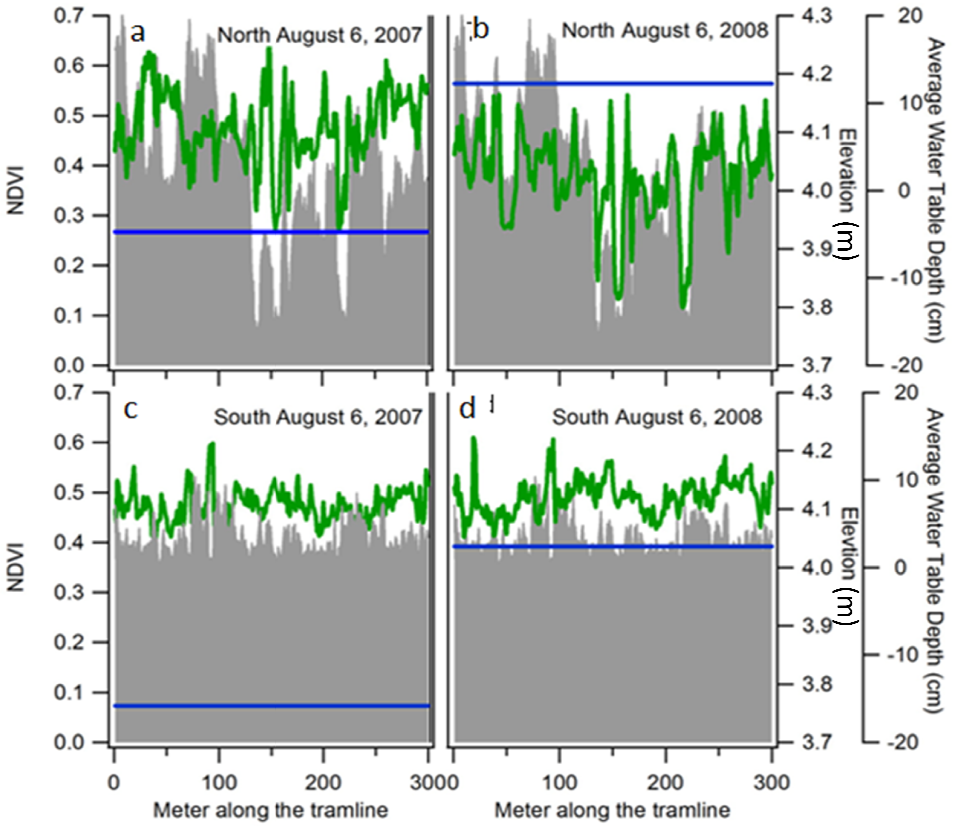

Figure 3.6. Plots of NDVI (green), microtopographic variation (gray) and mean WTD (blue) for the north and south tramlines on August 6th 2007 and 2008.

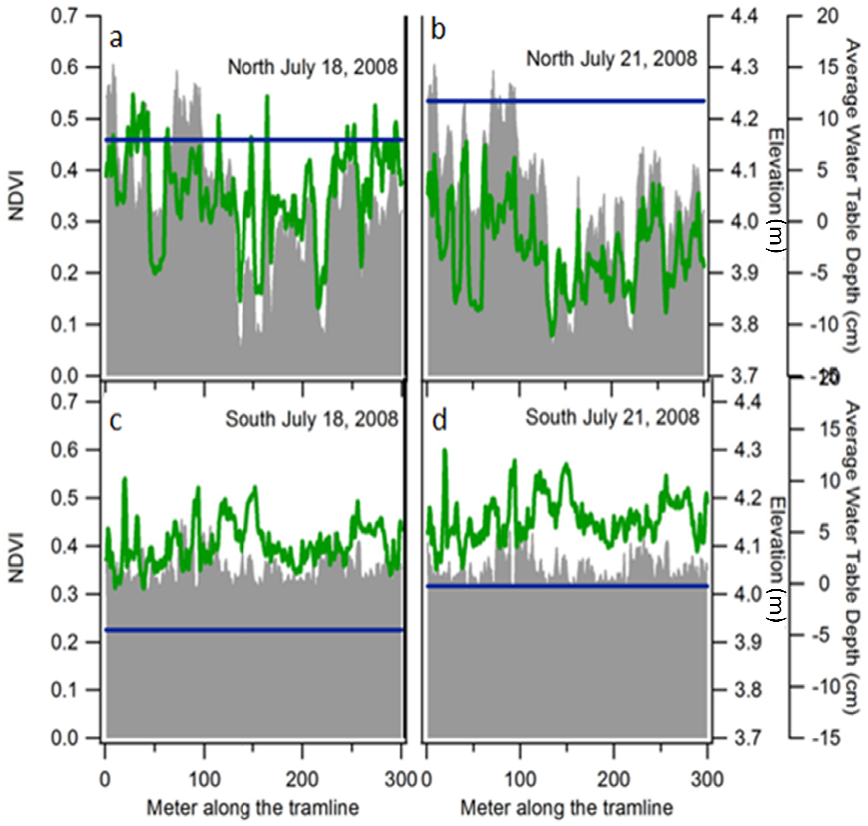

Figure 3.7. Here the green line indicates NDVI, the blue line indicates average water table depth and the grey line indicates elevation of the tramline area. The above figure shows how a rise in above ground water table depth on the north tramline area lowers the NDVI values on July 21, 2008 shown in 8b compared to the NDVI values for July 18, 2008 shown in 8a. This effect is similar to the effect observed in seasonal patterns of NDVI for north tramline on DOY 210 in figure 5c. Even though below ground water table depth was raised on the south tramline on July 21, 2008 shown in 8d compared to July 18, 2008 shown in 8c, the NDVI values did not decrease.

3.3.5 Environmental controls of land-surface phenology

The regression tree analysis performed on data from all years (2005-2009) was able to account for approximately 74% of the variability in the dataset (Fig. 3.8). The primary control of NDVI for DSSM ≥ 28 was WTD < 6.39cm. Between DSSM of 18 and 28, WTD ≥ 6.39cm was the primary control of NDVI.

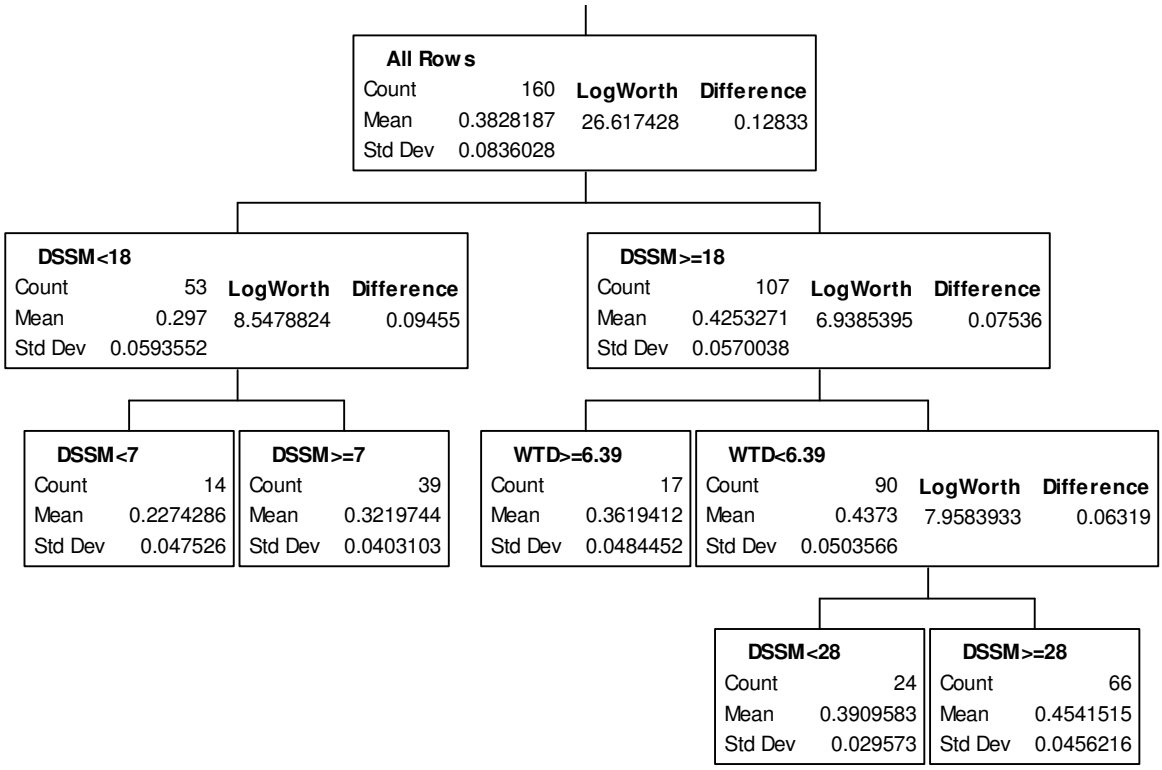

Figure 3.8. Regression tree analysis conducted on NDVI for all data collected between 2005-2009 (n = 160, R^2 = 0.74, No. of splits = 4).

3.3.6 Relationship between NDSWI-NDVI (surface hydrology and greenness)

Simultaneously plotting NDSWI and NDVI over the course of the snow free growing season showed a strong negative relationship (Fig. 3.9). Low values of NDVI were recorded when high values of NDSWI were also recorded and vice-versa (Fig. 3.9). This effect was particularly prominent at the north tramline during treatment years (2008 and 2009). Linear regression analysis between change in NDSWI and change in NDVI within a sampling period in 2008 and 2009 showed a strong correlation (R^2=0.69) for the flooded section while this relationship was not so strong for the control and the drained sections (R^2=0.29) (Fig. 3.10). At this time, WTD was largely below ground in the central and south treatment areas, further

suggesting that the measurement NDVI is only affected by dynamic fluctuations in WTD when WTD is below ground level. Linear regression analysis between NDSWI and NDVI calculated from the MODIS 16 day composite time series data for 2000 – 2010 between DOY 185 – 297 showed a R^2 value of 0.61 indicating that in the relationship between NDSWI and NDVI scales to the satellite scale (Fig. 3.11).

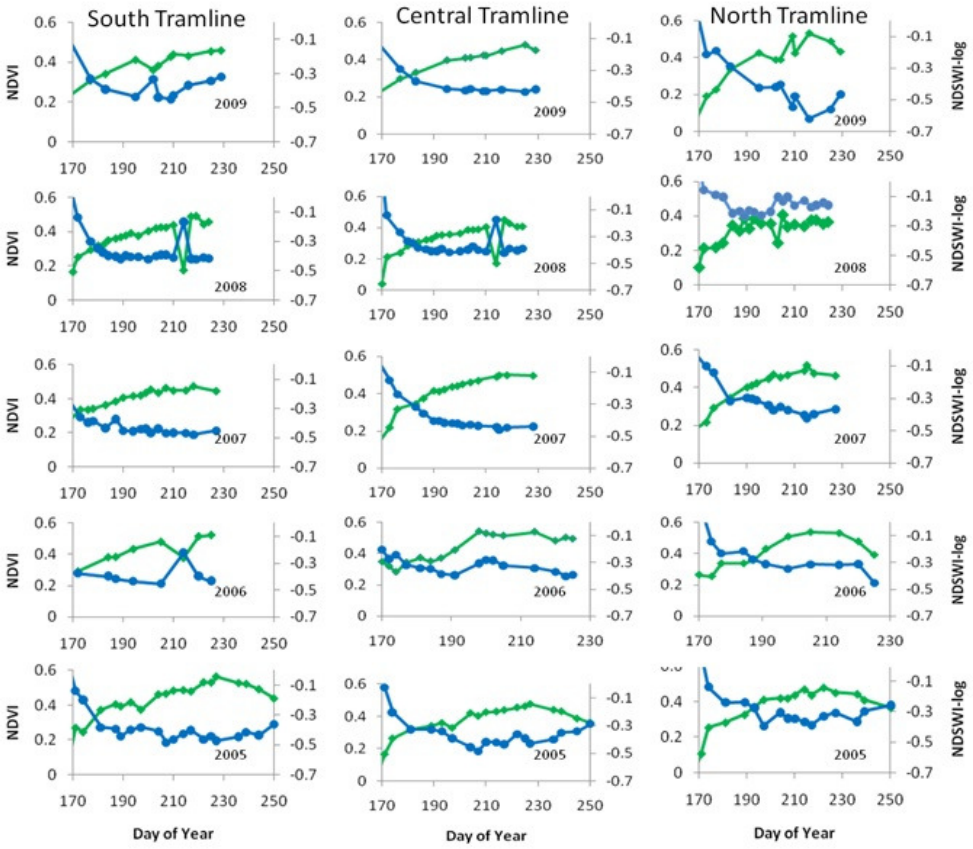

Figure 3.9. Seasonal dynamics of mean NDVI (green) and NDSWI-log (blue) for all three tramlines 2005 – 2009. 2005 – 2007 were pre-treatment years and 2008 – 2009 were treatment years. .

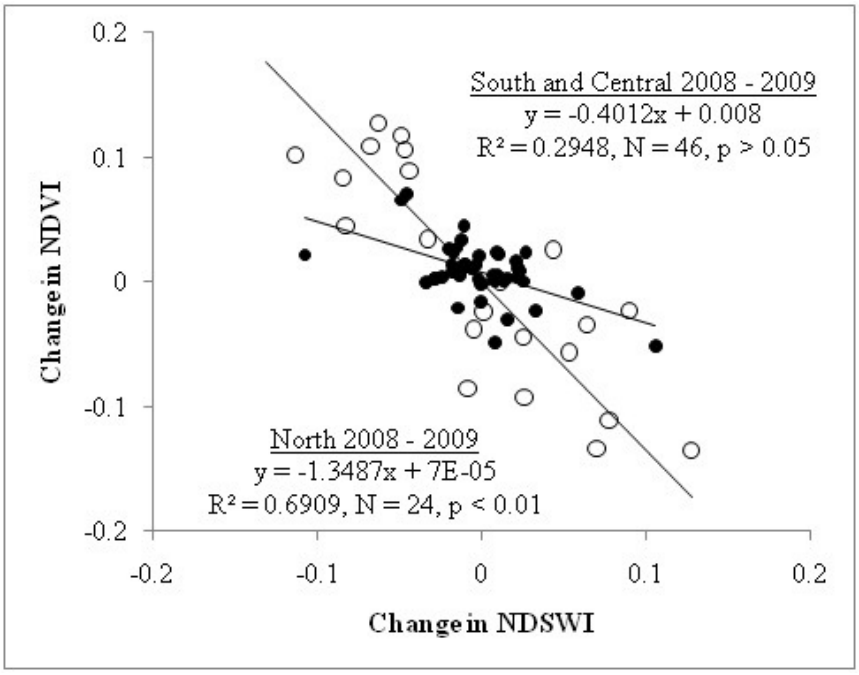

Figure 3.10. Relationship between the change in NDSWI and NDVI in a measurement period for the north (open circle), and the South and Central tramlines (solid circles) in 2008 and 2009. The north tramline area (flooded) showed a strong correlation indicating that change in surface water affects NDVI values.

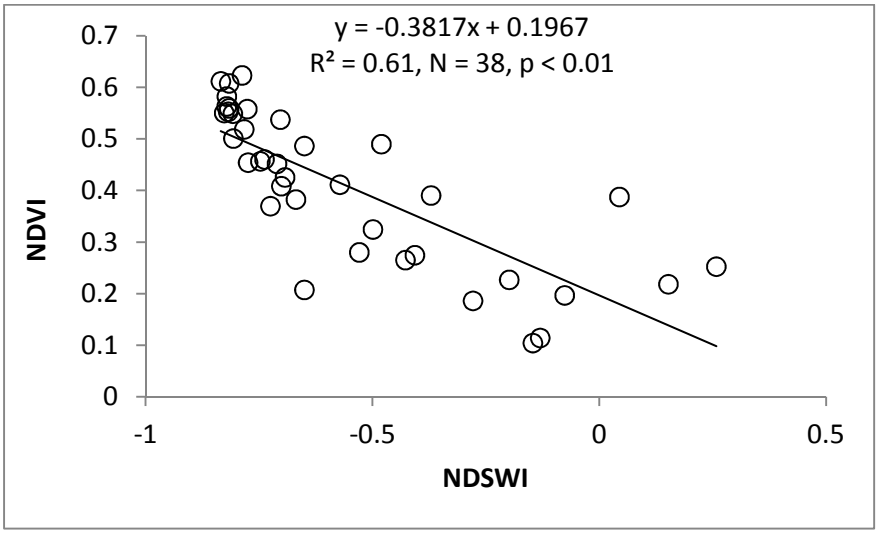

Figure 3.11. Relationship between NDSWI and NDVI using MODIS 8-day composite time series data for 2000 – 2010 between day 185 and day 297 for each year.

3.4 Discussion

The study of LSP using remote sensing (Friedl et al. 2006, Henebry et al. 2005), has seen significant progress over the past two decades (Zhang et al. 2006, White et al. 2005, Zhang et al. 2003, Myneni et al. 1997). Numerous studies have used time series vegetation indices derived from reflectance data acquired by satellite sensors to document and improve understanding of fundamental landscape to continental scale ecosystem properties (Bhatt et al. 2010, Jia et al. 2009, Running et al. 2008, Myneni et al. 1997). LSP is a key indicator of ecosystem dynamics that are susceptible to environmental change (Myneni et al. 1997). Detecting biotic responses such as phenology to a changing environment is essential for understanding the consequences of global change including impacts to ecosystem carbon balance (Merbold et al. 2009, Wolf et al. 2008) energy balance (Euskirchen et al. 2007, Chapin et al. 2005), and biodiversity (Foster et al. 2010). This study aimed to monitor seasonal and inter-annual trends in LSP and understand how LSP responds to altered surface hydrology and interannual climatic and other environmental variability using reflectance data from the robotic tram system. The robotic tram system used in the study provided an excellent platform to make continuous and repeatable ground-based measurement of LSP over the study period of 2005-2009 as part of the biocomplexity experiment.

We expected to observe substantial changes in LSP in response to the flooding and draining experiment. Instead, we observed a response to the experimental treatments that had a similar magnitude of variability to that associated with interannual variability. In retrospect, the LSP results are expected now that more detail on the interannual variability in WTD has been established. This study has shown that interannual variability in WTD is just as great as

experimental effects associated with the treatments, hence the treatments invoke realistic environmental states and serve to extend the opportunity to observe condition states that are plausible for the study site. Experimental flooding treatments in 2008 were not as consistent as those in 2009. The year 2008 was wetter and the capacity to flood was limited by the experimental infrastructure and natural topography which did not permit flooding beyond the level studied as water simply poured out over the top of the topographic margins intended to contain the treatment. Similar problems were minimal in 2009. These limitations in flooding treatments were visible in the LSP patterns for 2008 and 2009 as 2008 showed more fluctuations in the seasonal pattern of LSP than in 2009.

The 2006 seasonal pattern of NDVI showed the earliest snow-melt and highest peak season values for the control and the drying treatment areas. This was probably due to snow being removed in early spring for construction that extended the tramlines by 100m to the east of each of the tramlines for an extension of the tramlines. This finding supports previous finding that early snowmelt can result in higher peak season NDVI and productivity (Puma et al. 2007, Kimball et al. 2006).

The strong correlation between the south and central and north tramlines for NDVI and WTD indicated that values for the central and north tramlines can be modeled from the south tramline to assess the likely experimental impact of the draining and flooding experiments respectively. This was important for this experiment because it was unreplicated, and the treatments were held relative to interannual variability such that flooding during a dry year presents WTD's similar to what is experienced in the control treatment in a wet year. There was no marked difference in landscape phenology associated with the treatments. This finding is

similar to those reported by Olivas et al. (2011) and Zona et al. (2011) for CO2 flux. This is unlike findings reported for thaw depth where deeper thaw depths were reported for 2008 and 2009 for the flooding treatment area compared to 2006 and 2007 (Shiklomanov et al. 2010).

The effect of the treatment on LSP was more subtle than expected. To better understand factors controlling the spatiotemporal variability in the LSP patterns of the three treatment areas, regression tree analysis was used to analyze the interplay between NDVI and a range of factors shown by other studies to influence LSP and other ecosystem properties and processes. These included DSSM, daily average temperature, daily total PAR, and WTD for snow-free period of the growing season. Regression tree analyses do not allow for derivation of causation. Instead they are intended for the data mining and exploratory analyses that facilitate the discovery of tipping points and correlations with multiple and co-occurring environmental drivers. Here regression trees suggest that the spatiotemporal variability in NDVI was strongly controlled by DSSM and WTD thereby giving us new understanding of the environmental controls of NDVI spatiotemporal variability. We have known DSSM to be an important factor controlling seasonal NDVI but this appears to be the first ground based study in the arctic to show that variable surface hydrology can impact capacities to adequately determine NDVI.

More detailed analyses of LSP along tramlines on specific dates of measurement indicate both the challenge of acquiring NDVI in the presence of surface water strongly interferes with spectra used to derive NDVI. In this detailed study, the importance of micro-topography in influencing NDVI and surface water coverage was strongly apparent. Other studies have also shown how microtopographic variability can control ecosystem properties and processes such as species distribution (Henry 1998), soil moisture and WTD, surface energy budgets, trace gas flux

(Zona et al. 2011). Analysis for pre/post treatment variability and for short-term inter-annual variability showed that fluctuations in WTD and surface water cover had the greatest impact in low lying areas and NDVI decreased as WTD and surface water coverage increased. This phenomenon was observed between years, within a season and with environmental variability that was experienced over just a few days. Although there is likely to be some variability in the above ground green plant biomass that is measured as NDVI in such measurements, the majority of the variability experienced can be explained by surface water coverage, which appeared to be well described by NDSWI, a spectral index for estimating surface water cover and depth (Goswami et al. 2011).

The statistically strong relationship between NDSWI and NDVI in the MODIS 2km by 2km subset created for the study area also indicated that surface water could play an important role in controlling NDVI values at the satellite scales. The implications of this finding is important – especially for large scale studies in the Arctic that use satellite data where NDVI is used as an indicator of greening (Bhatt et al. 2010, Jia et al. 2009). Results from this study suggest that WTD is near the ground surface, greening can be documented as a result of drying.

3.5 Conclusions

This study characterized seasonal and interannual trends in land-surface phenology in an arctic tundra landscape for a period of five years and included measurement of pre and post flooding and draining treatment conditions in a large scale experimental manipulation. To our knowledge, no studies have reported such an extensive spatio-temporal dynamics of land-surface phenology in an arctic landscape using near surface remote sensing techniques. The overarching

goal of the study was to further understand the spatio-temporal dynamics and controls of LSP in an arctic tundra landscape using optical remote sensing and investigate if altered surface hydrology could impact LSP. We also sought to investigate these effects on data collected from ground and satellite platforms. Findings indicate there were no major differences between interannual patterns or treatment differences in land-surface phenology in the study area. There were some abrupt changes in intraseasonal patterns, which seemed to occur due to changes in surface hydrology as a result of experimental treatments and weather events such as snowfall events. A relatively high spatial resolution analyses also suggested that changes in land-surface phenology appeared to be related to changes in surface hydrology in areas of low lying microtopography where WTD was above ground. NDSWI and NDVI showed a strong negative relationship when water table was above ground level indicating that an increase in the cover of surface water, which is measureable with NDSWI, decreases NDVI and vice versa. These relationships held both at the high resolution tramline scale (plot level) and at the landscape level measured from reflectance derived from a globally orbiting satellite platform. Although widespread greening of the Arctic has been documented, this study suggests that if there has been a drying of landscapes similar to surface that of the study area, NDVI could have increased, not necessarily as a result of increased green plant biomass but because there is less water, which distorts accurate measurement of NDVI. Such drying of arctic landscapes has important implications for further understanding arctic ecosystem change and predicting the future state of the Arctic and Earth Systems.

Chapter 4: Relationships of NDVI, Biomass, and Leaf Area Index (LAI) for six key plant species in Barrow, Alaska

4.1 Introduction

High latitude arctic ecosystems are undergoing dramatic changes in response to climate change (Post et al. 2009, IPCC 2007, ACIA 2005, Hinzman et al. 2005, Smith et al. 2005). Arctic vegetation is particularly sensitive to climate change (Walker et al. 2005, Epstein et al. 2000, Myneni et al. 1997). A slight change in summer air temperatures, for example, has the capacity to cause major changes in plant growth (Arndal et al. 2009), vegetation structure (Riedel et al. 2005), phytomass (Epstein et al. 2008), species diversity, and shifts in altitudinal and zonal vegetation boundaries (Walker et al. 2005, Jia et al. 2002). Changes in vegetation biomass have important consequences for many components of the Arctic System including surface energy budgets (Chapin et al. 2005), permafrost (Shiklomanov, 2010) and hydrological cycles (Vorosmarty et al. 2008). Changes in plant growth also have important feedbacks to the Climate System through changes in ecosystem carbon balance (Schuur et al. 2009, McGuire et al. 2007). Therefore, understanding how vegetation biomass changes across different arctic ecosystems is key to understanding the future state of ecosystem structure and function in the Arctic.

Optical remote sensing is a valuable tool capable of assessing changes in plant biomass and other ecosystem properties and processes in response to climate change at multiple spatial scales panning leaf to ecosystem to global scales (Huemmrich et al. 2010, Sitch et al. 2007, Riedel et al. 2005, Boelman et al. 2003). Remote sensing, apart from being the only suitable tool for repeated assessment of vegetation properties such as phenology and biomass at regional to continental scales, is particularly well suited to monitoring changes in arctic ecosystems because of the logistical difficulties in accessing these vast and mostly unpopulated areas. Satellite based

sensors such as AVHRR, MODIS, Landsat have either daily coverage and/or accessible historical time series data of the Arctic, which provides opportunities for monitoring long term change (e.g. Bhatt et al. 2010, Olthof et al. 2008, Myneni et al. 1997) in factors such as biomass and leaf area index (LAI) (Riedel et al. 2005, Walker et al. 2003, Hansen 1991). Large scale studies in the Arctic have used optical remote sensing indices (i.e. NDVI) using data from satellite platforms to study long-term changes in vegetation greenness (Bhatt et al 2010, Olthof et al. 2008, Myneni et al. 1997). For a majority of these studies, ground-based data suitable for calibrating and validating remote sensing products are lacking.

Even though ground based validation of satellite-derived indices of biomass is well explored in other ecosystems (Soenen et al. 2010, Pontailer et al. 2003, Gamon et al. 1995), only a few studies have related plot level spectral reflectance indices to aboveground biomass or land-atmosphere CO_2 fluxes in the Arctic (Arndal et al. 2009, Epstein et al. 2008, Boelman et al. 2003). Some studies have related spectral reflectance to CO_2 fluxes to demonstrate the usefulness of NDVI in arctic landscape (Huemmrich et al. 2010, Puma et al. 2007, McMichael et al. 1999), while other studies have demonstrated the usefulness of spectral indices in estimating aboveground biomass (Epstein et al. 2008), and biomass and landscape age (Walker et al. 1995). However, total live plant biomass and net primary productivity is highly variable among arctic plant communities (Riedel et al. 2005, Shaver at al. 1996). More studies are required, therefore, to explore and establish fundamental relationships between optical measurements and ecosystem properties and processes in the Arctic.

In this study we explore the relationship between above-ground biomass, LAI and NDVI for six vascular plant species common in tundra near Barrow, Alaska (Johnson et al. 2011,

Hollister et al. 2006, Webber et al. 1978). To extrapolate these relationships to the landscape level and over decadal time scales in order to assess how ecosystem structure and function may have altered, we used plant community data from an International Polar Year Back to the Future (BTF) study (Callaghan et al. 2011, Villarreal et al. Accepted), which revisited sites established in Barrow during International Biome Program (IBP, Brown et al. 1980, Webber et al. 1978).

4.2. Method

4.2.1 Site Description

Data for this study were collected on or near the Barrow Environmental Observatory (BEO), Alaska, 71°17'01" N, 156°35'48" W. The site is situated on the northern-most point of the Alaskan Arctic Coastal Plain and has a low relief and an average elevation of 4 meters (Aguirre et al. 2008). Seventy two percent of the landscape near Barrow contains oriented lakes, drained thaw lake basins and small ponds (Hinkel et al. 2003). The region is underlain by continuous permafrost and includes thermokarst terrain typical of the Alaskan Arctic Coastal Plain (Brown et al. 1980), such as thaw lakes, high and low-centered polygons, shallow ponds and lakes. Active layer is generally less than 50 centimeters (Shiklomanov et al. 2010). Soils of the area have been described by Bockheim et al. (1999) and include cryoturbated gelisols, specifically Typic Aquorthels with high soil moisture content, Histoturbels, and Aquaturbels. The upper layer of this soil consists of carbon rich peat (ca. 50 kg/C/m^3) (Bockheim et al. 2001). Soils are generally moisture rich due to shallow drainage gradients, relatively low rates of evapotranspiration, and impeded drainage caused by ice-rich continuous permafrost (Liljedahl et al. 2011, Bockheim et al. 1999, Miller et al. 1998).

4.2.2 Biomass Harvest

Plant species selected for the study included *Arctophila fulva*, *Carex aquatilis*, *Dupontia fisheri*, *Eriophorum angustifolium*, *Eriophorum scheuchzeri* and *Petasites frigidus*. These six species are among the eight most common vascular plant species in the Barrow area (Webber et al. 1978, Johnson et al. 2011, Hollister et al. 2006). Twelve plots were selected for harvesting of above ground biomass (Table 4.1). The selected plots had dense mono-specific plant cover for a respective key plant species, which was considered to equate to 100% cover of the respective species. All plots were chosen so that there was no standing water present. Green fractions of the above ground plant biomass were harvested using a circular ring 23.3 cm in diameter. Green biomass within the plots was harvested and stored in zip-lock bags and kept cool. Harvested biomass was sorted within a few hours for any impurities then weighed using an Explorer Ohaus balance with accuracy of 0.0001g. Samples were then oven dried and weighed several times until no further loss in weight was recorded. The mean biomass for each species was calculated by averaging values for all plots for in which each species was found.

Biomass for each of the plots was also calculated as follows:

$$\text{Biomass} = \text{Dry Weight} * 0.054 \text{ gm/m}^2 \text{ ---------- Equation (4.1)}$$

Here 0.54 m^2 is the area of the harvest plots.

4.2.3 Spectral Data Collection

Spectral reflectance data for all the vegetation plots were collected before the plots were harvested using a dual-detector field portable spectrometer (Unispec DC, PP Systems,

Amesbury, MA, USA), which collects radiance (radiation from the target) and irradiance (radiation from the sky) simultaneously, thereby permitting correction of surface reflectance under varying sky conditions (Gamon et al. 2006a). The two detectors were cross-calibrated using a white panel with 99% reflectance (Spectralon, Labsphere, North Sutton, NH, USA) several times during spectral measurements. The Unispec-DC had a nominal range of operation between 303 and 1148 nm in 256 contiguous bands with a spectral resolution of approximately 3 nm and a full-width-half maximum of approximately 10 nm. The usable range of this detector (range with reasonable signal-to-noise) is approximately 400-1000 nm. The downward looking sensor has a field of view of 20 degrees and therefore to cover a plot size of diameter 23.3 cm, spectral scans were taken at a height of 78 cm above the plots. Measurements were taken around mid-day.

For each plot sampled, the normalized difference vegetation index (NDVI, Sims and Gamon 2003) was derived from the hyperspectral reflectance data (Equation 4.2). NDVI is indicative of the abundance of photosynthetically active vegetation (Rouse et al. 1974).

$$NDVI = (R800 - R680)/ (R800 + R680) \text{ ---------- Equation (4.2)}$$

Here R680 and R800 are reflectance values at 680nm, 800nm wavelengths respectively. Average NDVI for each species were calculated by averaging NDVI values for all plots in which each key plant species was found.

4.2.4 Calculation of Leaf Area Index (LAI)

Digital photos of the vegetation plots were taken before the plots were harvested using a Nikon Coolpix 5400 digital camera. The photos were taken with an automatic exposure looking vertically down at the plots to capture a rectangular area of roughly 50cm by 50cm. The color images were recorded in JPEG format and downloaded for further processing. LAI was derived from the digital images following the method given by Luo and Pattey (2010) and uses GreenCropTracker v.1.0 software developed by Agriculture and Agri-Food Canada. This software is provided free of cost and uses the IDL (Interactive Data Language) virtual machine freely available from ITT Corporation, USA and calculates vegetation green cover fraction and LAI from color digital images. The software applies a simple transformation to generate a feature representing greenness from three color channels i.e. Red (R), Green (G), and Blue (B):

$$\text{Greenness} = 2G - B - R$$

Here, R, G and B represent the intensity levels recorded for each color by the digital camera. The transformation uses the high contrast between the reflected intensity of green leaves and other background color associated with features like dead material, soil etc. A sequential threshold approach based on histogram analysis is used to calculate canopy vertical green fraction. LAI is estimated from the vertical gap fraction as follows Equation (4.3):

$$LAI = -2\ln(Po(0)) \quad \text{(Lui and Pattey, 2010)}\ldots\ldots\ldots \text{ Equation (4.3)}$$

In Equation (4.3) Po(0) refers to the gap fraction at a solar zenith angle zero. For a detailed derivation of this equation, refer to Lui and Pattey (2010). Average LAI values for each species were calculated by averaging all the plots for each species.

4.2.5 Data Analysis

To investigate statistical differences in NDVI, LAI and biomass among different species, one-factor ANOVA were performed using JMP v 7.0. Average values for each of the above mentioned parameters for each of the species were calculated and plotted as bar graphs using Excel 2007. Error bars indicating one standard deviation were added to each data series. To explore how NDVI and LAI relate to biomass, linear regression analyses were performed for all species combined and for only the graminoids using data from all plots and all species. Biomass regression models were developed with NDVI, LAI as individual inputs.

To investigate decadal time scale change, biomass was modeled for five species i.e. *Arctophila fulva*, *Carex aquatilis, Dupontia fisheri, Eriophorum angustifolium, Eriophorum scheuchzeri,* using mean percent cover data available for these species for 1972 and 2008 in the Barrow IBP study sites. Using biomass data measured for these species for the hundred percent species cover harvest plots, biomass were estimated for these particular species for 1972 and 2008 were calculates using the percent cover data available for the Barrow IBP study sites. This helped us to investigate if we could use our method to model biomass in decadal time scale using existing data which could potentially be helpful in understanding how arctic plant communities have changed over decadal time scales in response to climatic and other change is imperative (Finzi et al. 2011).

4.3. Results

Plots that were selected for this study were free from standing water and were deemed to have hundred percent vegetation cover for the respective species of interest. *Dupontia fisheri* had the highest NDVI (0.87) closely followed by *Arctophila fulva* (0.82) and *Petasites frigidus* (0.77). *Eriophorum scheuchzeri* had the lowest NDVI values (0.50). *Arctophila fulva* had the highest LAI (3.53) followed by *Dupontia fisheri* (2.49), *Carex aquatilis* (1.88), *Petasites frigidus* (1.74), and *Eriophorum scheuchzeri* had the lowest LAI (0.56). *Arctophila fulva* had the highest aboveground biomass (136.81 g/m2) followed by *Dupontia fisheri* (43.48 g/m2), *Carex aquatilis* (40.09 g/m2) and *Eriophorum angustifolium* (36.66 g/m2). *Eriophorum scheuchzeri* had the lowest biomass among all the species studied (11.66 g/m2) (Table 4.1 and Fig. 4.1).

Table 4.1. Summary of NDVI, LAI, and biomass measurements for the six key plant species.

Species	No. of Plots	Avg. NDVI	Avg. LAI	Avg. Biomass (g/m2)	Graminoid (Yes/No)
Arctophila fulva	4	0.82 ± 0.133	3.53 ± 0.416	136.81 ± 44.042	Yes
Carex aquatilis	3	0.68 ± 0.133	1.88 ± 0.416	40.09 ± 44.042	Yes
Dupontia fisheri	1	0.87 ± 0.133	2.49 ± 0.416	43.48 ± 44.042	Yes
Eriophorum angustifolium	1	0.79 ± 0.133	1.49 ± 0.416	36.66 ± 44.042	Yes
Eriophorum scheuchzeri	2	0.50 ± 0.133	0.56 ± 0.416	11.66 ± 44.042	Yes
Petasites frigidus	3	0.77 ± 0.133	1.74 ± 0.416	30.66 ± 44.042	No

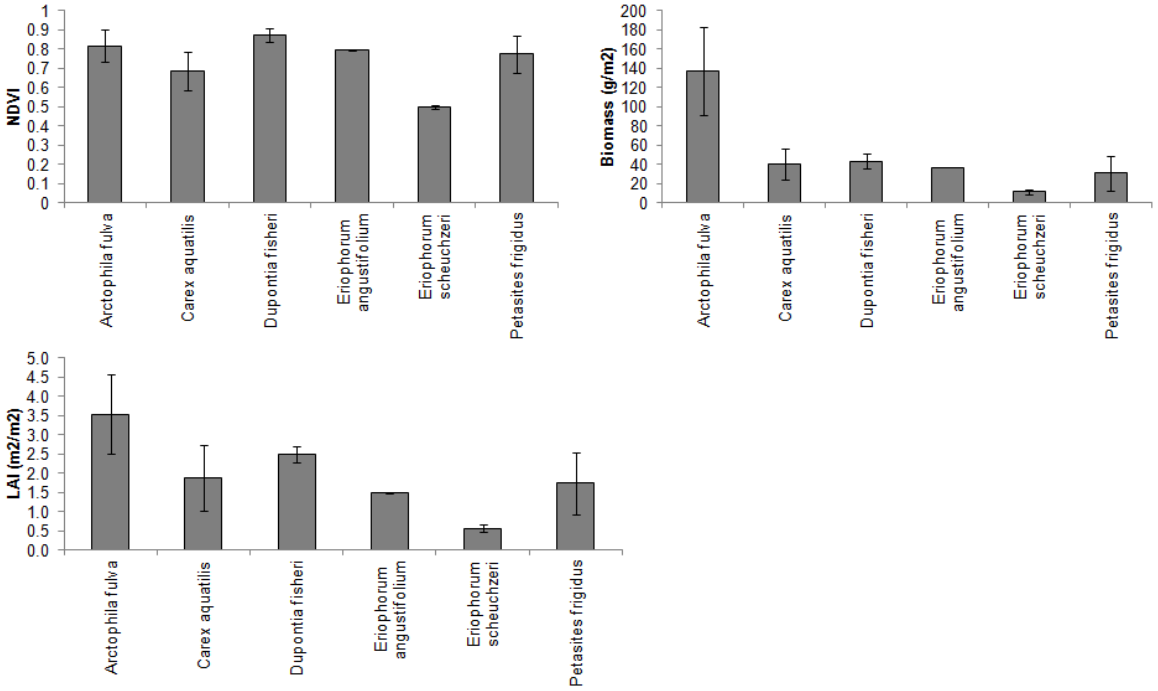

Figure 4.1. Average values of NDVI, Biomass and LAI for each of the key plant species. Error bars represent ± one standard error.

NDVI showed strong exponential relationships with both LAI (Figs. 4.2a, 4.2b) and aboveground biomass (Figs. 4.2c, 4.2d). The relationship between NDVI and LAI for graminoids was slightly stronger with $R^2 = 0.85$ compared to that for all species combined while correlations between NDVI and biomass for graminoids was stronger ($R^2 = 0.82$) compared to that for all species combined ($R^2 = 0.70$). All the relationships between NDVI, LAI and biomass showed strong exponential relationships with $R^2 \geq 0.7$, indicating that NDVI saturates at higher biomass and LAI values. The relationship between LAI and biomass was slightly stronger for graminoids ($R^2 = 0.88$) compared to the relationships for all species combined ($R^2 = 0.86$) (Fig. 4.3).

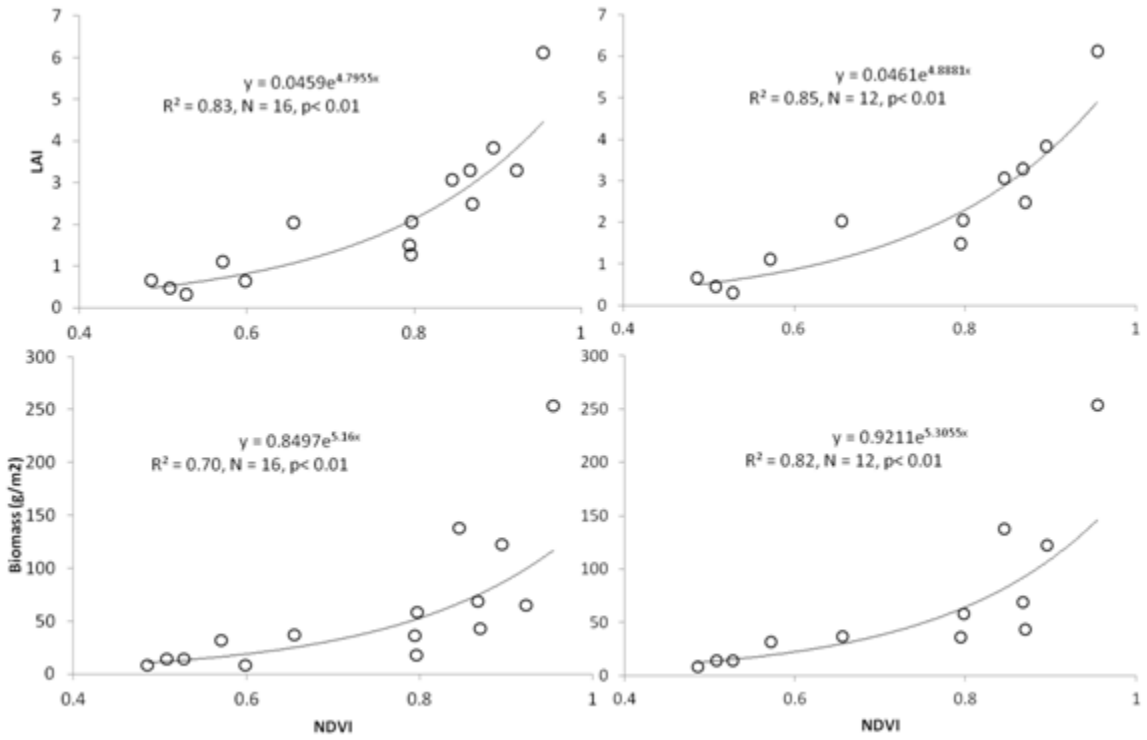

Figure 4.2. Correlations between NDVI and LAI and Biomass for all species combined (left figures) and for graminoids only (right figures). All the relationships showed strong exponential relationships with $R^2 \geq 0.7$, indicating that NDVI saturates at higher biomass and LAI values.

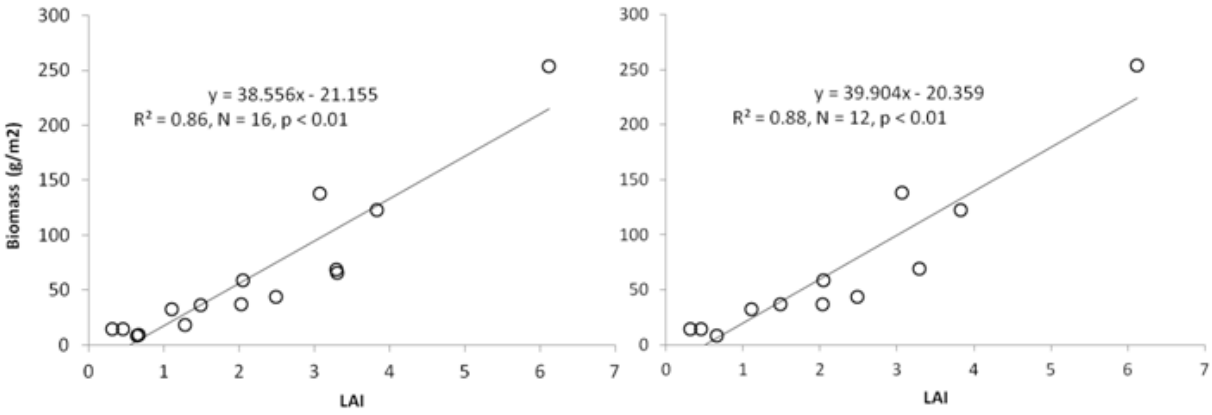

Figure 4.3. Correlations between LAI and Biomass for all species combined (left figures) and for graminoids only (right figures). Biomass showed a strong linear relationships with LAI for both correlations ($R^2 = 0.86$ all species, $R^2 = 0.88$ graminoids).

Analysis of the species percent cover change for the IBP plots for 1972 and 2008 showed that *Carex aquatilis* and *Eriophorum angustifolium* decreased in cover between 1972 and 2008 while *Arctophila fulva* and *Dupontia fisheri* increased in cover (Fig. 4.4a). Similarly, modeling of biomass showed that *Carex aquatilis* and *Eriophorum angustifolium* had a predicted decreased biomass in 2008 compared to 1972 while *Arctophila fulva* and *Dupontia fisheri* had increased predicted biomass cover in 2008 compared to 1972 (Fig. 4.4b). A 2.8% increase in percent cover for *Arctophila fulva* showed a 124% increase in biomass while a 3.4% increase in percent cover for *Dupontia fisheri* showed a 14.93% increase in biomass between 1972 and 2008. The 13.36% decrease in percent cover for *Carex aquatilis* suggested a 33.92% decrease in of biomass whereas a 1.59% decrease in percent cover for *Eriophorum angustifolium* showed a 14.65% decrease in biomass. As *Eriophorum scheuchzeri* had very low percent cover and biomass, it was not included in this analysis.

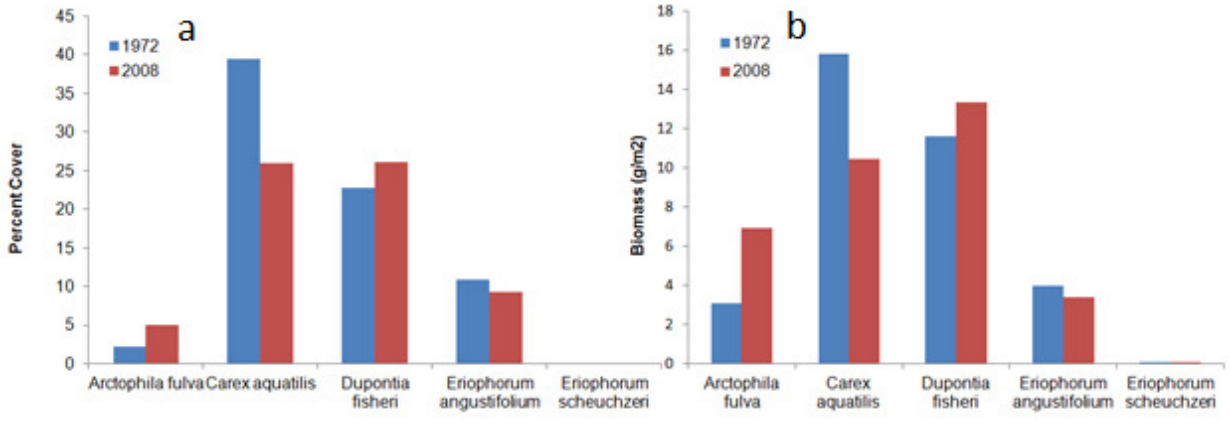

Figure 4.4. Measured decadal change in percent cover and modeled biomass for key species in the Barrow IBP study area. The greatest percent and magnitude of increase in cover was recorded for *Arctophila fulva* and decrease for *Carex aquatilis*. The greatest percent and magnitude of increase in biomass was modeled for *Arctophila fulva* and decrease for *Carex aquatllis*.

4.4. Discussion

In the Arctic, ecosystem properties such as standing plant biomass appears to be sensitive to phenomenon associated with climate change such as warming (Bhatt et al. 2010, Hollister et al. 2006, Walker et al. 2005, Epstein et al. 2000). Changes in vegetation biomass have important consequences for many components of the Arctic system including surface energy balance and permafrost (Euskirchen et al. 2007, Chapin et al. 2005), hydrology (Post et al. 2009, Hinzman et al. 2005) and wildlife. Optical remote sensing is the only feasible tool for regional scale monitoring and assessment of change in vegetation properties such as biomass and LAI (Stow et al. 2004), which is essential for understanding processes such as land-atmosphere carbon balance (Merbold et al. 2009, Wolf et al. 2008), and therefore, the future state of the Arctic and Earth Systems as they respond to climate change (IPCC 2007, ACIA 2005). Establishing sound spatiotemporal relationships between remote sensing products and ground based measurements underpins capacities of being able to extrapolate ecosystem properties and processed from the plot level to landscape and global scales (Boelman et al. 2003). This study aimed to develop such relationships between above ground biomass, LAI and NDVI for six common plant species found in tundra near Barrow, Alaska using ground based plot level measurements. To explore the potential of scaling these relationships over decadal time scales, data from a historic plant community resampling effort associated with the International Polar Year Back to the Future (BTF) study (Callaghan et al. 2011) were used that resampled sites formerly associated with the IBP field site near Barrow (Villarreal et al. Accepted).

The results showed that the NDVI values for the six species studied varied within a range of ~ 0.3 with corresponding change in values in LAI and biomass. The strong relationships

between NDVI and biomass and LAI for the species studied support the use of NDVI as a spectral index for indirectly measuring plant community structure. The strong relationship between NDVI and biomass found in this study is similar to studies conducted in other tundra ecosystems including tussock tundra (Boelman et al. 2003), shrub and high arctic tundra (Walker et al. 2003). While Boelman et al. (2003) reported a linear relationship between NDVI and biomass, Walker et al. (2003) reported an exponential relationship between NDVI and biomass, similar to our finding. Further investigation of these relationships throughout the growing season could be helpful to strengthen these relationships.

The strong exponential relationships between NDVI and biomass and NDVI and LAI suggest that NDVI saturates for higher values of biomass (> 100 g/m^2) and LAI (> 2 m^2/m^2). On the other hand, the strong linear relationship between LAI and biomass suggests that there is no saturation in the measurement of biomass from LAI. The saturation of NDVI for higher biomass and LAI is well reported for non-arctic studies (Santin-janin et al. 2009, Huete et al. 2002) whereas these relationships are reported to be both linear (Boelman et al. 2003) and exponential (Walker et al. 2003) in the Arctic. Our vegetation plots were chosen to have 100 percent species cover without any standing water and minimal litter and standing dead matter. This probably resulted in an unusually high LAI and biomass, suggesting the linearity of the relationship between LAI and biomass requires more extensive exploration in the Arctic.

It is important to understand how arctic plant communities have changed over decadal time scales in response to climatic and other changes to understand the potential impact on biodiversity and ecosystem functional processes such as those associated with land-atmosphere carbon exchange (Finzi et al. 2011). Findings from the decadal extrapolation of plant cover

values to biomass, for the former IBP plots suggest that three species had increased biomass while three species had decreased biomass from 1972 to 2008. This finding shows that the rate of change of biomass for some species can be different which might cause non-linear trends in greening in different tundra ecosystems as species respond differently to change. Our finding is similar to the findings of Lara et al. (Accepted) who reported that ecosystem function in different plant communities within a tundra landscape have changed at different rates over decadal time scales. To better understand the non-linear change observed for specific species in our study, more studies similar to this are needed in tundra ecosystems in Barrow as well as in other tundra ecosystems to assess which species could act drivers of such non linear changes.

4.5. Conclusions

This study found strong plot level correlations between NDVI and biomass and LAI for six key plant species that are relatively common in tundra near Barrow, Alaska. These findings are similar to other published studies focusing on other tundra ecosystems elsewhere in the Arctic (Epstein et al. 2008, Riedel et al. 2005, Boelman et al. 2003). However, NDVI was found to saturate at an approximate biomass of 100 g/m^2 and an LAI of 2 m^2/m^2, which suggests that greening of tundra could be linked to a relatively small change in species cover. LAI was not found to saturate with an increase in biomass. Extrapolating results over multiple decades to hypothesize trajectories of change in biomass, LAI and NDVI, highlight the potential importance of species level change, which has the potential to cause non-linear change in various metrics of ecosystem structure and function. Overall, results reaffirm the applicability of NDVI for large scale assessment of vegetation change in the Arctic and highlight the need for additional species

specific and multi-scale studies, which are likely to facilitate interpretation of drivers and mechanisms of change derived at large spatial scales using remote sensing approaches.

Chapter 5: Development of Cyberinfrastructure (CI) for better management and quality control of hyperspectral data for robotic tram system

5.1 Introduction

Understanding the environment in which we live and how human activities and other natural changes affect it has always been regarded as one of the most important and challenging problems in science. In recent times, there has been increasing urgency to further understand and predict how the future state of the Earth System is going to be impacted by global change in order to forecast how humans will need to adapt. This urgency is motivating several paradigm shifts in the ecological and environmental sciences (NSF Cyberinfrastructure Vision for 21st Century, 2007):

- Environmental sciences are becoming a more data-driven science and this itself is causing the need to improve trust and integrity in the data collected.
- There has been an increased reliance on data collected by other researchers and multidisciplinary scientific networks (e.g. NEON, and Fluxnet) to address global scale scientific questions (e.g., how are global biogeochemical cycles being impacted by climate change? How does seasonal climate variability impact the virulence of infectious diseases?).
- Environmental scientists are increasingly using advanced field-based instrument technologies such as sensor arrays and autonomous vehicles for continuous high frequency measurements of various environmental data.
- The need to improve spatiotemporal and organizational scaling of environmental properties and processes from small (e.g. leaf level) to large scales (e.g. global), and large to small scales has also increased, requiring new computational approaches to modeling and

algorithm development, scaling of uncertainty, and data reduction, exploration and visualization.

The need for advancing environmental science research has been a focus for the establishment of national scientific priorities and this can be highlighted in several reports including *Cyberinfrastructure Vision for 21st Century* (NSF, 2007), *Towards an Arctic Observing Network* (NRC, 2006), *Grand Challenges in Environmental Science* (NAS, 2001); *Environmental Science and Engineering for the 21st Century* (NSF, 2000), *Our Common Journey: A Transition Toward Sustainability* (NAS, 1999). Many of these reports have highlighted the infrastructure needed to advance the environmental sciences, including comprehensive and automated data collection and management systems. In addition, there has been an increased awareness of the need to improve modern observing systems, further utilize powerful supercomputers and high-speed communication links, and develop tools to improve access to high quality data streams and data archives. This need for infrastructure development also highlights the need for optimizing data streams, instituting quality assurance procedures, and managing, archiving and integrating large volumes of multivariate data and automated data processing tools.

Interestingly, the emerging data needs in the multidisciplinary environmental sciences have led to a "data paradox". Huge volumes of multifarious data are now being generated to meet scientific needs, but the human resources and cyberinfrastructure required to support this growth has arguably been lacking for most disciplines in the environmental sciences. As such, environmental scientists are facing new challenges in documenting, managing, and accessing, and processing such large and diverse volumes of data.

Many of the challenges facing the environmental sciences as described above as a whole were encountered during this project and allowed for the exploration and prototype development of a range of cyberinfrastructure that ultimately benefited the science presented in this thesis so far. This chapter documents the development of these cyberinfrastructure, which aided data management and documentation, quality control and access to some ground based hyperspectral data of spectral signatures of vegetation. These developments were facilitated by a range of collaborations within the environmental sciences (John Gamon, University of Alberta; Fred Huemmrich, NASA Goddard), and interdisciplinary efforts with the computer sciences (Ann Gates, Paulo Pinheiro, Irbis Gallegos, and Leonardo Saylandia associated with UTEP's Cyber-ShARE Center of Excellence). Below, the data volume challenge associated with the robotic tram system which created a similar 'data paradox' as mentioned above is highlighted as are the various cyberinfrastructure that helped address this issue.

5.2 Data Paradox with the Robotic Tram System

The robotic tram system associated with the biocomplexity project consisted of three 300m tramlines (Goswami et al. 2011). Hyperspectral data in the visible to near IR range of the spectrum were collected at every meter of each of the tramlines two to three times per week using a Unispec DC portable spectrometer (PP Systems, Amesbury, MA, USA). The Unispec DC collects data in two channels at the same time, one for radiance and one for irradiance in 256 wavebands. For each run of the robotic tram, a total of 300 spectral data files were collected per tramline, which resulted in the collection of 900 spectral data files after each full day of sampling (3 tramlines x 300 data files/tramline). Each spectral data file consisted of reflectance

measurements for 256 wavebands, thus, following a full day's worth of data collection, a total of 230,400 data points were collected. In one field season, approximately 30 sample-days of data were collected, depending on logistic constraints, weather, and technical difficulties. As a result, for one field season the tram system generates a total of 27,000 spectral data files and 13,824,000 data points. For the duration of the study (2005 – 2009), more than 135,000 spectral data files were collected. This totals to more than 69,120,000 data points during the study period. The volume and complexity of data for the entire project were compounded with ancillary measurements such as digital photographs of tramline footprint areas (~ 5,000 photographs), micrometeorological data from the automatic weather station (AWS) collected at 1 minute interval creating a steady stream of data from multiple sensors (~2,073,600), and other physical environmental measurements including WTD, soil moisture and thaw depth (~20,000 data points).

Thus, the robotic tramline project associated with the biocomplexity project also experienced data management problems similar to any modern day data intensive environmental science project. High spatio-temporal sampling was conducted using several different data collection methods and technologies; these were sensitive to data quality issues due to human, technological, and environmental conditions and limitations; large volumes of data were collected, managed, and shared between investigators; and a range of different processing, algorithm development, and ecological scaling was executed. Development of key cyberinfrastructure met many of these challenges and included the development of workflows and ontologies for documentation of scientific process, quality control specifications and

screening software and automated data processing tools in addition to improved metadata documentation procedures. These are described below.

5.3. Development of Workflows and Ontologies for the Robotic Tram System

5.3.1. What is ontology?

An ontology is a "specification of a conceptualization" or a description of concepts and relationships that can exist for an agent or a community of agents (Noy and McGuinness, Ontology 101, web reference). Ontologies capture knowledge about a certain domain of interest by defining concepts and relationships among them within that domain (Baadar et al. 2003). Ontologies can be machine-readable, providing the means for data discovery and integration (Jones et al. 2006). Ontologies are being used successfully in a number of biological and medical informatics projects to capture processes and create vocabularies for data discovery (Bard and Rhee 2004, Rosse and Mejino 2003). Here we describe the development of ontologies for the robotic tram system associated with the biocomplexity project through the use of the software WDO-It (Pinheiro da Silva et al. 2007), developed in the Trust Laboratory at the University of Texas at El Paso.

5.3.2 Ontology for Ecological Research

Ecology is an inherently multidisciplinary science that explores how physical and biological factors and their inter-relationships establish the structure and function of living systems (Madin et al. 2007). The range of data needing ecological analyses are typically very broad, requiring input from non-biological fields such as geography, oceanography, and

hydrology. To address broader synthetic problems, ecological studies often need extensive scientific collaboration and generate a diverse and voluminous collection of data (Callaghan et al. 2011). Current methods for discovering, exploring, mining, analyzing and visualizing ecological data are inefficient and constrain synthesis efforts (Pickett et al. 1994) relative to breakthroughs that have been made in other disciplines (Chen, 1976; Batini et al. 1992, Hammer and Macleod, 1999) such as space science (Sterling et al. 1995), geological science (Keller et al. 2006) and oceanography.

Effective data discovery is particularly problematic in ecology, where mostly small and focused studies employ ad hoc data management solutions often consisting of flat files or spreadsheets with minimal formal structure and little to no metadata documentation (Madin et al. 2007). The knowledge within the ecological domain can be represented with the help of ontologies, (Baader et al, 2003), which can be understood by machines and thus provide improved capacities for comprehensive data discovery and integration (Jones et al. 2006). Here we provide an overview of a Semantic Abstract Workflow (SAW) and ontology developed for the robotic tram system associated with the Biocomplexity experiment. This SAW was developed using WDO-IT (Pinheiro et al. 2007), a software tool developed in the UTEP Trust Laboratory.

5.3.3 WDO-It

WDO-It is a novel software tool for defining ontologies that enable domain experts to encode concepts categorized as data (e.g., raw measurements and derived data such as maps and graphs), methods (i.e, services, processes, or functions), and relationships among these concepts

(Pinheiro et al. 2007). It was originally developed to record a collection of data-method relationships in geosciences (Gates et al. 2007). The tool captures a Workflow- Driven Ontology (WDO) (Salayandia et al. 2006), i.e., a task ontologies. Task Ontologies are vocabulary described in a domain to describe tasks or activities of that domain. WDO-It helps users (e.g., scientists or any domain experts) generate abstract workflows using the graphical user interface (GUI) and refine the WDO based on evaluation of the abstract workflow.

Semantic Abstract Workflows (SAWs), defined through WDO-It (Fig. 5.1), are graphical structures that model data flow of a defined process, using concepts associated with the WDO. The graphical structure contains three types of entities:

1. Rectangle-shaped nodes represent activities of the process
2. Oval-shaped nodes represent data sources and sinks
3. Directed edges connecting the nodes represent the data of the process.

The connection and direction of an edge determines whether data is flowing from a source, is flowing to a sink, is input to an activity, or is output from an activity. Furthermore, edges link nodes to represent data dependency between them (Fig. 5.1). WDOs and SAWs are used to document existing scientific processes, design new scientific processes, establish common vocabularies about a scientific process and to understand the scientific processes of others researchers.

Here WDO-It (Fig. 5.1) was used to develop SAWs and ontologies for the robotic tram system data collection and data processing routine. The vocabulary for the robotic tramline system was assembled through review of the literature (Gamon et al. 2006a, Gamon et al. 2006b) and instrument manual (Unispec DC manual, PP Systems, Amesbury, MA, USA), as well as

through experiences from hands on training on using the robotic tramline system for research purposes. SAWs for the reflectance data collection (Fig. 5.2), metadata collection (Fig. 5.3) and reflectance data processing (Fig. 5.4) are shown below.

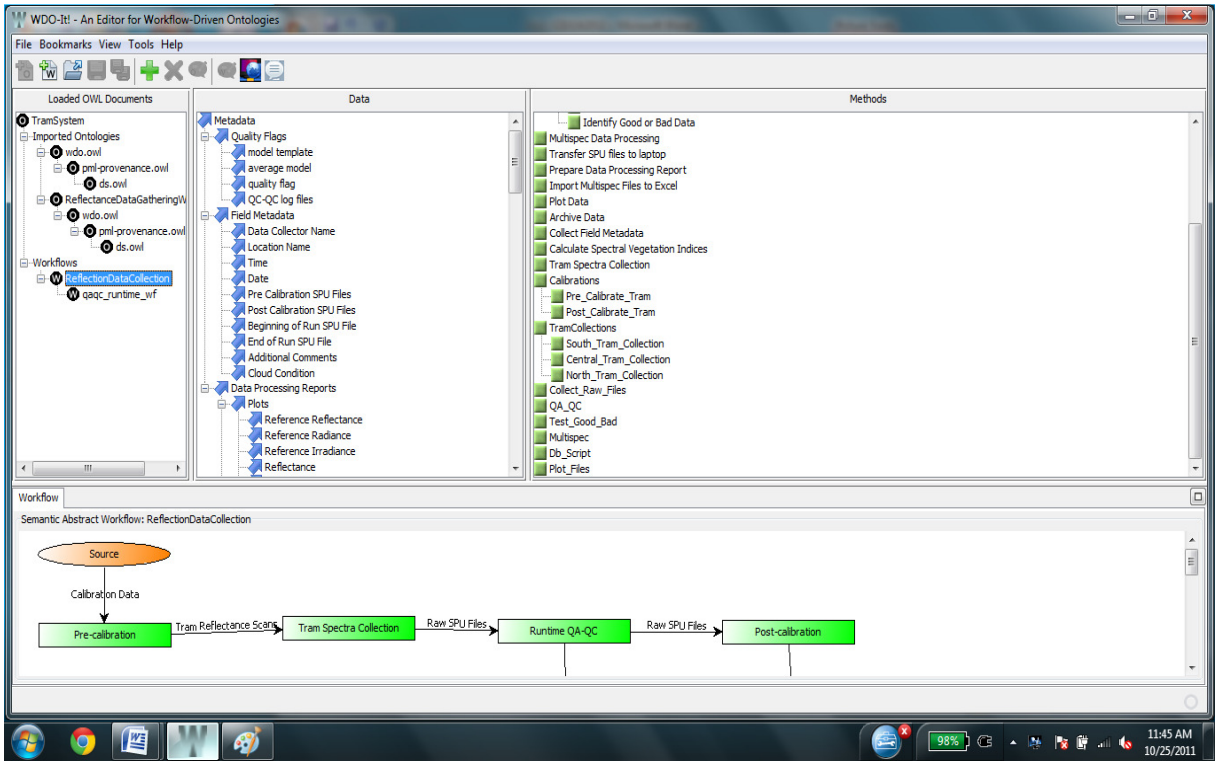

Figure 5.1. Screenshot of the WDO-It graphical user interface (GUI)

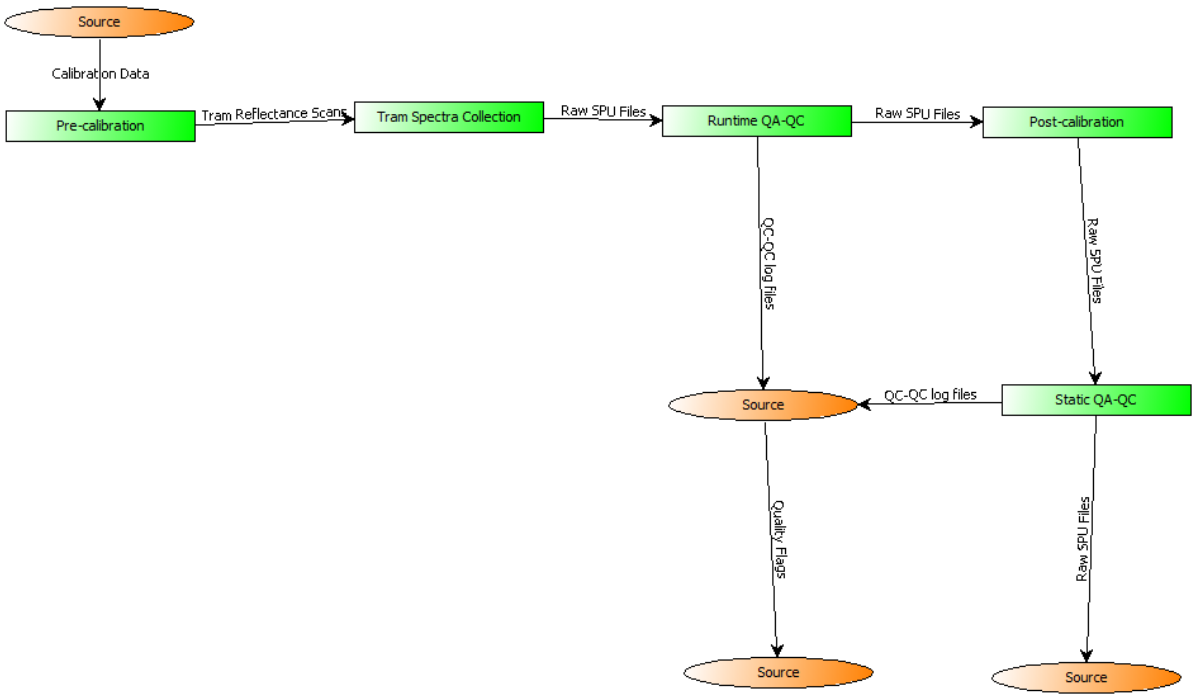

Figure 5.2. Workflow captured in WDO-It describing how reflectance data is gathered from the robotic tram system.

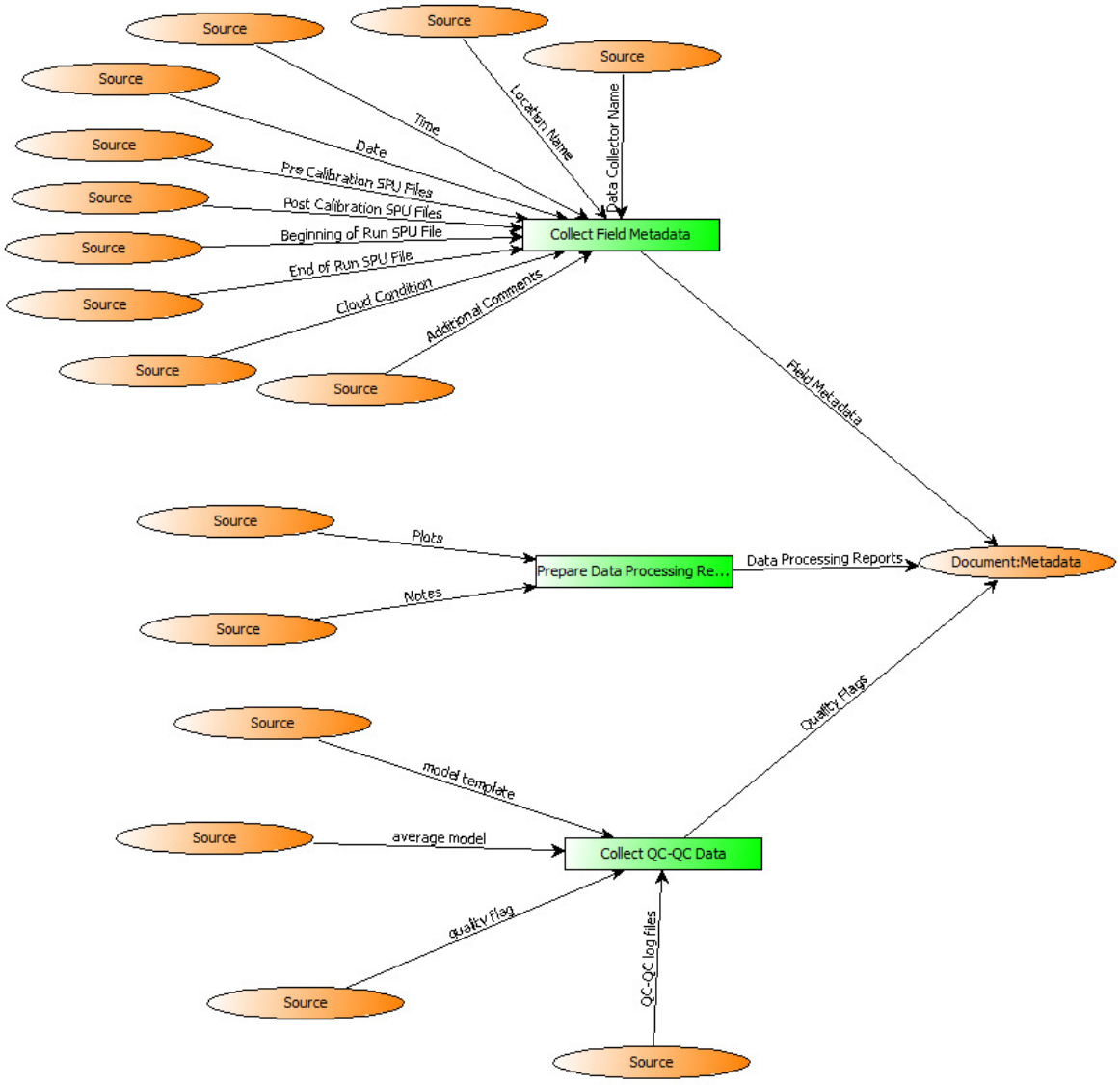

Figure 5.3. WDI-It workflow describing how metadata is collected for the robotic tram system.

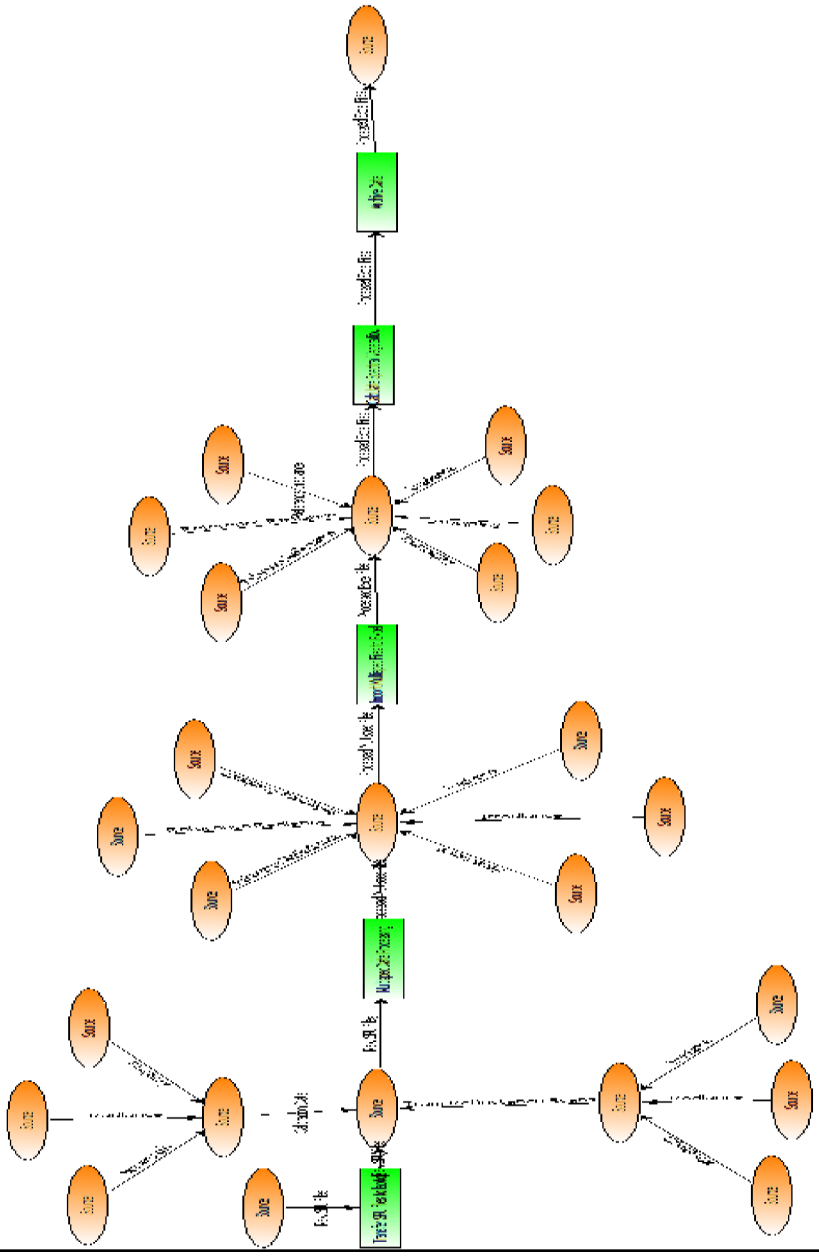

Figure 5.4. WDO-It workflow for data processing for the robotic tram system.

SAWs and WDOs developed in this study have been used to capture the processes in a similar study in the Chihuahuan Desert at the Jornada Experimental Range, where UTEP's systems ecology laboratory has established a 110 meter long tram system. Although no data were collected to quantitatively evaluate this transfer of knowledge support, it is my opinion that students new to remote sensing and robotic tram systems became more familiar and quicker compared to the immediate learning curve required for the establishment and maintenance of this project. Following review, it is expected that this workflow will be made available on the SpecNet website, where we hope others will also find this tool useful, adopt the protocols as outlined, and subsequently improve capacities for cross-site intercomparison.

5.4 Development of QA/QC Specifications and Tools

5.4.1. Background and Rationale

The traditional method of quality checking hyperspectral data from a robotic tram system was time consuming, was somewhat open to human error, and lacked automation of data quality checking procedures. Following the establishment of the tram system in 2005 and the 30% expansion of this in 2006, it became particularly apparent that near real time data quality checking greatly improve the efficiency of operating the tram system and facilitate prompt error detection, thereby saving valuable field time. On several occasions, effort associated with an entire day's data collection was wasted because a sometimes easy to fix problem was not noted soon after its inception. This scenario was particularly common when thick fog or mist prevailed, causing interference with the optical signature recorded through the fibreoptics on the spectrometer. Additionally, the traditional method of data quality checking required expert

knowledge and detailed observation and subjective decision making. On several occasions, quality checking appeared to be somewhat erroneous and subject to the operator's level of experience. Although all data were thoroughly screened by a single experienced person for all of the data chapters presented above, this proved to be time consuming and for some problems noted late in the quality checking process, required the entire data series to be re-screened.

To address the challenges associated with the verification of hyperspectral data collected using robotic tram systems, the Data Assessment Run-Time (DART) Monitoring Framework was developed in collaboration with colleagues from UTEP Cybershare Center – specifically Irbis Gallegos (PhD student), who lead the software engineering backing this project and Dr Ann Gates. Specifically, DART was designed to interface with a wireless data stream from the robotic tram system established as a component of the Barrow Biocomplexity flooding and draining experiment (Goswami et al, 2011). DART applies software engineering principles and techniques including both run-time verification and formal methods. DART is intended to detect deviations from an "idealized" set of data for a period in a given growing season (referred to as the *representative data set* hereafter) that is formulated from expert knowledge and historical data. The deviations identify and flag data points that demonstrate environmental variability outside of an expected state and/or instrument malfunction.

A manuscript of the DART effort has been published (Gallegos et al, NAFIPS IEEE, 2011), and the appendix contains a copy of the manuscript. The software has been alpha tested, and requires further hardening before it being released. My specific contribution to this study was in developing the conceptual framework that evolved from my need for quality checking of the robotic tramline data in the biocomplexity project. I suggested using good quality historical data

from the robotic tramline to develop condition states that could be used as reference to check for quality state of the collected data being tested. I prepared the reference dataset from the historical data for every week for one growing season, suggested the threshold values to be used for quality checking at different times of the growing season. Additionally, I also helped in developing the user interface from a user perspective and as a potential user. I also facilitated the field testing of the software in Barrow, Alaska, helped setting up the wireless network by creating an adhoc network for data streaming from the robotic tram system to the base station. I also contributed to the paper published for this work by writing specific sections and reviewing the paper.

5. 4.2 Tool Overview

The Data Assessment Run-time (DART) Monitoring (Figs. 5.5, 5.6) works in a similar manner to a software engineering run-time monitoring system with minor adaptations to accommodate data processing. For the DART framework, a data property is a logical statement about data values associated with hyperspectral sensor readings. With DART, a user specifies a set of data properties of interest, which document the data quality checks that will monitor the sensor readings. DART is intended to detect deviations from an "ideal" set of data that is derived from expert knowledge and historical data, i.e., the representative data set. DART can operate in either a *near-real time* mode or a *post-collection* mode. The *near-real time* mode allows scientists to verify the data at near-real time as the data are wirelessly streamed from the tram cart to a computer. In *near-real time* mode, DART is given a path to a run-time folder, and continually checks data stored as new files in the folder, i.e., files sent by a spectrometer. *Post-*

collection mode is used to verify data that has already been collected and stored but requires verification.

The system requires three input files to function:

1. A "Run-time Data File" (obtained from a run-time folder) that contains the raw data and metadata collected by the spectrometer on the tram cart at a given interval in time or position along the tramline.
2. An expert-validated "Representative Data Set File" (stored in the "Representative Data Set Repository") that contains averaged set of historical data from a previous collection period
3. An expert-validated "Property Specification File" (stored in the "Specification Repository") that contains the data properties to be verified.

The "Representative Data Set Repository" stores hyperspectral reflectance files from previous sampling periods. These are *representative data sets* that contain averaged hyperspectral reflectance data considered representative for a particular sampling location and time of the growing season. A representative data set is compared to unverified data collected by the tram system that corresponds to the given sampling location and seasonal time period. The property specifications file contains threshold values used for specifying range tolerances between the actual readings and the values of the representative data set. Specifications are described in XML files according to the quality thresholds expected for each week of the growing season and for an area of interest.

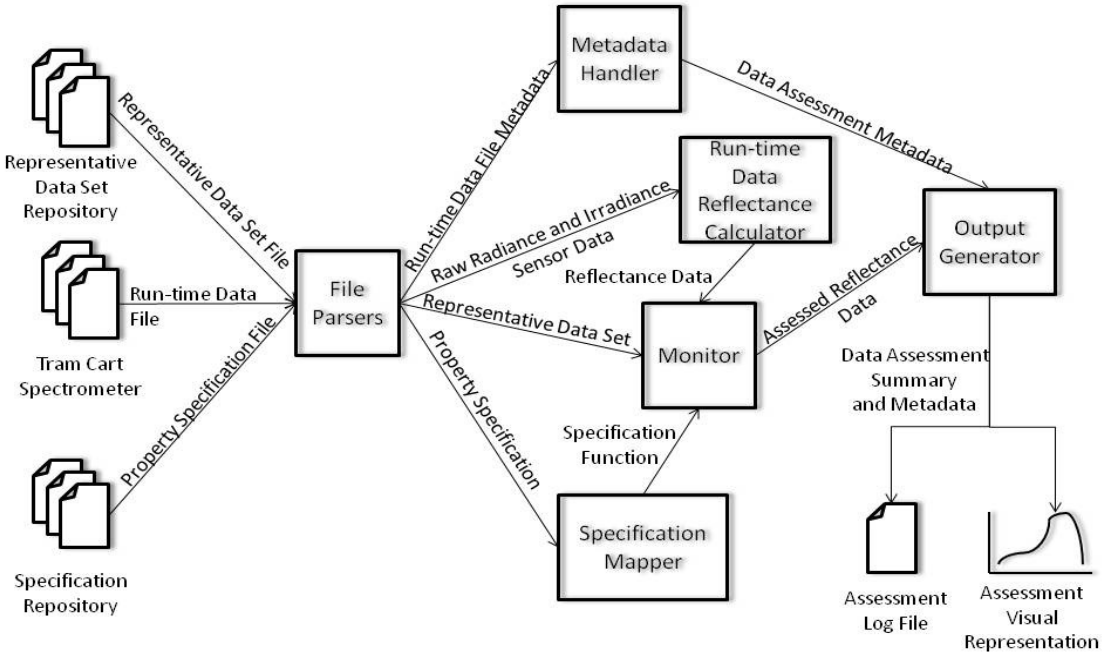

Figure 5.5. Flow of data in the Data Assesment Run-time (DART) framework. Rectangles represent modules in the system

DART performs data assessment by assigning data assessment flags to individual reflectance values, ranges of interests, and "Run-time Data Files." For individual reflectance values, DART determines the deviation of the reflectance value from the "ideal" data values. Given a set of predefined thresholds provided by the user, DART compares the reflectance deviations to such thresholds and classifies the severity of the deviation. For every wavelength value in a specific range, the absolute difference (AD) between the derived reflectance value and the representative seasonal value is calculated and compared to a predefined threshold (T); if AD is less than or equal to T, the derived reflectance value is not considered a deviation. If the AD deviates from T, the assessment flag changes accordingly (Table 5.1).

Table 5.1. Tolerance ranges used in DART to Assess Hyper-Spectral Data given An Absolute difference (AD) Between a calculated reflectance value, a representative value, and a data assesment threshold (T)

Flag	Condition	Description
00D	$AD \leq T$	No deviations found.
01D	$T < AD \leq T+0.1$	Small deviation found.
02D	$T+0.1 < AD \leq T+0.2$	Medium deviation found.
03D	$AD > 0.2$	Large deviation found.

5.4.3 Software field Testing

For field testing of the software, a case study was conducted on the robotic tram system located in the Barrow Environmental Observatory near Barrow, Alaska (Goswami et al. 2011) during the 2008 field season. The tram cart was modified to include a laptop on which DART was executed. The laptop on the cart was accessible remotely through a point to point wireless connection, allowing data transfer at near-real time. Although field trials performed well, the majority of data for the 2008 seasonal data was assessed using DART's post-processing mode due to limited wireless connectivity with the central and northern tramlines.

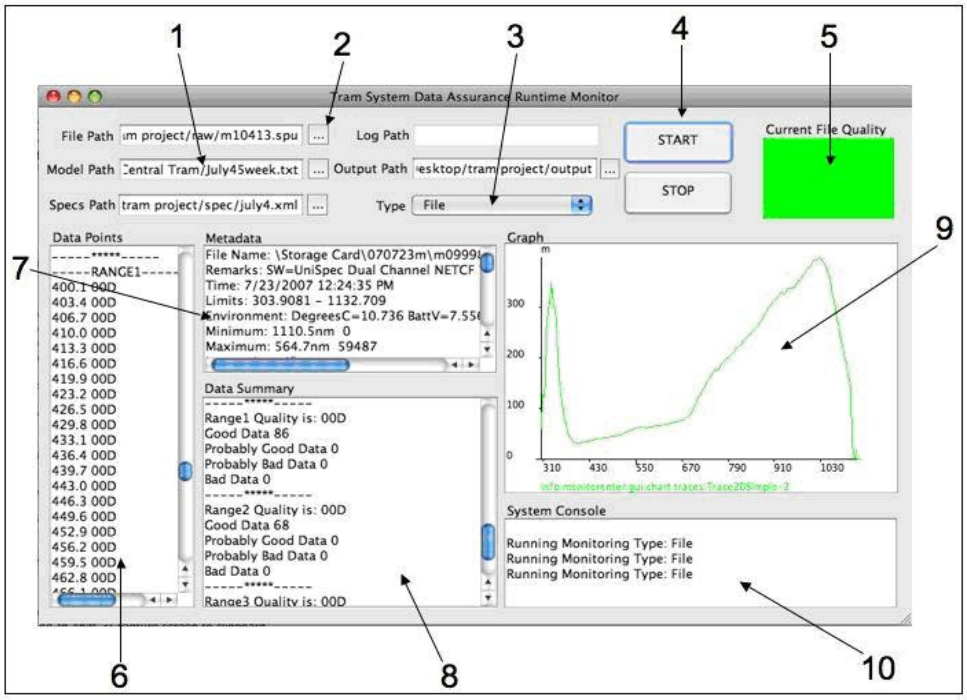

Figure 5.6. Graphical user interface (GUI) for the DART software. Here the numbers 1 – 10 represent different features of the software : 1. Input – Output Paths, 2. File choice, 3. Verification type, 4. Start and stop button, 5. File status, 6. Data point quality, 7. Metadata, 8. Data quality summary, 9. Graph, 10. System output.

Representative data sets for the 2008 season were created using historical data gathered in 2007. The representative data sets included average weekly reflectance data constructed from 2007 post-processed data for the three tramlines. This resulted in 27 representative data sets - nine per tramline, and one for every week of the 2007 season. Thirteen specification files containing expected threshold values for different times of the season and delimiters were made to define ranges of scientific interest in the spectra. The specification files contained properties defined for three ranges of scientific interest within the optimal range in the spectra (i.e., 400-1000 nm) and two noise ranges outside the optimal range. The thresholds and the delimiter selections were based on the scientist's knowledge acquired over time.

A total of 81 tram runs were processed using DART, for a total of 24,690 spectral files, and 7,407,000 spectral readings for the 2008 season. Six additional days were unprocessed because the measurements were taken with a different spectrometer than the one used to create the seasonally representative data sets; thus, even though the specifications could be reused for these measurements, representative data sets for the new spectrometer were unavailable.

The hyperspectral data at the beginning of the season was expected to contain large deviations due to the presence of snow and melting snow. DART correctly identified (Fig. 5.7) the expected "largely deviated" (03D) data during this period - a transition period from June 18 (Day 169) to June 30 (Day 181), and the expected "no deviations" (00D) for the rest of the season for the North and Central tramlines. Technical problems appear to have influenced data obtained from the South tramline at odd times throughout the season.

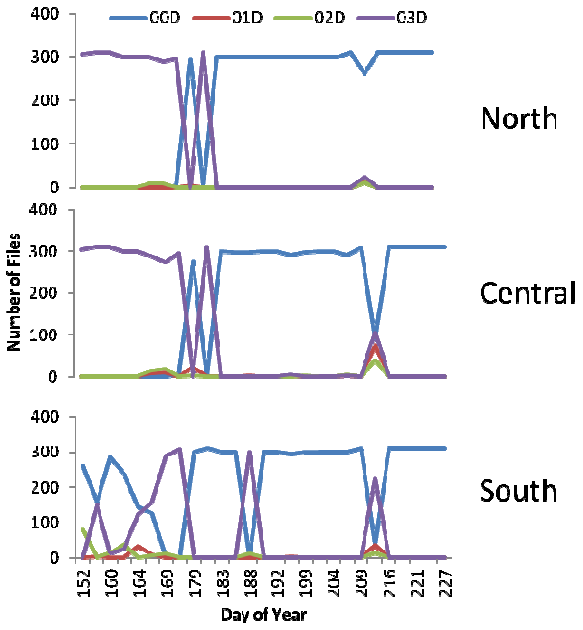

Figure 5.7. DART data assessment results distribution for the 2008 field season.

The case study identified two types of properties: data properties and instrument properties. Data properties specify expected values and relationships related to field data readings i.e., noise ranges, and data values outside the specified thresholds for spectral ranges. Instrument properties specify expected instrument behavior and relationships by defining examining attributes and instrument functions based on reading (e.g., low voltage, bad fiber optic, and loose connections). The case study also showed that software engineering run-time verification techniques can be adapted to be used as data assessment techniques. For a detailed description of the field testing please refer to the published manuscript in the appendix of this dissertation (Gallegos et al. 2011).

5.5 Development of Web-based Vegetation Spectral Library (VSL)

5.5.1 Remote Sensing and Spectral Libraries

Spectral characteristics of vegetation and other land surfaces are often used to study ecosystem structure and function at large spatial scales. Spectra can be used to *'train'* classifications of satellite imagery or model land-atmosphere carbon flux for example. These types of analysis, as well as other remote sensing using data derived from spacecraft, manned or unmanned aircraft, requires access to a knowledge base of spectral profiles for known land and vegetation surfaces. The Vegetation Spectral Library (VSL) (http://www.spectrallibrary.utep.edu) is an example of a web based cyberinfrastructure tool intended to make such a knowledge base freely available to international scientific research communities and anyone who takes an interest in the spectral signature data of vegetation. There are only a few comparable web based initiatives (Curry et al. 2011). The only two web-based

spectral libraries are the U.S. Geological Survey (USGS) Spectral Library for minerals, and the ASTER Spectral Library available at the NASA Jet Propulsion Lab (JPL) for a collection of spectra from a range of materials including data from the USGS Spectral Library and the Johns Hopkins University (JHU) Spectral Library that specializes in minerals and meteorites with some snow and vegetation spectra. Only the ASTER spectral library offers search capabilities over their data sets. Therefore, the VSL is an important contribution to the remote sensing community with its web-based platform and enhanced data browsing/search capabilities.

5.5.2 Description of the library

The VSL was created using a PostgreSQL database interfaced to a Plone web interface (Fig. 5.8). The application is hosted on a server in the Systems Ecology Laboratory at the University of Texas at El Paso. Currently, the library includes 235 datasets collected from around the world, data from several arctic locations, the Antarctic Peninsula and offshore islands, and several locations in the Chihuahuan Desert.

The data in the library is freely available to web based users who can download the data directly from the web-based library. Users can either browse (Fig. 5.9) or search (Fig. 5.10) for data according to location, site name, landcover type, and other parameters such as sky conditions, time of day, and sampling instrument (Details on the appendix). Data are coupled to metadata (Fig. 5.13) and digital images (Fig. 5.14) of vegetation or land surfaces from which spectral signatures have been derived. The users can also view (Fig. 5.10) and plot the data online (Fig. 5.12).

There are two levels of users for the library, administrator and general users. The administrator has the ability for higher level data management and can manage user profiles and access (add, remove, restrict user privileges), manage data (upload, modify, delete), and manage written content on the site. General users can browse and search for data and download this data in ASCII format. If the general user wants to contribute data to the library (Fig. 5.15), s/he can request permission by sending an email to the site administrator. Once approved, s/he can upload data and metadata to the library. Metadata requires that a prescribed format is met (Fig. 5.16). The metadata form and the upload data form are explained in detail in the online help menu (Fig. 5.17). Screen shots below are intended to display the various functionalities of the library and web interface.

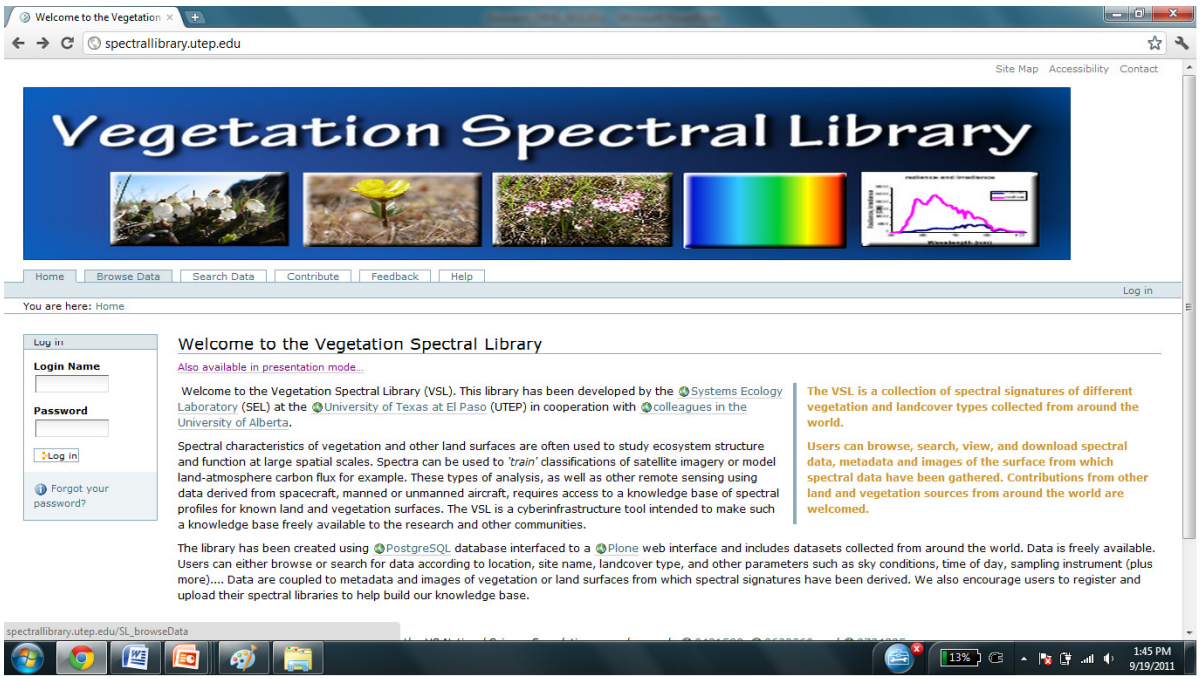

Figure 5.8. Plone web interface for the vegetation spectral library.

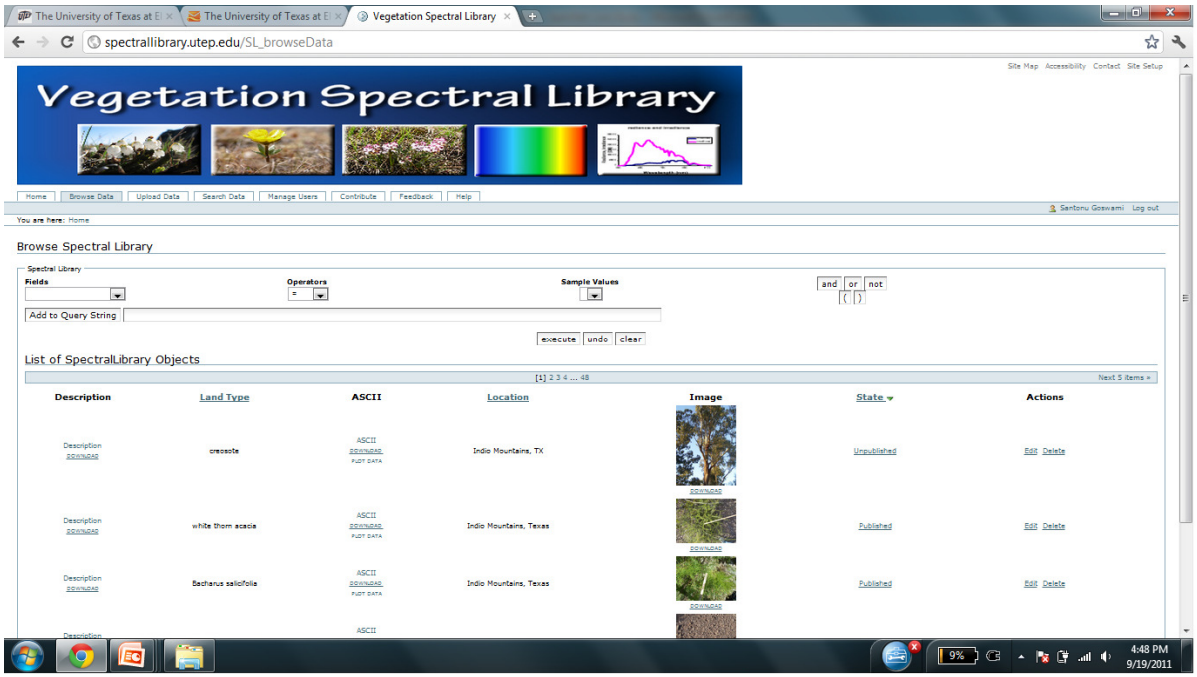

Figure 5.9. Screen shot of the Vegetation Spectral Library browsing data functionality.

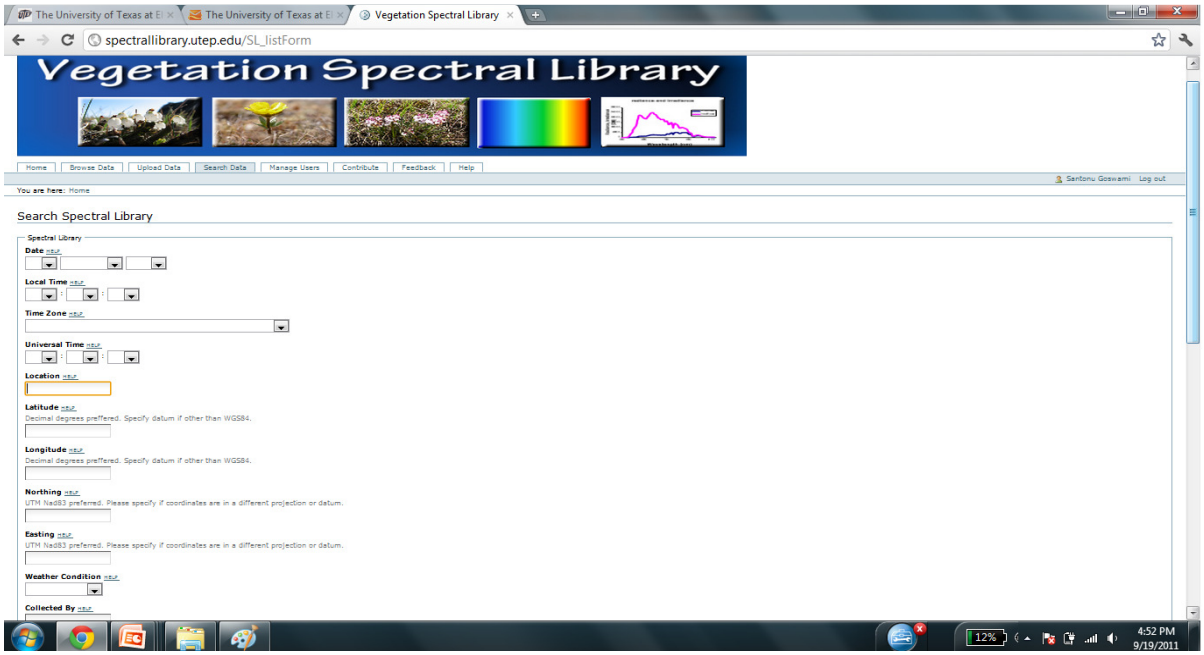

Figure 5.10. Screen shot of the Vegetation Spectral Library searching for data functionality.

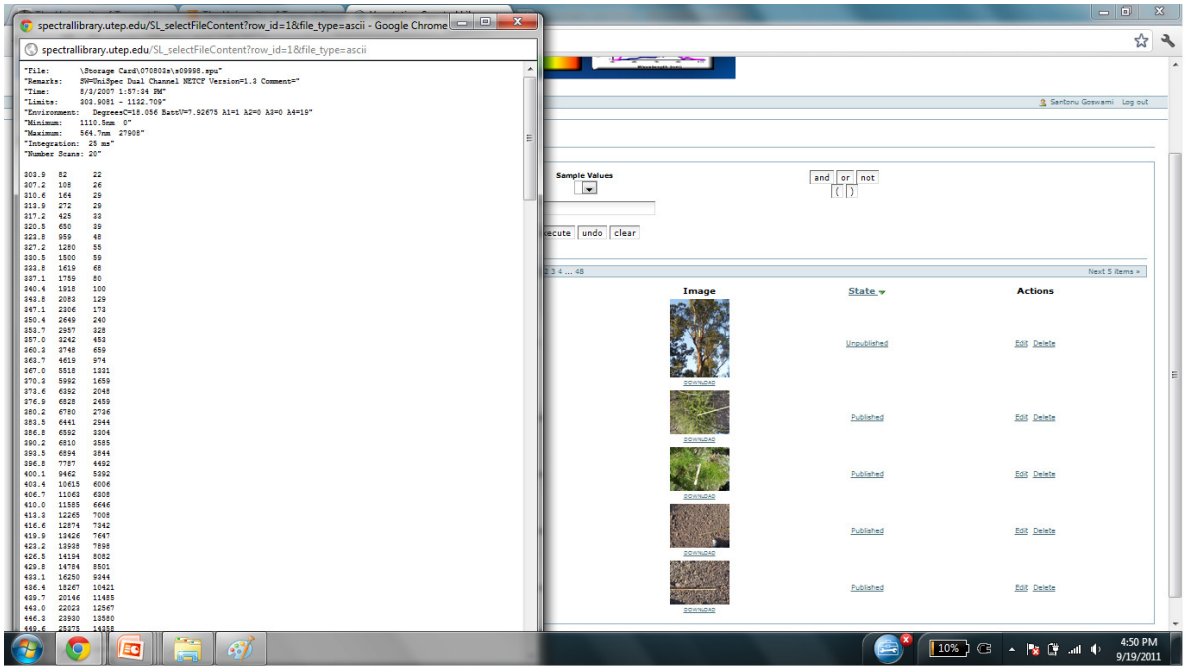

Figure 5.11. Screen shot of the Vegetation Spectral Library showing how spectral data files can be viewed online.

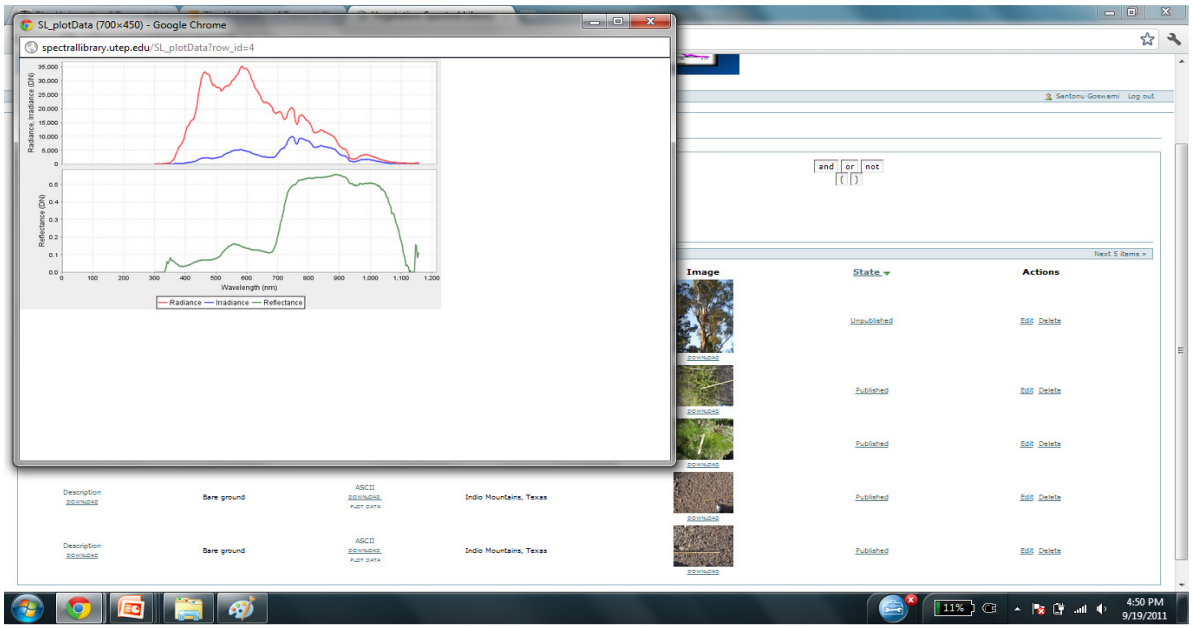

Figure 5.12. Screen shot of the Vegetation Spectral Library showing how plotting of spectra can be produced online on-the-fly.

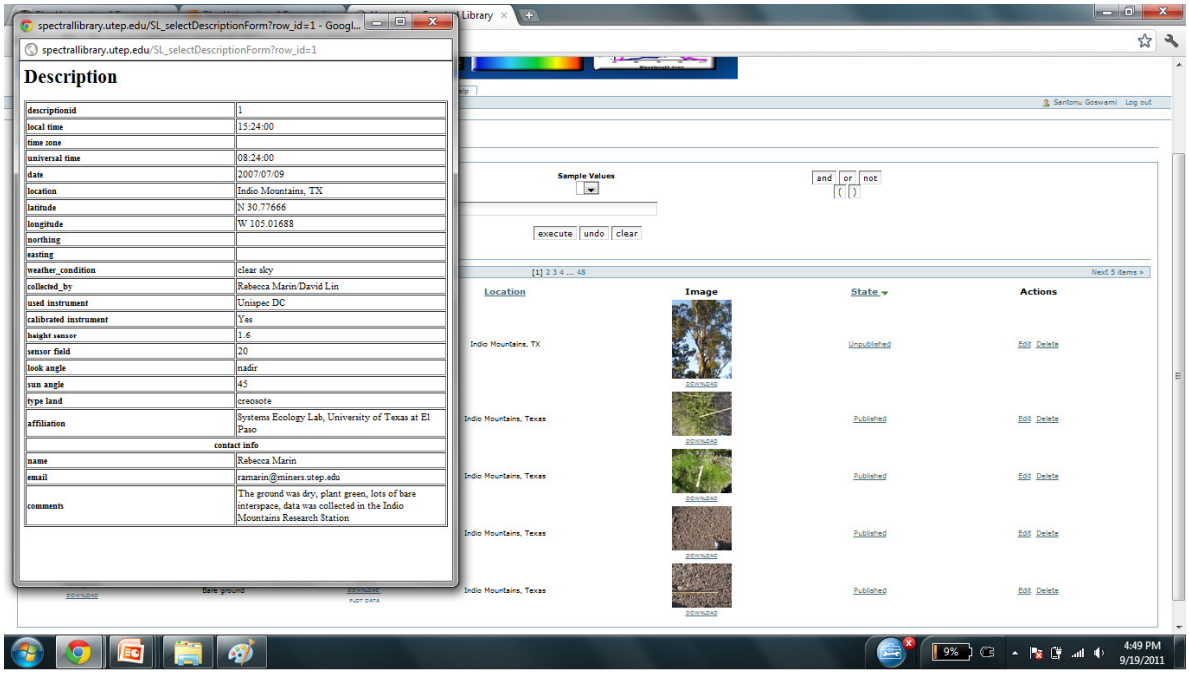

Figure 5.13. Screen shot of the Vegetation Spectral Library showing how metadata can be viewed online.

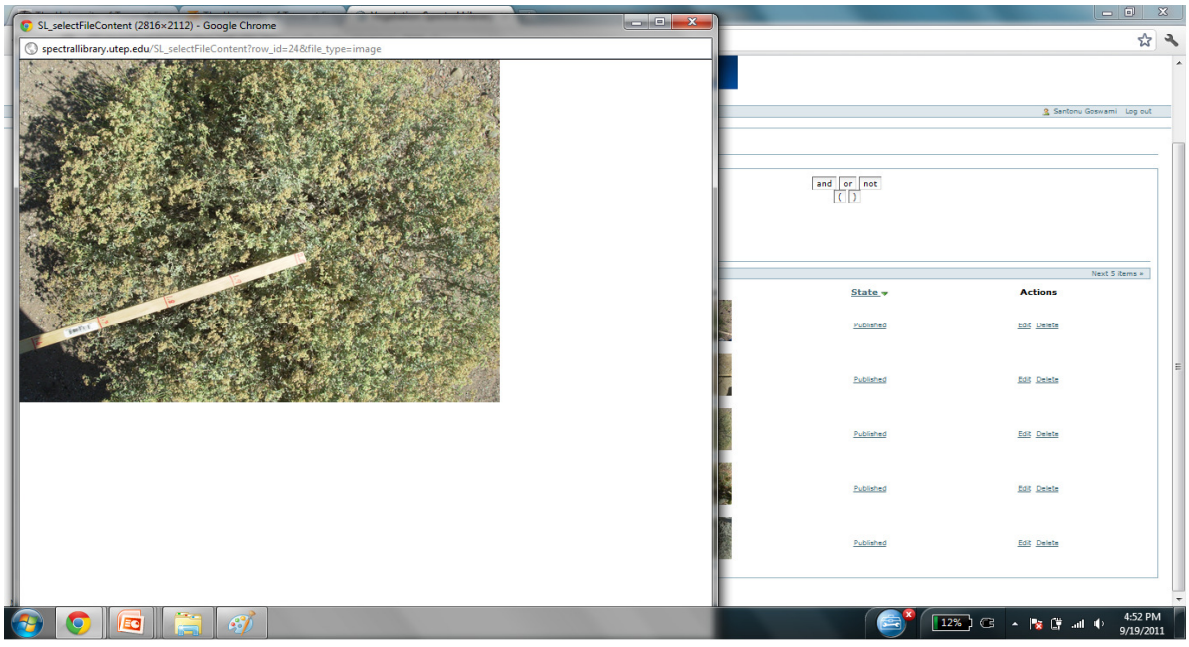

Figure 5.14. Screen shot of the Vegetation Spectral Library showing how images associated with a respective data file can be viewed online.

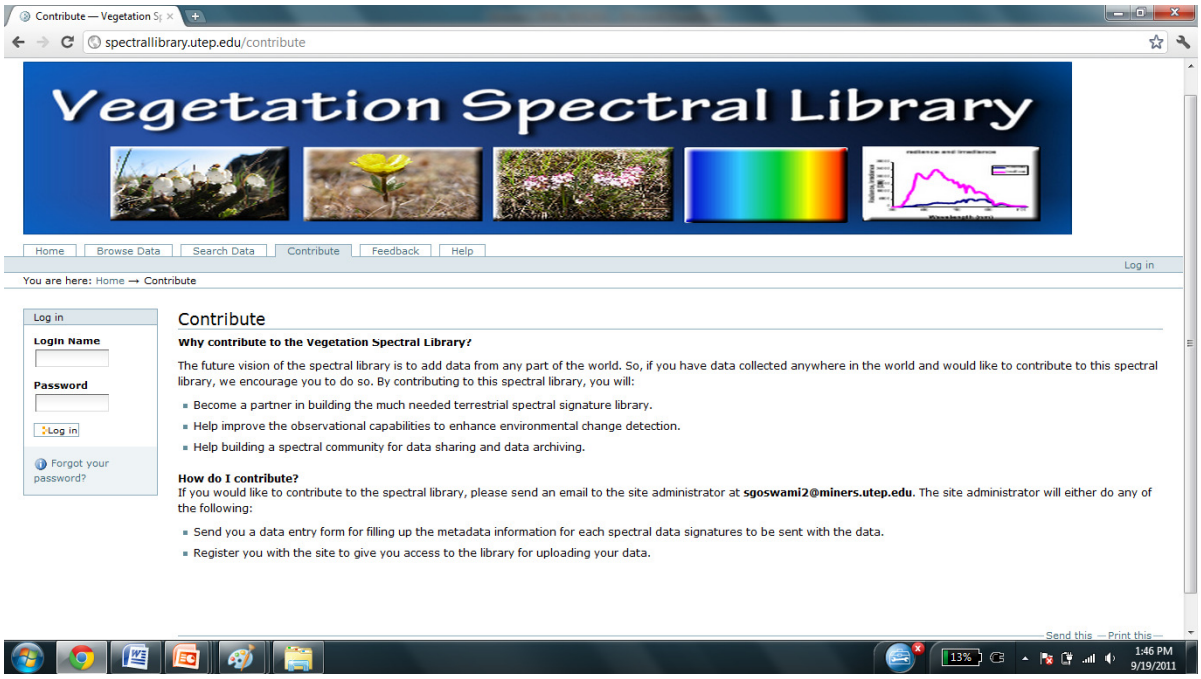

Figure 5.15. Screen shot of the Vegetation Spectral Library showing how requests to the library can be attained.

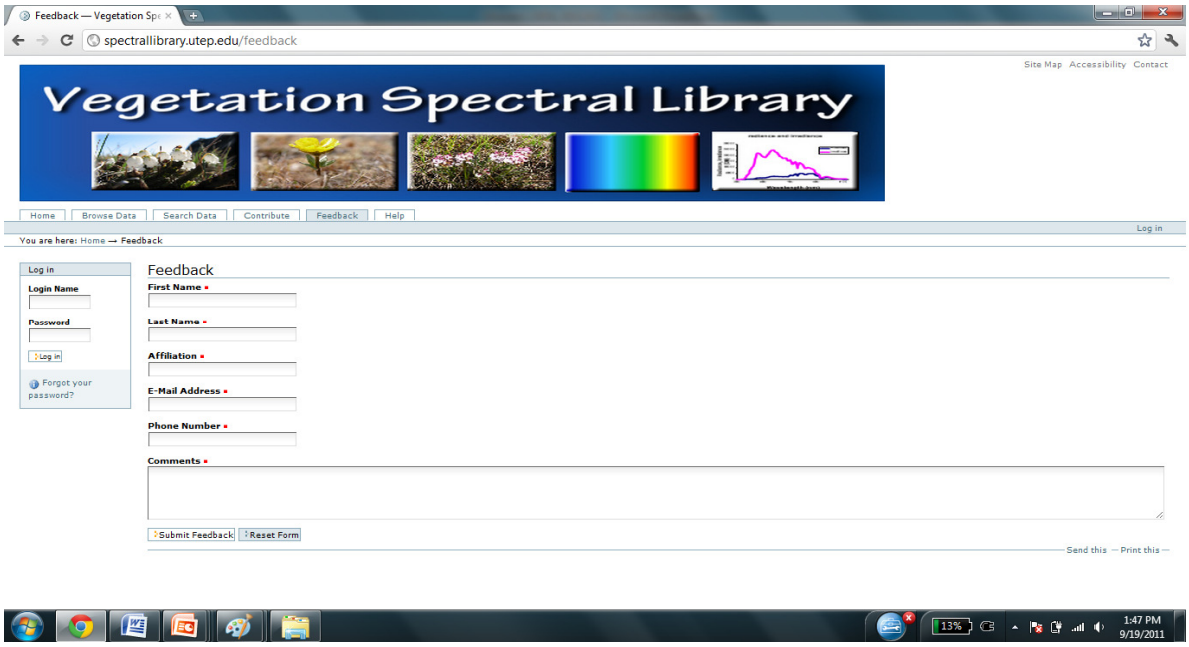

Figure 5.16. Screen shot of the Vegetation Spectral Library and the online form for data submission to the library. This form is available only to users approved by the administrator of the site.

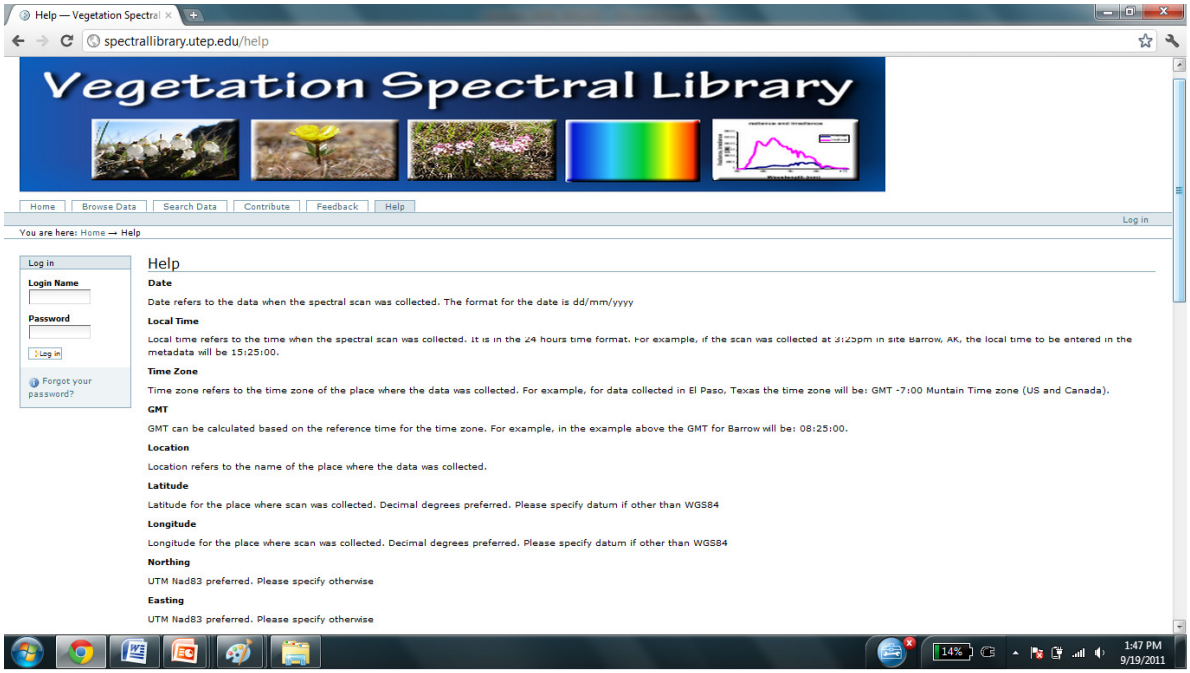

Figure 5.17. Screen shot of the Vegetation Spectral Library showing the help menu which is available online. Users can find detailed information about the metadata, data types available etc.

5.5.3 User statistics

Google analytics was added to the site in December 13, 2008 to track web traffic. This facilitates monitoring of visitors use the library and from they have accessed the site. The latter is providing important information for the potential geographic needs of the user community (Fig. 5.18). Statistics from Google analytics shows that during the period 12/01/2008 – 11/03/2011, a total of 2,179 users visited the site from 84 countries around the world. The top ten countries visiting the VSL were United States, Russia, India, Canada, Brazil, Germany, Taiwan, United Kingdom, Malaysia and Bulgaria (Table 5.2). Germany had the highest percent new visits with 86.67% and Taiwan had the lowest percentage of new visits at 2.5%.

Table 5.2. The following table shows the top ten countries by number of visitors and percent new visits during the period 12/01/2008 – 11/03/2011.

Country	Visits	% New Visits
United States	791	53.10
Russia	369	31.71
India	76	81.58
Canada	76	64.47
Brazil	73	19.18
Germany	45	86.67
Taiwan	40	2.50
United Kingdom	38	52.63
Malaysia	36	55.56
Bulgaria	34	50.00

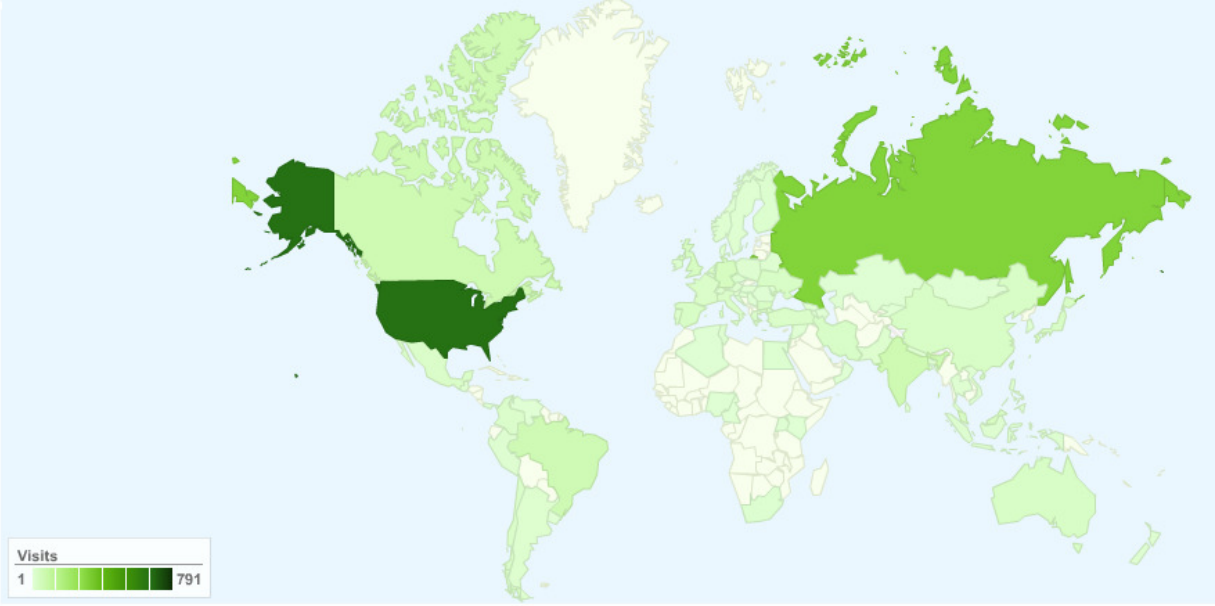

Figure 5.18. Country from which VSL was accessed during the period 12/13/2008 – 11/03/2011. The website had a total of 10,919 page views from 2,179 visitors from 84 countries and six continents.

5.6 Discussion

With newer and existing initiatives focused on environmental data collection and increasingly higher spatial and temporal resolutions and for larger areas of coverage (e.g. National Ecological Observatory Network (NEON), Ocean Observatories Initiative (OOI), Large-Scale, Engineering Analysis Network for Environmental Research (CLEANER), Flux Network (FluxNet), Spectral Network (SpecNet), AsiaFlux, EuroFlux), the volume and complexity of environmental data is likely to grow exponentially given the range of advancements in sensor and communication technologies. While the instrumentation and hardware performance has produced large volumes of complex data, it is becoming increasingly clear that such development needs to be coupled to the development of new cyberinfrastructure

to ensure that scientific needs are being met (NSF Cyberinfrastructure vision for the 21st century, 2007). To address the environmental science 'data paradox' there is a need for sophisticated data processing software, visualization tools, middleware and scientific applications to enhance scientific discovery and improved understanding.

Many of the greater challenges of data management facing the modern day data-driven environmental science projects were experienced in this project – the "data paradox". Many of these challenges were in part overcome through the exploration, adoption and development of various cyberinfrastructure, which included work flows and ontologies, data quality specification and verification tools, and a web based spectral library. The learning from the efforts documented in this chapter agrees with other similar environmental science studies (Keller et al. 2006, Williams et al. 2006) that automation of data quality control, processing and archiving, improved metadata documentation, the application of workflow and ontologies for documentation of data flows and scientific process greatly enhances the efficiency and effectiveness of the data collection, verification and management. Traditionally, ecological data has been difficult to discover, explore and use due to the many ad hoc data management solutions utilized, which often consisted of flat files or spreadsheets with minimal formal structure with little to no metadata documentation (Madin et al. 2007). Improved metadata documentation and development of ontologies and workflows provide a way for future data discovery and integration (Jones et al. 2006). Ontology and workflows for the robotic tramline system work as a first step towards documenting the data collection and data processing process from which other researchers are likely to benefit. The QA/QC software (DART) system uses a set of algorithms to determine the percentage of data falling within specified thresholds. Results

of automated checks are displayed in color-coded tables, plots and data assessment reports. The automated process of capturing uncertainty in data quality for the robotic tram data in near real time allow relatively untrained field assistants and new scientists unfamiliar with the system to specify and verify data properties in near real-time as data via post-processing. This feature has the capacity to help scientists identify anomalies in data and data assessment properties and procedures. The web based vegetation spectral library provides a relatively unique example of a web-based tool that can be used for data sharing and web-visualization of these data. User statistics demonstrate a clear need for these tools internationally. As these tools are refined further, it is hoped that large research collaborations such as SpecNet (Gamon et al. 2010, Gamon et al. 2006b) can act as a gateway for tool sharing with a broader community.

5.7. Conclusions

In this study, several new cyberinfrastructure tools have been developed for the robotic tram system associated with the biocomplexity experiment to address paradoxical data challenges typical within the environmental sciences. The experiences gained throughout the process were invaluable and provided first hand experiences and insights into how modern cyberinfrastructure can help a data intensive project. The work described is by no means a complete cyberinfrastructure for the robotic tram system but it is amongst the first to address several challenges that constrain the efficiency and effectiveness of the system. Although there are still numerous challenges that need to be met in order to develop a complete end to end cyberinfrastructure for the robotic tram system, the effort was successful.

Chapter 6: General Discussion

Compared to other ecoregions on Earth, the Arctic appears to be experiencing the most pronounced impacts from climate change (IPCC 2007, ACIA 2005). Recent observations indicate that the Arctic has undergone numerous changes over the past century (Kaufman et al. 2009). Significant and concurrent changes include a general greening of the Arctic since the 1980s (Bhatt et al. 2010, Myneni et al. 1997), increased shrub dominance (Sturm et al. 2005), a rise in permafrost temperature (Osterkamp and Romanovsky 1999), and a loss of arctic lake area (Smith et al. 2005).

This dissertation provides an investigation of ecosystem dynamics within a large-scale hydrological manipulation experiment using hyperspectral remote sensing and a robotic tram system. This study produced several key findings:

- A new spectral index was developed called the Normalized Difference Surface Water index (NDSWI, Goswami et al. 2011), which can be used to monitor vegetated the surface hydrological dynamics of tundra landscapes at multiple spatial scales (ground level to satellite level) throughout the snow free period.
- The presence of surface water showed a profound effect on reflectance spectra which are used to generate the Normalized Difference Vegetation Index (NDVI), a measure of above ground green plant biomass. Results suggest that decadal greening trends documented for the study area and elsewhere in the Arctic where standing surface water is prominent could be a result of drying in combination with, or instead of an increase in phytomass.

- NDVI increased exponentially with both LAI and Biomass for all the key species we studied. Findings from the decadal time extrapolation of plant cover values to biomass for the former IBP plots suggest that three species had increased biomass while three species had decreased biomass from 1972 to 2008. Our finding that biomass change occurred at different magnitudes for different species due to change in percent cover highlights the importance of understanding species level change in different tundra ecosystems in the Arctic landscape. The non-linearity in biomass change for some species over decadal time scale shows that greening trends in different tundra ecosystems in the Arctic might be non-linear or may be a result of a relatively small change in species cover.
- Development of modern cyberinfrastrucutre tools for improved hyperspectral reflectance data management and quality control were able to address some of the key data and informational challenges associated with this project, which generated large volumes of data. Similar challenges have been noted in other fields of environmental science, suggesting that solutions provided for this study could also be useful to other environmental science applications.

6.1. Synthesis of this Dissertation

Detailed discussions and summaries of individual research objectives are provided in each chapter. The following summarizes findings related to the specific objectives outlined in Section 1.4.

The aim of research objective 1 was to develop an optical remote sensing method that can estimate surface water depth (SWD) and surface water cover (SWC) for vegetated arctic tundra landscapes.

A spectral index was developed and named as the Normalized Difference Surface Water Index (NDSWI, Goswami et al. 2011). The index was able to accurately estimate SWC and SWD in the biocomplexity flooding and draining experimental area, which is situated in a vegetated thaw lake basin on the northern Arctic Coastal Plain of northern Alaska. We compared NDSWI to Equivalent Water Thickness (EWT) and the Water Band Index (WBI), two other spectral indices that have been widely used to estimate surface hydrological properties with remote sensing approaches (Green et al. 2006, Sims and Gamon 2003, Roberts et al. 1997, Gao and Goetz 1995, Penuelas et al. 1993), and found NDSWI was a better predictor of SWD, SWC, and WTD within the study area. Although this study shows a strong potential of NDSWI to be used as an index of SWD and SWC, we caution that further testing is required to determine the spatio-temporal scalability of NDSWI across multiple sensing platforms, and a broader range of land cover types, and regimes of surface hydrology than tested to date. This is particularly important for tundra landscapes where WTD is close to or above the ground surface, as surface water was shown to confound measurement of NDVI in such landscapes. Because NDSWI can be derived from a range of satellite platforms, it was possible to characterize the surface hydrology of the study area and evaluate the performance of the experimental flooding and draining experiment. Like many other large-scale experimental manipulations in the ecological sciences, the focal flooding and draining experiment used in this study was unreplicated, was a logistic and operational challenge, and displayed a high degree of 'natural' variability in land

cover and surface hydrology within and between treatment areas. A distinct advantage of NDSWI over the other spectral indices tested in this study is that it can be readily adapted to a range of satellite remote sensing platforms because of the commonality of the two wavebands used (460nm – blue, 1000nm – IR). Considering the importance of surface hydrology to ecosystem processes and properties such as carbon dioxide and methane flux (Merbold et al. 2009, Wolf et al. 2008), surface energy balance (Euskircken et al. 2007, Chapin et al. 2005), plant phenology and response to warming (Walker et al. 2006, Arft et al. 1999), and geomorphic processes (McNamara and Kane 2009, Lawrence and Slater 2005), the potential for NDSWI to facilitate the advancement of modeling and spatial extrapolation of these processes from plot to regional scales seems promising. Similar to how satellite-derived NDVI is increasingly being used to model land atmosphere carbon flux, leaf area index, or plant biomass (Running et al. 2004), we believe that, pending further testing and refinement, NDSWI could be applied in a similar manner to improve models of carbon dioxide or methane fluxes, which are highly dependent on surface hydrology (Merbold et al. 2009). If possible, this could facilitate the development of spatially explicit models that estimate net greenhouse warming potential through the combination of land-atmosphere carbon dioxide and methane flux models. Such development, including ground, air and satellite-based estimates of NDSWI, could be integrated within regional studies or observatories focused on carbon dynamics recommended recently by McGuire et al. (2009).

The aim of research objective 2 was to characterize five years of land-surface phenology in the study area using hyperspectral reflectance.

Seasonal and inter-annual dynamics of LSP were monitored in the study area to further understand how LSP responds to altered surface hydrology and interannual climatic and other environmental variability. The robotic tram system used in the study provided an excellent platform to make continuous and repeatable ground-based measurement of LSP over the study period 2005-2009. It was expected that substantial changes in LSP would occur in response to the flooding and draining experiment. Instead, little to no response was detected. The earliest snowmelt was recorded for 2006, which also showed the greatest peak season NDVI for the control and the drained treatment areas. The early snowmelt for 2006 was probably a result of snow being removed in early spring for construction of the extensions to the tramlines but supports previous finding that early snowmelt may lead to increased peak season productivity (Kimball et al. 2006). The effects of the hydrological treatments on LSP were subtle. Regression tree analysis suggested that the spatiotemporal variability in NDVI were strongly controlled by a gamut of factors that interact concomitantly and differ in their relative importance. WTD was, however, identified as a controlling factor in the spatiotemporal variability in NDVI. With increasing SWD, NDVI values were lowered and vice versa. This effect was more prominent in sampling areas with lower elevations with surface water cover. Further analyses of LSP along tramlines on specific dates of measurement at meter resolution highlighted the challenge of acquiring NDVI in the presence of surface water, which strongly interferes with spectra used to derive this index. In this detailed study, the importance of micro-topography to NDVI and surface water coverage was strongly apparent. Generally, low lying areas of the experimental

basin showed higher peak season NDVI compared to high elevation areas. This effect was more prominent in the flooded treatment area, which had greater topographic variability compared to the central and south treatment areas. Fluctuations in WTD and surface water cover had the greatest impact on low lying areas where NDVI decreased as WTD and surface water coverage increased. This phenomenon was observed between years, within a season and with environmental variability that was experienced over just a few days. Although there is likely to be some variability in the above ground green plant biomass that is measured as NDVI in such measurements, the majority of the variability experienced can be explained by surface water coverage, which appeared to be well described by NDSWI. When WTD was above ground, NDVI and NDSWI were negatively correlated and when WTD was below ground NDVI and NDWSI were weakly positively correlated. This relationship held in an analysis of a 2000-2010 MODIS 2km by 2km subset created for the study area, indicating that surface water could play an important role in determining how NDVI is determined at the satellite scale. The primary implication of this finding is that measurement of NDVI could be compromised as an indicator of arctic greening (*sensu* Bhatt et al, 2010, Jia et al, 2009) in areas where SWC prevails.

The aim of research objective 3 was to develop relationships between NDVI, Biomass and LAI for six key vascular plant species found in the study area.

The six species studied were *Arctophila fulva*, *Carex aquatilis*, *Dupontia fisheri*, *Eriophorum angustifolium*, Eriophorum scheuchzeri and *Petasites ftigidus*. NDVI values varied within a range of ~ 0.3, with corresponding differences in LAI and biomass also. The strong relationships between NDVI and biomass and LAI for all species studied support the use of

vegetation indices as an indicator of plant green biomass and landscape greenness in the Arctic. Further investigation of these relationships throughout the growing season could be helpful to further understand the seasonality of this relationship. The strong relationships between NDVI and biomass found in this study are similar to studies conducted in other arctic landscapes (Epstein et al. 2008, Boelman et al. 2003). Arctic vegetation is particularly sensitive to climate change (Walker et al. 2005, Epstein et al. 2000) and understanding how vegetation biomass changes over time and between different arctic ecosystems is an urgent challenge. Changes in vegetation biomass have important consequences for many components of the Arctic system including the status of the permafrost (Shiklomanov et al. 2010) and hydrology (Hinzman et al. 2005). Optical remote sensing is a valuable tool for assessing changes in biomass and LAI (Riedel et al. 2005, Pontailler et al. 2002) in response to climate change at multiple spatial and temporal scales (Boelman et al. 2003). Remote sensing is well suited to high latitude ecosystems because of the remoteness and the logistical challenges to working in these regions (Stow et al. 2004). Therefore, developing algorithms that relate spectral properties with ecosystem properties in plot level studies and assessing if these relationships hold at larger spatial scales is important for the scaling of uncertainty. To explore how these relationships might hold over decadal time scales, we used data from an International Polar Year Back to the Future (BTF) study (Villarreal et al. In review, Callaghan et al. 2011) near Barrow and modeled decadal time scale changes in biomass for the selected species from changes in percent cover data measured at this site several decades apart. Three species appear to have increased in biomass while three species had decreased in biomass between 1972 and 2008. This finding was similar to the findings of Lara et al. (Accepted) for plant community types dominated by the species studied. Our finding that

biomass change occurred at different magnitudes for different species due to change in percent cover highlights the importance of understanding how different species change in different tundra ecosystems in the Arctic landscape. This finding shows that rate of change in biomass for some species can be different and not necessarily related to cover, which could cause non-linear trends in greening in different tundra ecosystems and/or greening of such landscapes may be caused by a relatively small change in species cover.

The aim of research objective 4 was to develop and test cyberinfrastructure tools that enhance the collection and quality control of hyperspectral data for robotic tram systems.

The need for increased spatio-temporal monitoring using the robotic tramline project in the biocomplexity experiment faced similar challenges to the environmental sciences generally. Many of these challenges were in part overcome through the exploration, adoption and development of various cyberinfrastructure, which included work flows and ontologies, data quality specification and verification tools, and a web based spectral library. Traditionally, ecological data has been difficult to discover, explore and use due to the many ad hoc data management solutions utilized, which often consisted of flat files or spreadsheets with minimal formal structure with little to no metadata documentation (Madin et al. 2007). Improved metadata documentation and development of ontologies and workflows provide a way for future data discovery and integration (Jones et al. 2006). Ontology and workflows for the robotic tramline system work as a first step towards documenting the data collection and data processing processes from which other researchers are likely to benefit. The QA/QC software (DART) system uses a set of algorithms to determine the percentage of data falling within specified

thresholds. Results of automated checks are displayed in color-coded tables, plots and data assessment reports. The automated process of capturing uncertainty in data quality for the robotic tram data in near real time allowed relatively untrained field assistants and new scientists unfamiliar with the system to specify and verify data properties in near real-time via post-processing. This feature has the capacity to help scientists identify anomalies in data and data assessment properties and procedures. The web based vegetation spectral library provides a relatively unique example of a web-based tool that can be used for data sharing and web-visualization of these data. User statistics demonstrate a clear need for these tools internationally. As these tools are refined further, it is hoped that large research collaborations such as SpecNet (Gamon et al. 2010, Gamon et al. 2006b) can act as a gateway for tool sharing with a broader community. Several new cyberinfrastructure tools have been developed for the robotic tram system in this research objective to address the paradoxical data challenges associated with the system, which are similar within today's environmental sciences. The experiences gained throughout the process were invaluable and provided first hand experiences and insights into how modern cyberinfrastructure can help a data intensive project. The work described is by no means a complete cyberinfrastructure for the robotic tram system but it is amongst the first to address several challenges that constrain the efficiency and effectiveness of the system. We succeeded to some extent but there are still numerous challenges that need to be met in order to develop a complete end to end cyberinfrastructure for the robotic tram system.

6.2 Suggestions for Future Research

As discussed throughout this dissertation, reflectance signals were profoundly affected by the presence of surface water in the study area. This created aberrations in NDVI signals when surface water was present. NDVI is widely used as a metric for monitoring LSP in the Arctic as well as in the other ecosystems. Findings from this study indicate, however, that NDVI can be compromised when surface water is present. A combination of NDSWI and NDVI suggests that plant and water signals can be studied together and the likelihood of surface water interfering with plant signals can be assessed. Future research should consider studying the relationship between NDSWI and NDVI in greater detail and at more localities determine and optimize monitoring of LSP in the Arctic using remote sensing at multiple scales. Similar to NDVI, the newly developed index NDSWI can also be applied to sensors from multiple platforms including satellite based sensors.

Large scale studies have used NDVI derived from satellite based measurements to assess long-term changes in greenness of the circumpolar arctic (Bhatt et al. 2010, Myneni et al. 1997). Based on NDVI as an indicator of change, these studies have made conclusions about the magnitude and locations of "greening" which infers that mostly biomass production has increased in the circumarctic region. Our findings suggest that an increase in NDVI does not necessarily imply an increase in biomass, but may also be due to the drying of arctic landscapes not taken into account by these larger scale and lower resolution studies. Future research should explore these effects at multiple spatial scales to investigate the "greening of the Arctic" may also be an indicator of a drying of the Arctic.

This dissertation strongly supports the need for the development of modern end to end cyberinfrastructure system and advanced instrumentation in data-intensive environmental science projects through interdisciplinary collaboration. In this study we have made an effort to develop cyberinfrastructure for the robotic tram system associated with the biocomplexity experiment to address key data challenges. The experiences gained throughout the process were invaluable and provided first hand experiences and insights into how modern cyberinfrastructure can help a data intensive project such as this one. Further research should consider the design and development of cyberinfrastructure for enhanced automatic operation.

6.3 Conclusions

This chapter concludes this dissertation by integrating and summarizing various research objectives posed in Section 1.4 and throughout the dissertation research. Overall findings further highlight the challenges of multi-scale remote sensing in arctic landscapes and provide improved understanding of several ecosystem properties and processes, and how these are best measured with remote sensing approaches. Additionally, this study showed that existing capacities for interdisciplinary environmental research were improved through cyberinfrastructure development.

References

Adams J.B., & Gillespie, J.R. (2006) Remote *Sensing of Landscapes with Spectral Images: A Physical Modeling Approach*, Cambridge University Press, Cambridge.

ACIA. (2005). Impacts of a Warming Arctic: Arctic Climate Impact Assessment. *Cambridge University Press, Cambridge*.

Aguirre A., Tweedie C.E., Brown J., Gaylord A., (2008). Erosion of the Barrow Environmental Observatory Coastline 2003–2007, Northern Alaska, *Proceedings of the Ninth International Conference on Permafrost, Fairbanks, Alaska USA*.

AON Report: Toward an Integrated Arctic Observing Network, (2006). *National Academics Press.*

Arft, A. M., Walker, M. D., Gurevitch, J., Alatalo, J. M., Bret-Harte, M. S., Dale, M., Diemer, M., Gugerli, F., Henry, G. H. R., Jones, M. H., Hollister, R. D., Jonsdottir, I. S., Laine, K., Levesque, E., Marion, G. M., Molau, U., Molgaard, P., Nordenhall, U., Raszhivin, V., Robinson, C. H., Starr, G., Stenstrom, A., Stenstrom, M., Totland, O., Turner, P. L., Walker, L. J., Webber, P. J., Welker, J. M., Wookey, P. A., (1999). Responses of tundra plants to experimental warming: meta-analysis of the international tundra experiment. *Ecological Monographs*, 69, 491-511.

Arndal M.F., Illeris L., Michelsen A., Albert K., Tamstorf M. P., Hansen B. U., (2009). Seasonal variation in gross primary production, plant biomass, and carbon nitrogen pools in five high arctic vegetation types, *Arctic Alpine Research*, 41, 164 – 173.

Baader, F., D. Calvanese, D. McGuinness, D. Nardi, P. Patel-Schneider (2003). The Description Logic Handbook: Theory, Implementation, and Applications. Cambridge University Press.

Bard, J. R. L., S. Y. Rhee (2004). Ontologies in biology: design, applications and future challenges. Nat. Rev., Genet. 5, 213–222.

Batini, C., S. Ceri, S. B. Navathe (1992). ConceptualDatabaseDesign:An Entity-Relationship Approach. Benjamin Cummings, Redwood City, CA.

Bhatt, U. S., D. A. Walker, M. K. Reynolds, J. C. Comiso, H. E. Epstein, G. S. Jia, R. Gens, J. E. Pinzon, C. J. Tucker, C. E. Tweedie & P. J. Webber (2010). Circumpolar arctic tundra vegetation change is related to sea ice decline, *Earth Interactions*, 14.

Bockheim, J. G., L. R. Everett, K. M. Hinkel, F. E. Nelson & J. Brown (1999). Soil organic carbon storage and distribution in arctic tundra, Barrow, *Soil Science Society of America Journal*, 63, 934-940.

Boelman, N. T., M. Stieglitz, et al. (2003). Response of NDVI, biomass, and ecosystem gas exchange to long-term warming and fertilization in wet sedge tundra. *Oecologia* 135(3): 414-421.

Brando V. E., Anstee J. M., Wettle M., Dekker A. G., Phinn S. R., Roelfsema C. (2009). A physics based retrieval and quality assessment of bathymetry from suboptimal hyperspectral data, *Remote Sensing of Environment,* 113, 755–770.

Brock J.C., Wright C.W., Clayton T.D., A. Nayegandhi, (2004). Lidar optical rugosity of coral reefs in Biscayne National Park, Florida, *Coral Reefs,* 23(1), 48–59.

Brock J.C., Wright C.W., Kuffner I.B., Hernandez R., Thompson P., (2006). Airborne lidar sensing of massive stony coral colonies on patch reefs in the northern Florida reef tract, *Remote Sensing of Environment,* 104(1), 31–42.

Brown J, Miller P. C., Tieszen L. L., Bunnel F. L. (1980). An Arctic Ecosystem: the Coastal Tundra at Barrow, Alaska, *Stroudsburg, Pa.: Dowden, Hutchinson & Ross*, (US/IBP synthesis series; v. 12)**,** 571.

Callaghan, T. V., C. E. Tweedie et al. (2011). Multi-Decadal Changes in Tundra Environments and Ecosystems: Synthesis of the International Polar Year-Back to the Future Project (IPY-BTF), AMBIO, 40(6):705-716.

Callaghan, T. V., L. O. Bjorn, Y. Chernov, T. Chapin, T. R. Christensen, B. Huntley, R. A. Ims, M. Johanasson, D. Jolly, S. Jonasson, N. Matveyeva, N. Panikov, W. Oechel, G. Shaver, S. Schaphoff & S. Sitch (2004). Effects of changes in climate on landscape and regional processes, and feedbacks to the climate system, *Ambio*, 33, 459-468.

Chapin F. S., Sturm M., Serreze M. C., McFadden J. P., Key J. R., Lloyd A. H., McGuire A. D., Rupp T. S., Lynch A. H., Schimel J. P., Beringer J., Chapman W. L., Epstein H. E., Euskirchen E. S., Hinzman L. D., Jia G., Ping C.-L., Tape K. D., Thompson C. D. C., Walker D. A., Welker J. M., (2005). Role of Land Surface Changes in Arctic Summer Warming, *Science* 310:5748, 657-660.

Chen, P.P., (1976). The entity-relationship model: toward a unified view of data. ACM TODS 1, 9–36.

Curry, R. C. Kiddle, R. Simmonds, G. Z. Pastorello (2011). An On-line Collaborative Data Management System, Proceedings of Gateway Computing Environments Workshop (GCE) IEEE.

Engstrom R, Hope A , Kwon H, Stow D, (2008). The relationship between soil moisture and NDVI near Barrow, Alaska, *Physical Geography*, 29(1), 38-53.

Euskirchen E . S., Mcguire A. D., Chapin F.S. (2007), Energy feedbacks of northern high-latitude ecosystems to the climate system due to reduced snow cover during 20th century warming, *Global Change Biology*, 13, 2425–2438.

Gallegos I., S. Goswami, A. Q. Gates, C. E. Tweedie, J. A. Gamon (2011). Towards Near-Real Time Data Property Specification and Verification for Arctic Hyperspectral Sensor Data, In *Proceedings of the North American Fuzzy Information Processing Society Conference (NAFIPS) 2011*.

Gamon J. A., C. Coburn, L. B. Flanagan, K. F. Huemmrich, C. Kiddle, G. A. Sanchez-Azofeifa, D. R. Thayer, L. Vescovo, D. Gianelle, D. A. Sims, A. F. Rahman, G. Z. Pastorello (2010). SpecNet revisited: bridging flux and remote sensing communities, *Canadian Journal of Remote Sensing*, 2010, 36:(S2) S376-S390, 10.5589/m10-067

Gamon, J. A., Y. F. Cheng, H. Claudio, L. MacKinney & D. A. Sims (2006a) A mobile tram system for systematic sampling of ecosystem optical properties. *Remote Sensing of Environment,* 103, 246-254.

Gamon, J. A., A. F. Rahman, J. L. Dungan, M. Schildhauer & K. F. Huemmrich (2006b) Spectral Network (SpecNet) - What is it and why do we need it? *Remote Sensing of Environment,* 103, 227-235.

Gamon, J. A., K. Kitajima, et al. (2005). "Diverse optical and photosynthetic properties in a neotropical dry forest during the dry season: Implications for remote estimation of photosynthesis." Biotropica **37**(4): 547-560.

Gamon, J. A., L. Serrano, J. S. Surfus (1997). The photochemical reflectance index: an optical indicator of photosynthetic radiation use efficiency across species, functional types, and nutrient levels. *Oecologia*, 112(4), 492-501.

Ganguly S., Schull M. A., Samanta A., Shabanov N. V., Milesi C., Nemani R. R., Knyazikhin Y., Myneni R. B., (2008). Generating vegetation leaf area index earth system data record from multiple sensors. Part 1: Theory, *Remote Sensing of Environment*, 112, 4333 – 4343.

Gao B.C. and Goetz A.F.H. (1995). Retrieval of equivalent water thickness and information related to biochemical components of vegetation canopies from AVIRIS data, *Remote Sensing of Environment*, 52 (3), 155–16.

Gao, B.C. (1996). NDWI – A normalized difference water index for remote sensing of vegetation liquid water from space, *Remote Sensing of Environment*, 58(3), 257-266.

Gates, A. Q., G. R. Keller, F. Salcedo, P. Pinheiro da Silva, L. Salayandia (2007). The Gravity Data Ontology: Laying the Foundation for Workflow-Driven Ontologies. In *Proceedings of the Second International Conference on Geospatial Semantics*, Mexico City, Mexico, November 29-30, 2007.

Goswami, S., J. A. Gamon, and C. E. Tweedie (2011), Surface hydrology of an arctic ecosystem: Multiscale analysis of a flooding and draining experiment using spectral reflectance, *J. Geophys. Res.*, *116*, G00I07, doi:10.1029/2010JG001346.

Green R. O., Painter T. H., Roberts D. A., and Dozier J., (2006). Measuring the expressed abundance of the three phases of water with an imaging spectrometer over melting snow, *Water Resources Research*, 42(10), W10402.1-W10402.12.

Hammer, J., D. McLeod (1999). Resolution of representational diversity in multidatabase systems. In: Elmagarmid, A., M. Rusinkiewicz, A. Sheth (Eds.), Management of Heterogeneous and Autonomous Database Systems, vol. 4. Morgan Kaufmann, San Francisco, pp. 91–117. 413 pp.

Hinkel K.M., Eisner W. R., Bockheim J. G., Nelson F. E., Peterson K. M., Dai X., (2003). Spatial Extent, Age, and Carbon Stocks in Drained Thaw Lake Basins on the Barrow Peninsula, Alaska, *Arctic, Antarctic, and Alpine Research*, 35(3), 291-300.

Hinzman L. D., Bettez N. D., Bolton W. R., Chapin F. S., Dyurgerov M. B., Fastie C. L., Griffith B., Hollister R. D., Hope A., Huntington H. P., Jensen A. M., Jia G. J., Jorgenson T., Kane D. L., Klein D. R., Kofinas G., Lynch A. H., Lloyd A. H., McGuire A. D., Nelson F. E., Oechel W. C., Osterkamp T. E., Racine C. H., Romanovsky V. E., Stone R. S., Stow D. A., Sturm M., Tweedie C. E., Vourlitis G. L., Walker M. D., Walker D. A., Webber P. J., Welker J. M., Winker K. S., Yoshikawa K., (2005). Evidence and implications of recent climate change in terrestrial regions of the Arctic, *Climate Change*, 72, 251-298.

Hobbie, J. E., B. J. Peterson, N. Bettez, L. Deegan, W. J. O'Brien, G. W. Kling, G. W. Kipphut, W. B. Bowden & A. E. Hershey (1999). Impact of global change on the biogeochemistry and ecology of an Arctic freshwater system. *Polar Research,* 18, 207-214.

Hochberg E. J., Atkinson M. J., Andréfouët S. (2003). Spectral reflectance of coral reef bottom-types worldwide and implications for coral reef remote sensing. *Remote Sensing of Environment,* 85, 159 –173.

Hope A. S., Pence K. R., Stow D. A., (2004). NDVI from low altitude aircraft and composited NOAA AVHRR data for scaling Arctic ecosystem fluxes, *International Journal of Remote Sensing*, 25(20), 4237 – 4250.

Hudson J. M. G., G. H. R. Henry (2009). Increased plant biomass in a High Arctic heath community from 1981 to 2008, *Ecology*, 90(10), 2657-2663.

Huemmrich K.F., Kinoshita G., Gamon J.A., Houston S., Kwon H., Oechel W.C. (2010) Tundra Carbon Balance Under Varying Temperature and Moisture Regimes. *Journal of Geophysical Research, 115, GOOI02,doi: 10.1029/2009JG001237.*

Illeris L., Christensen T. R., Masterpanov M., (2004). Moisture effects on temperature sensitivity of CO_2 exchange in a subarctic heath ecosystem, *Biogeochemistry*, 70(3), 315-330.

IPCC, 2007: Summary for Policymakers. In: Climate Change 2007: The Physical Science Basis. Contribution of Working Group I to the Fourth Assessment Report of the Intergovernmental Panel on Climate Change [Solomon, S., D. Qin, M. Manning, Z. Chen, M. Marquis, K.B. Averyt, M.Tignor and H.L. Miller (eds.)]. Cambridge University Press, Cambridge, United Kingdom and New York, NY, USA.

Irish J. L. and White T. E., (1998). Coastal engineering applications of high-resolution lidar bathymetry*, Coastal Engineering*, 35(1-2), 47 – 71.

Jia, G. S. J., H. E. Epstein & D. A. Walker (2003). Greening of arctic Alaska, 1981-2001. *Geophysical Research Letters,* 30.

Jonasson S., Castro J., Michelsen A., (2004). Litter, warming and plants affect respiration and allocation of soil microbial and plant C, N and P in arctic mesocosms, *Soil Biology and Biochemistry*, 36(7), 1129 – 1139.

Jones, M.B., Schildhauer, M., Reichman, O.J., Bowers, S. (2006). The New Bioinformatics: integrating ecological data from the gene to the biosphere. Ann. Rev. Ecol. Evol. Syst. 37, 519–544.

Kasischke E. S., Bourgeau-Chavez L. L., Rober A. R., Wyatt K. H., Waddington J. M., Turetsky M. R. (2009). Effects of soil moisture and water depth on ERS SAR backscatter measurements from an Alaskan wetland complex, *Remote Sensing of Environment*, 113, 1868–1873.

Kaufman, D. S., D. P. Schneider, N. P. McKay, C. M. Ammann, R. S. Bradley, K. R. Briffa, G. H. Miller, B. L. Otto-Bliesner, J. T. Overpeck & B. M. Vinther (2009). Recent Warming Reverses Long-Term Arctic Cooling, *Science,* 325, 1236-1239.

Kimball J. S., Zhao M., McDonald K.C., Running S.W., (2006). Satellite Remote Sensing of Terrestrial Net Primary Production for the Pan-Arctic Basin and Alaska, *Mitigation and Adaptation Strategies for Global Change*, 11(4), 783-804.

La Puma, I. P., T. E. Philippi, et al. (2007). Relating NDVI to ecosystem CO2 exchange patterns in response to season length and soil warming manipulations in arctic Alaska, Remote Sensing of Environment, 109(2): 225-236.

Laidler G.J, Paul M., Treitz P.M., Atkinson D.M. (2008). Remote Sensing of Arctic Vegetation: Relations between the NDVI, Spatial Resolution and Vegetation Cover on Boothia Peninsula, Nunavut, *Arctic*, 61(1), 1-3.

Liljedahl, A.K., L. D. Hinzman, Y. Harazono, D. Zona D., C. E. Tweedie, R. D. Hollister, R. Engstrom, W. C. Oechel (2011). Nonlinear controls on evapotranspiration in Arctic coastal wetlands, Biogeosciences Discuss., 8, 6307-6344, 2011, doi:10.5194/bgd-8-6307-2011.

Lara M. J., S. Villarreal, D. R. Johnson[1], R. D. Hollister, P. J. Webber, C. E. Tweedie, Estimated change in tundra ecosystem function from 1972 to 2010 near Barrow Alaska, Accepted, Environmental Research Letters.

Lawrence, D. M., and A. G. Slater (2005), A projection of severe near-surface permafrost degradation during the 21st century, *Geophysical Research Letters*, 32, L24401.

Lepers, E., E. F. Lambin, A. C. Janetos, R. DeFries, F. Achard, N. Ramankutty & R. J. Scholes (2005). A synthesis of information on rapid land-cover change for the period 1981-2000, *Bioscience,* 55, 115-124.

Mazéas, O., Von Fischer J. C., Rhew R. C., (2009). Impact of terrestrial carbon input on methane emissions from an Alaskan Arctic lake, *Geophysical Research Letters*, 36, L18501, doi:10.1029/2009GL039861.

McGuire D. A., Chapin F. S., Walsh J. E., Wirth C., (2006). Integrated regional changes in arctic climate feedbacks: Implications for the global climate system, *Annual review of environment and resources*, 31, 61-91.

McGuire D. A., Anderson L. G., Christensen T. R., Dallimore S., Guo L., Hayes D. J., Heimann M., Lorenson T. D., Macdonald R. W., Roulet N., (2009). Sensitivity of the carbon cycle in the Arctic to climate change, *Ecological Monographs*, 79(4), 523-555.

McNamara J. P., Kane D. L., (2009). The impact of a shrinking cryosphere on the form of arctic alluvial channels, *Hydrological Process*, 23, 159–168.

Meade NG, Hinzman LD, Kane DL, (1999). Spatial estimation of soil moisture using synthetic aperture radar in Alaska, Satellite Applications for Energy Budgets and the Hydrological Cycle, Book Series: *Advances in Space Research*, 24(7), 935-940.

Merbold L., Kutsch W. L., Corradi C., Kolle O., Rebmann C., Stoy P. C., Zimov S. A., Schulze E. D., (2009). Artificial drainage and associated carbon fluxes (CO_2/CH_4) in a tundra ecosystem, *Global Change Biology*, 15(11), 2599-2614.

Miller, L. L., Allard M., Hinkel, K. M., Nelson, F. E., Outcalt, S. I., Paetzold, R. F. (1998). Spatial and temporal patterns of soil moisture and thaw depth at Barrow, Alaska, U.S.A. *Collection Nordicana*, 57, 731-737.

Myneni, R. B., C. D. Keeling, C. J. Tucker, G. Asrar & R. R. Nemani (1997). Increased plant growth in the northern high latitudes from 1981 to 1991, *Nature,* 386, 698-702.

National Science Foundation (2007). Cyberinfrastructure Vision for 21st Century Discovery, March 2007.

Oberbauer S. F., Tweedie C. E., Welker J. M., Fahnestock J. T., Henry G. H. R., Webber P. J., Hollister R. D., Walker R. D., Kuchy A., Elmore E., Starr G., (2007). Tundra CO_2 fluxes in response to experimental warming across latitudinal and moisture gradients, *Ecological Monographs*, 77(2), 221-238.

Olivas, P. C., S. F. Oberbauer, C. E. Tweedie, W. C. Oechel, D. Lin, A. Kuchy (2011). Effects of Fine-Scale Topography on CO(2) Flux Components of Alaskan Coastal Plain Tundra:

Response to Contrasting Growing Seasons, Arctic Antarctic and Alpine Research 43(2): 256-266.

Olivas, P. C., S. F. Oberbauer, C. E. Tweedie, W. C. Oechel, A. Kuchy (2010). Responses of CO(2) flux components of Alaskan Coastal Plain tundra to shifts in water table, Journal of Geophysical Research-Biogeosciences 115.

Olthof, I., D. Pouliot, R. Latifovic & W. J. Chen (2008). Recent (1986-2006) Vegetation-Specific NDVI Trends in Northern Canada from Satellite Data, *Arctic,* 61, 381-394.

Osterkamp, T. E. & V. E. Romanovsky (1999). Evidence for warming and thawing of discontinuous permafrost in Alaska, *Permafrost and Periglacial Processes,* 10, 17-37.

Peters, D. P. C., P. M. Groffman, K. J. Nadelhoffer, N. B. Grimm, S. L. Coffins, W. K. Michener & M. A. Huston (2008) Living in an increasingly connected world: a framework for continental-scale environmental science. *Frontiers in Ecology and the Environment,* 6, 229-237.

Peñuelas, J., Filella, I., Biel, C., Serrano, L., Savé, R. (1993). The reflectance at the 950–970 nm region as an indicator of plant water status, *International Journal of Remote Sensing*, 14(10), 1887-1905.

Petrescu, A. M. R., Huissteden, J., Jackowicz-Korczynski, M., Yurova, A., Christensen, T. R., Crill, P. M., Bäckstrand, K., and Maximov, T. C. (2008). Modeling CH_4 emissions from arctic wetlands: effects of hydrological parameterization, *Biogeosciences Discuss*, 5, 3195–3227.

Phinn S., C. Roelfsema, A. Dekker, V. Brando, J. Anstee (2008). Mapping seagrass species, cover and biomass in shallow waters: An assessment, of satellite multi-spectral and

airborne hyper-spectral imaging systems in Moreton Bay (Australia), *Remote Sensing of Environment*, 112, 3413–3425.

Pickett, S.T.A., J. Kolasa, C. G. Jones (1994). Ecological Understanding: The Nature of Theory and the Theory ofNature. Academic Press, San Diego.

Ping Chien-Lu, Michaelson G. J., Jorgenson M. T., Kimble J. M., Epstein H., Romanovsky V. E., Walker D. A. (2008). High stocks of soil organic carbon in the North American Arctic region, *Nature Geoscience,* 1, 615 – 619.

Pinheiro da Silva, Paulo; L. Salayandia, A. Q. Gates (2007). WDO-It! A Tool for Building Scientific Workflows from Ontologies. *Departmental Technical Reports (CS).* Paper 201.

Post E., Forchhammer M. C., Bret-Harte M. S., Callaghan T. V., Christensen T. R., Bo Elberling, Fox A. D., Gilg O., Hik D. S., Høye T. T., Ims R. A., Jeppesen E., Klein D. R., Madsen J., McGuire D. A., Rysgaard S., Schindler D. E., Stirling I., Tamstorf M. P., Tyler N. J. C., van der Wal R., Welker J., Wookey P. A., Schmidt N. M., Aastrup P. (2009). Ecological Dynamics Across the Arctic Associated with Recent Climate Change, *Science*, 325, 5946, 1355-1358.

Roberts D. A, Green R. O., Adams J. B., (1997). Temporal and spatial patterns in vegetation and atmospheric properties from AVIRIS, *Remote sensing of environment*, 62(3), 223-240.

Rosse, C., J. L. V. Mejino Jr. (2003). A reference ontology for bioinformatics: the Foundational Model of Anatomy. J. Biomed. Inform. 36, 478–500.

Running S. W., Nemani R. R., Heinsch F. A., Zhao M., Reeves M., Hashimoto H., (2004). A continuous satellite-derived measure of global terrestrial primary production. *BioScience*. 54(6), 547-560.

Sanchez –Azofeifa G, Castro K, Wright S. J., Gamon J., Rivard B., Kalacska M., Schnitzer S. (2009). Differences in leaf traits, leaf internal structure, and spectral reflectance between two communities of lianas and trees : Implications for remote sensing in tropical environments. *Remote Sensing of Environment.* 113(10), 2076-2088.

SAON Report: Observing the Arctic: Report of the Sustaining Arctic Observing Network Initiative Group, www.arcticobserving.org, available, December, (2008).

Salayandia, S., P. Pinheiro da Silva, A. Q. Gates, F. Salcedo (2006). Workflow-Driven Ontologies: An Earth Sciences Case Study. *Proceedings of the 2nd IEEE International Conference on e-Science and Grid Computing*, p. 17, Amsterdam, Netherlands, December 2006.

Schuur, E. A. G. and B. Abbott (2011). Climate change: High risk of permafrost thaw, *Nature* 480, 32–33, doi:10.1038/480032a.

SEARCH: Study of Environmental Arctic Change: Plans for Implementation During the International Polar Year and Beyond. Report of the SEARCH Implementation Workshop, May 23 - 25, 2005.

Serrano L., Ustin S. L., Roberts D. A., Gamon J. A., Penuelas J., (2000). Deriving Water Content of Chaparral Vegetation from AVIRIS Data, *Remote Sensing of Environment*, 74(3), 570–581.

Serreze, M. C., J. E. Walsh, F. S. Chapin, T. Osterkamp, M. Dyurgerov, V. Romanovsky, W. C. Oechel, J. Morison, T. Zhang & R. G. Barry (2000). Observational evidence of recent change in the northern high-latitude environment, *Climatic Change,* 46, 159-207.

Sims D. A., Gamon J. A., (2003). Estimation of vegetation water content and photosynthetic tissue area from spectral reflectance: a comparison of indices based on liquid water and chlorophyll absorption features, *Remote Sensing of Environment*, 84(4), 526–537.

Sitch S., McGuire A. D., Kimball J., Gedney N., Gamon J., Engstrom R., Wolf A., Zhuang Q., Clein J., McDonald K. C. (2007). Assessing the Carbon Balance of Circumpolar Arctic Tundra Using Remote Sensing and Process Modeling, *Ecological Applications*, 17(1), 213-234.

Smith, L.C., Sheng, Y., MacDonald, G.M., Hinzman, L.D. (2005). Disappearing Arctic Lakes. *Science* 308(5727):1429, DOI: 10.1126/science.1108142.

Smith L.C. (1997). Satellite Remote Sensing of River Inundation Area, Stage, and Discharge: A Review, *Hydrological Processes*, 11, 1427 – 1429.

Storlazzi C.D., Logan J.B. and Field M.E., (2003). Quantitative morphology of a fringing reef tract from high-resolution laser bathymetry: Southern Molokai, Hawaii, *Geological Society of America Bulletin* 115, 1344–1355.

Stow, D.A., Hope A., McGuire D., Verbyla D., Gamon J., Huemmrich F., Houston S., Racine C., Sturm M., Tape K., Hinzman L., Yoshikawa K., Tweedie C. E., Noyle B., Silapaswan C., Douglas D., Griffith B., Jia G., Epstein H., Walker D., Daeschner S., Petersen A., Zhou L., Myneni R.,(2004). Remote sensing of vegetation and land-cover change in Arctic Tundra Ecosystems, *Remote Sensing of Environment*, 89(3), 281–308.

Stoy P. C., Williams M., Spadavecchia L., Bell R. A.' Prieto-Blanco A.' Evans J. G.' Van Wijk M. T. (2009). Using Information Theory to Determine Optimum Pixel Size and Shape for Ecological Studies: Aggregating Land Surface Characteristics in Arctic Ecosystems, *Ecosystems*, 12(4), 574-589.

Sturm, M., T. Douglas, C. Racine & G. E. Liston (2005). Changing snow and shrub conditions affect albedo with global implications, *Journal of Geophysical Research-Biogeosciences,* 110.

Sturm, M., C. Racine & K. Tape (2001). Climate change - Increasing shrub abundance in the Arctic, *Nature,* 411, 546-547.

Tape, K., M. Sturm & C. Racine (2006). The evidence for shrub expansion in Northern Alaska and the Pan-Arctic, *Global Change Biology,* 12, 686-702.

Tarnocai, C., J. G. Canadell, E. A. G. Schuur, P. Kuhry, G. Mazhitova, S. Zimov (2009). Soil organic carbon pools in the northern circumpolar permafrost region, *Global Biogeochemical Cycles,* 23.

Teh Y. A., M. O., Atwood A. R., Abel T. and Rhew R. (2009). Hydrologic Regulation of Gross Methyl Chloride and Methyl Bromide Uptake from Alaskan Arctic Tundra, *Global Change Biology,* 15, 330-345.

Ustin S.L., Roberts D.A., Pinzo´ J., Jacquemoud S., Gardner M., Scheer G., Castaneda C. M., Palacios-Orueta A., (1998). Estimating Canopy Water Content of Chaparral Shrubs Using Optical Methods, *Remote Sensing of Environment*, 65(3), 280-291.

Vanderbilt V.C., Khanna S., Ustin S.L. (2007). Impact of pixel size on mapping surface water in subsolar imagery, *Remote Sensing of Environment*, 109(1), 1–9.

Villarreal S., R. D. Hollister, D. R. Johnson, M. J. Lara, P. J. Webber, C. E. Tweedie, Tundra vegetation change near Barrow, Alaska (1972-2010), Accepted, Environmental Research Letters.

Wahren, C. H. A., M. D. Walker & M. S. Bret-Harte (2005) Vegetation responses in Alaskan arctic tundra after 8 years of a summer warming and winter snow manipulation experiment. *Global Change Biology,* 11, 537-552.

Walker M. D., Wahren C. H., Hollister R. D., Henryd G. H. R., Ahlquist L. E., Alatalo J. M., Bret-Harte M. S., Calef M. P., Callaghan T. V., Carroll A. B., Epstein H. E., Jónsdóttir I. S., Klein J. A., Magnússon B., Molau U., Oberbauer S. F., Rewa S. P., Robinson C. H., Shaver G. R., Suding K. N., Thompson C. C., Tolvanen A., Totland Ø., Turner P. L., Tweedie C. E., Webber P. J., Wookey P. A., (2006). Plant community responses to experimental warming across the tundra biome. *PNAS*, 103(5), 1342-1346.

Wedding L.M., Friedlander A. M., McGranaghan M., Yost R. S., Monaco M. E., (2008). Using bathymetric lidar to define nearshore benthic habitat complexity: Implications for management of reef fish assemblages in Hawai, *Remote Sensing of Environment*, 112(11), 4159-4165.

Wolf A., Blyth E., Harding R., Jacob D., Keup-Thiel E., Goettel H., Callaghan T., (2008). Sensitivity of an ecosystem model to hydrology and temperature, *Climate Change*, 87(1-2).

Zona D, Oechel W.C., Peterson K.M., Clements R.J., Paw U K.T., Ustin S.L. (2009) Characterization of the carbon fluxes of a vegetated drained lake basin chronosequence on the Alaskan Arctic Coastal Plain, accepted, *Global Change Biology*.

Appendix 1:

Surface hydrology of an arctic ecosystem: Multiscale analysis of a flooding and draining experiment using spectral reflectance

Santonu Goswami,[1] John A. Gamon,[2,3,4] and Craig E. Tweedie[1]

Received 6 March 2010; revised 7 June 2010; accepted 11 June 2010; published 20 January 2011.

[1] In the Arctic, surface hydrology plays an important role in controlling plant community composition and ecosystem processes such as land-atmosphere carbon and energy balance. Investigating how climate change in this region will affect surface hydrology and subsequent biotic, atmospheric, and climatic feedbacks could be key to understanding the future state of the Arctic and Earth systems. Improved methods for monitoring surface hydrology at large spatial scales are needed in the Arctic. Near Barrow, Alaska, a large-scale experiment with flooded, drained, and control treatment areas, each exceeding 9 ha, was initiated during summer 2008 following 3 years of monitoring under nonmanipulative conditions. Throughout the 2008 growing season, hyperspectral reflectance data were collected in the visible to near-infrared (IR) range using a 300 m long robotic tram system. Water table depth, surface water depth, and percent surface water cover were also measured. A spectral index (Normalized Difference Surface Water Index (NDSWI)) was developed using reflectance in the IR region (R_{1000} strong absorbance) and blue region (R_{460} poor absorbance). NDSWI was strongly correlated with both surface water depth and surface water cover, and was used to monitor spatial and temporal patterns of surface hydrology in the experimental treatment. Using 2002 and 2008 Quickbird satellite imagery, the index was also used to examine differences in NDSWI between experimental treatments. Using this approach, we demonstrate that the flooded treatment was significantly different from the other two treatments (drained and control) and that the new index can be used to monitor surface hydrology in arctic wetlands.

Citation: Goswami, S., J. A. Gamon, and C. E. Tweedie (2011), Surface hydrology of an arctic ecosystem: Multiscale analysis of a flooding and draining experiment using spectral reflectance, *J. Geophys. Res.*, *116*, G00I07, doi:10.1029/2010JG001346.

1. Introduction

[2] Climate change appears to be most pronounced at high northern latitudes [*Intergovernmental Panel on Climate Change*, 2007; *Arctic Climate Impact Assessment*, 2005]. Many of the observed [*Post et al.*, 2009; *Hinzman et al.*, 2005; *Smith et al.*, 2005] and modeled [*McGuire et al.*, 2009; *Sitch et al.*, 2007] climate change responses in arctic tundra ecosystems are related to altered surface hydrology. In the Arctic, the importance of surface hydrology on surface energy budgets [*Chapin et al.*, 2005; *Euskirchen et al.*, 2007], land-atmosphere carbon exchange [*Merbold et al.*, 2009; *Wolf et al.*, 2008], plant phenology and response to warming [*Arft et al.*, 1999; *Walker et al.*, 2006], and geomorphic processes [*Lawrence and Slater*, 2005; *McNamara and Kane*, 2009] are well recognized. Based on experimental evidence, observations and modeling, alteration of surface hydrology in arctic terrestrial ecosystems is likely to change a variety of interconnected ecosystem processes such as primary productivity [*McGuire et al.*, 2006; *Oberbauer et al.*, 2007; *Illeris et al.*, 2004], methanogenesis [*Mazéas et al.*, 2009; *Merbold et al.*, 2009; *Petrescu et al.*, 2008], nutrient cycling [*Arndal et al.*, 2009; *McGuire et al.*, 2009; *Jonasson et al.*, 2004] and land cover or plant community change [*Walker et al.*, 2006; *Smith et al.*, 2005].

[3] The degree to which changes in land-atmosphere carbon exchange dynamics will interact with and offset the balance and stability of the substantial store of soil organic carbon in the Arctic [*Tarnocai et al.*, 2009; *Ping et al.*, 2008] is a primary concern [*McGuire et al.*, 2009]. If the increased primary productivity predicted for the Arctic does not balance the net loss of CO_2 equivalent carbon loss to the atmosphere, a positive feedback to regional and potentially the global climate system will occur [*Kimball et al.*, 2006]. This positive feedback response to warming in the Arctic is likely to be controlled by soil moisture and surface hydrology [*McGuire et al.*, 2006; *Huemmrich et al.*, 2010], so there is a need to monitor these parameters and determine

[1]Environmental Science and Engineering Program, University of Texas at El Paso, El Paso, Texas, USA.
[2]Department of Biological Sciences, California State University, Los Angeles, California, USA.
[3]Desert Research Institute, Reno, Nevada, USA.
[4]Now at Department of Earth and Atmospheric Sciences and Department of Biological Sciences, University of Alberta, Edmonton, Alberta, Canada.

0148-0227/11/2010JG001346

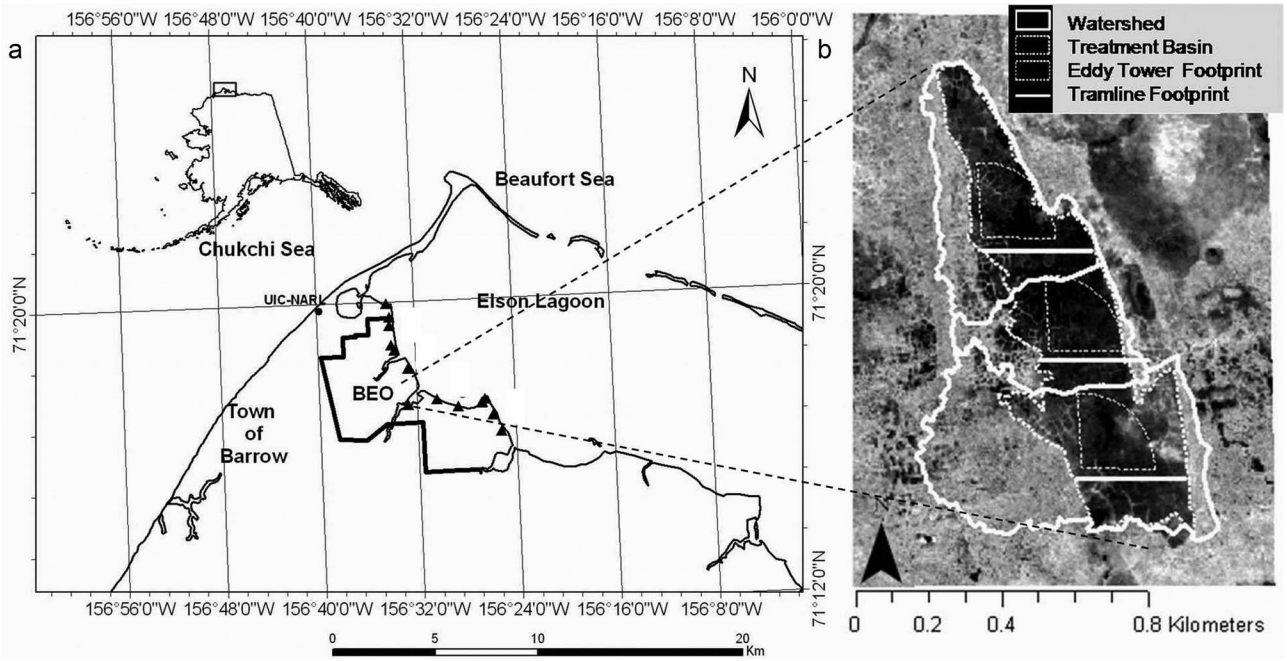

Figure 1. (a) Location of the Barrow Environmental Observatory (BEO) near Barrow, Alaska. (b) The location of the study area. The experimental design of the Biocomplexity experiment includes experimentally flooded (north) and drained (central) treatments, and a control section (south) (Figure 1b). Watersheds for each treatment and the inundated basin areas are highlighted (Figure 1b). The straight lines indicate the three sampling transects ("tramlines"). The idealized footprints of the three flux towers associated with the experiment are indicated by pie-shaped semicircles.

how they are changing over time and space to better understand the future state of the arctic system. Substantial efforts before, during, and now following the 2007–2009 International Polar Year have focused on improving environmental observing capacities in the Arctic, particularly the future fate and transport of the Arctic soil organic carbon store [*Arctic Observing Network*, 2006]. Such efforts highlight the importance of observations that span plot to global scales. Because of the many advantages remote sensing offers to such scaling challenges, the development of remote sensing approaches and technologies in an integrated arctic observing network is a key priority.

[4] Several remote sensing methods have been developed for monitoring surface hydrology or soil moisture over large spatial scales. To assess the state of surface hydrology in terrestrial ecosystems, remote sensing has been used to monitor inundation area [*Smith*, 1997; *Smith et al.*, 2005], snowpack [*Green et al.*, 2006], and vegetation water content [*Roberts et al.*, 1997; *Ustin et al.*, 1998; *Serrano et al.*, 2000]. Radar remote sensing using microwave electromagnetic radiation has been used successfully for assessing soil moisture status in some arctic landscapes [*Kasischke et al.*, 2009; *Meade et al.*, 1999]. While radar is useful for estimating inundation area, the return signal is easily confounded by wind or the presence of vegetation that can alter the backscatter properties [*Smith*, 1997]. Light Detection and Ranging (LiDAR) remote sensing has also been used in habitat mapping [*Wedding et al.*, 2008], coral reef structure [*Storlazzi et al.*, 2003; *Brock et al.*, 2004, 2006], and the bathymetry of coastal regions [*Irish and White*, 1998]. Optical remote sensing methods (using visible or near-infrared wavelengths) can penetrate water bodies, and have been applied to bathymetry [*Brando et al.*, 2009; *Legleiter and Roberts*, 2009], seagrass mapping [*Phinn et al.*, 2008] and coral reef assessment [*Hochberg et al.*, 2003]. Additionally, optical remote sensing has often been used to evaluate vegetation moisture content through reflectance indices based on water absorption bands [*Sims and Gamon*, 2003]. Examples of the latter include the Water Index (sometimes called the Water Band Index) based on reflectance at the 970 nm water band [*Peñuelas et al.*, 1993], and the Normalized Difference Water Index [*Gao*, 1996] based on the 1240 nm water band. Some methods apply a form of Beer's law to fit the water absorption coefficient spectrum to a reflectance spectrum, yielding an "Equivalent Water Thickness" (EWT) [*Gao and Goetz*, 1995; *Roberts et al.*, 1997; *Sims and Gamon*, 2003; *Green et al.*, 2006]. Based on the assumption of Beer's law, which states that reflected or transmitted light is related to the exponent of the amount of an absorbing compound, EWT offers a physically based alternative to other index based methods for assessing vegetation water content [*Gao and Goetz*, 1995]. To the extent that water bodies or vegetation behave according to Beer's law, and to the extent that calculation of EWT is based on a full spectrum (multiple bands rather than two bands), it seems that EWT should offer a superior method of assessing moisture status, but not all studies have supported this conclusion [*Serrano et al.*, 2000; *Sims and Gamon*, 2003]. Consequently, the "best" method for retrieving surface hydrology information with optical remote sensing remains an open question and a key challenge.

[5] Most of the optical remote sensing methods for assessing surface moisture properties utilize one or more water absorption features present in reflectance spectra [*Green et al.*, 2006]. Because these methods employ water absorption bands, they readily saturate, are easily confounded by atmospheric water vapor, and the vapor absorption bands overlap with liquid water features [*Sims and Gamon*, 2003; *Green et al.*, 2006]. These issues create practical problems for quantitative retrieval of surface moisture measurements, particularly in areas with high atmospheric moisture such as the Arctic. Additionally, instrument limitations (e.g., low signal to noise) and artifacts (e.g., "second-order" or "stray light" errors) in certain spectral regions (e.g., the 970 nm water band) often confound a clear interpretation of water signals, particularly with silicon photodiode detectors [*Sanchez-Azofeifa et al.*, 2009].

[6] To our knowledge, optical remote sensing has not been applied to assess surface water depth, a sensitive indicator of surface hydrology and soil moisture in the Arctic, especially on the coastal plain of northern Alaska. One goal of this study was to develop a spectral index from optical remote sensing that could be used to estimate surface water depth and surface water cover, and to characterize changes in surface hydrological properties at multiple spatial and temporal scales. To maximize the prospects for scaling, we specifically sought an index that could be least confounded by atmospheric moisture, would be relatively free from instrument errors, and would be commonly available from ground-based, airborne or satellite-borne instruments. Another key goal of this study was to evaluate the treatment effect associated with the Biocomplexity experiment, a large-scale flooding and draining manipulation conducted in northern Alaska near the city of Barrow to assess the impact of altered soil moisture status on land-atmosphere carbon, water and energy balance. Like other large-scale experimental manipulations, the Biocomplexity experiment was unreplicated and required the development of new environmental metrics to capture changing surface properties across a large treatment area. Our goal was to develop an index that could be used to evaluate hydrological treatment effects across a heterogeneous, dynamic landscape, and to evaluate discrepancies between various sampling "footprints" (flux towers, optical sampling transects, and the entire treatment basin).

2. Methods

2.1. Study Area

[7] The study was conducted within the Biocomplexity flooding and draining experiment on the Barrow Environmental Observatory (BEO) near Barrow, Alaska, 71°17′01″N, 156°35′48″W (Figure 1). The BEO is situated on the Alaskan Arctic Coastal Plain and has a low relief with an average elevation of 4 m [*Aguirre et al.*, 2008]. Seventy two percent of the landscape near Barrow contains oriented lakes, vegetated drained thaw-lake basins and small ponds [*Hinkel et al.*, 2003]. The Biocomplexity experimental area is located in a series of three coalesced drained thaw-lake basins that include moist and wet tundra vegetation dominated by graminoid tundra (C. E. Tweedie et al., Land cover classification and change detection near Barrow, Alaska using QuickBird satellite imagery, submitted to *Arctic, Antarctic, and Alpine Research*, 2010). The study site is underlain by continuous permafrost and includes thermokarst terrain typical of the Alaskan Arctic Coastal Plain [*Brown et al.*, 1980], as well as thaw lakes, high- and low-centered polygons, shallow ponds and lakes, and a shallow active layer that is generally less than 50 cm in the experimental basin [*Shiklomanov et al.*, 2010]. Soils of the area are described by *Bockheim et al.* [1999] and include cryoturbated gelisols, specifically typic aquorthels with high soil moisture content, histoturbels, and aquaturbels. The upper layer of this soil consists of carbon rich peat (ca. 50 kg/C/m^3) [*Bockheim et al.*, 1999]. Soils are generally moisture rich due to shallow drainage gradients, relatively low rates of evapotranspiration, and impeded drainage caused by ice-rich continuous permafrost [*Bockheim et al.*, 1999; *Miller et al.*, 1998].

[8] Winter is generally long, dry and cold and the summers are relatively short, moist and cool [*Brown et al.*, 1980]. The sun is above the horizon continuously from 10 May to 2 August, and below the horizon from 18 November to 24 January [*Brown et al.*, 1980]. Air temperature remains below freezing for 9 months of the year and can fall below freezing during any of the 3 summer months. A gradual warming trend begins in April, and snowmelt typically occurs in early June. Wind speed varies little during the year, averaging 5.3 m/s, with the fall months being the windiest. Fog and low cloud persist throughout the summer and the relative humidity generally exceeds 80% from June through September. Mean June–August precipitation is 58.4 mm [*Engstrom et al.*, 2008].

2.2. Experimental Infrastructure

[9] As part of the Biocomplexity experiment, water tables were manipulated in a vegetated thaw-lake basin to investigate the impact of variation in soil moisture on land-atmosphere carbon, water and energy balance. In 2008 (the year of this study), following 3 years of baseline measurements (2005–2007), the lake basin was divided into three treatments, a flooded section (+10 cm water table depth), a drained section (−10 cm water table depth), and a control section where the water table was maintained relative to water levels outside the manipulation area (Figure 1b). The experimental infrastructure established for this site includes a robotic tram system similar to that described by *Gamon et al.* [2006]. The tram system consists of three 300 m long transects ("tramlines") with one tramline located in each of the three treatment areas. Each tramline spanned the entire width of the lakebed and was oriented east–west to avoid midday shading of the south side (the sampling footprint of the tramline). An eddy covariance flux tower designed to measure trace gas flux for each of the treatment areas [*Zona et al.*, 2009] was situated adjacent to each of the tramlines (Figure 1b). A range of other collaborative studies were conducted throughout the experimental area, including several featured in this special issue [*Olivas et al.*, 2010; *Shiklomanov et al.*, 2010]. The infrastructure established for the Biocomplexity experiment provided an ideal research platform for this study as it established the capacity to repeatedly assess the surface spectral properties of the same land cover type affected by contrasting surface hydrology regimes throughout the snow-free period.

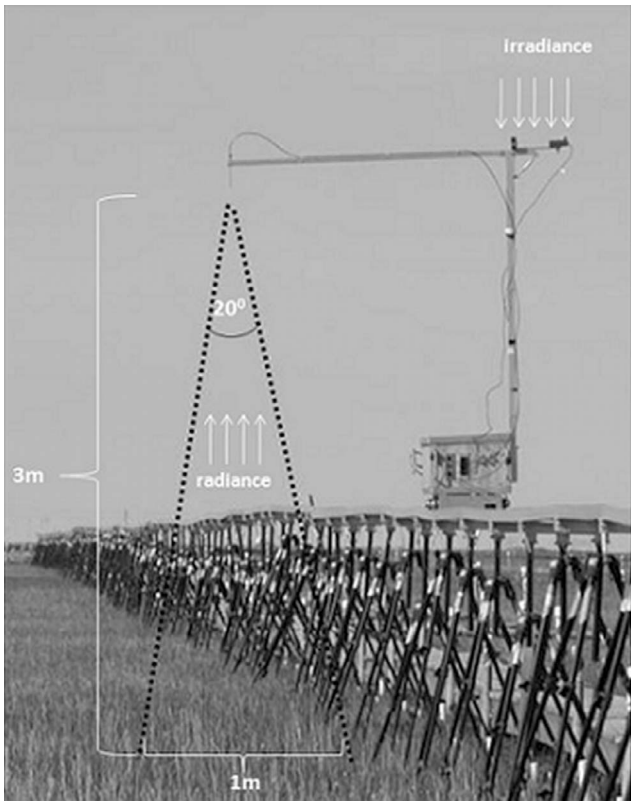

Figure 2. The robotic cart used for collection of hyperspectral reflectance data at the Biocomplexity experiment near Barrow, Alaska. Illustration of the cart riding on an elevated 300 m long tramline. Radiance and irradiance are sampled each meter along the tramline. The field of view for radiance measurements is illustrated by the dotted lines outlining the spectrometer field of view at the foreoptic.

2.3. Reflectance Measurements

[10] Field reflectance data used in this study were collected from early June 2008 to late August 2008. This period spanned the majority of the 2008 snow-free period for the study site. Spectral data were obtained using a dual-detector field portable spectrometer (Unispec DC, PP Systems, Amesbury, MA, USA), which collects radiance (radiation from the target) and irradiance (radiation from the sky) simultaneously, thereby permitting correction of surface reflectance under varying sky conditions [*Gamon et al.*, 2006]. The two detectors were cross-calibrated using a white panel with 99% reflectance (Spectralon, Labsphere, North Sutton, NH, USA) at the beginning and at the end of each set of measurements along each tramline. Our Unispec-DC had a nominal range of operation between 303 and 1148 nm in 256 contiguous bands with a spectral resolution of approximately 3 nm and a full width at half maximum of approximately 10 nm. The optimal range of this detector (range with reasonable signal to noise) is approximately 400–1000 nm, which was used to limit the spectral range used in most subsequent analyses.

[11] Along each tramline, reflectance data were collected by placing the field spectrometer on a semiautonomous robotic cart [*Gamon et al.*, 2006], which traveled along each of the 300 m long tramlines in a west–east direction (Figure 2). The cart speed was set to approximately 1 m every 5 s, allowing each 300 m long tramline to be sampled in approximately 25 min. A mechanical switch mounted on the base of the robotic cart was triggered when the cart passed over crossbars situated at every meter along each tramline. This activated the spectrometer to make a measurement. Three hundred spectral measurements were made along each tramline every time the robotic cart was operated. Each tramline was sampled up to three times per week if rain and mist did not prevail. The downward looking foreoptic was positioned at approximately 3 m above the ground and provided a field of view of approximately 20 degrees from the tip of the foreoptic. This equated to approximately a 1 m diameter sampling footprint at ground level (Figure 2). By repeating measurements throughout the snow-free period, the tram system enabled us to obtain a spatially explicit time series of surface reflectance of the same land cover type under different surface hydrology regimes. Reflectance was calculated as the ratio of the two channels, corrected by the mean cross-calibration spectrum measured for each run of the cart along each tramline (see *Gamon et al.* [2006] for details). Reflectance data were processed using the software Multispec (Version 5.1, available at http://specnet.info), which calculated interpolated reflectance at 1 nm intervals between 303 and 1148 nm.

2.4. Surface Hydrology

[12] Water table depth was measured manually every 10 m along each tramline every time spectral measurements were made, using a method similar to that described by *Olivas et al.* [2010]. Perforated PVC tubing with a diameter of 4 cm was placed in holes drilled in to the tundra, leaving approximately 20 cm of tubing above ground level. A ruler was used to measure the height of the water table relative to ground level. When the water level was below the surface, water table depth was considered negative and positive when the water table was above the surface. In cases of below ground water (negative water table depth values), surface water depth was assigned a value of zero; consequently, surface water depth simply refers to positive water table depth values (i.e., areas of visible standing water).

[13] Percent surface water cover was determined by running supervised classifications of digital color photographs using image processing software (ENVI, Version 4.2, ITT Visual Information Solutions, Boulder, CO, USA). Photos of each tramline footprint (matching the optical sampling areas) were acquired on 18 July 2008, using a digital camera (Coolpix 5400, Nikon) that was mounted on the boom of the robotic cart and triggered manually using an electronic shutter cable. The photo locations were also adjacent to water table depth measurements (i.e., every 10 m along each of the three tramlines; n = 90), allowing direct comparison with water table depth and surface water depth measurements.

2.5. Reflectance and Surface Hydrology

[14] The development of a spectral index suitable for characterizing surface hydrology (water table depth, surface water cover and surface water depth) required the assessment of spectral sensitivity to surface water. To do this,

reflectance was measured at separate locations along the tramline having different surface water cover, water table depth, and surface water depth. Additionally, reflectance at every 10 nm from 400 to 1000 nm was regressed with surface water cover, water table depth and surface water depth collected every 10 m along the tram line on 18 July 2008. Both linear and logarithmic regressions were run to determine the best fit for each.

[15] We used the regression equations from the analysis described above to derive two versions of a surface water index, the "Normalized Difference Surface Water Index" (NDSWI). The first version of NDSWI calculated the normalized difference of reflectance at 460 nm and 1000 nm ("NDSWI-linear," equation (1) below). The second version of NDSWI used a similar equation and the same reflectance bands but required reflectance to be log transformed ("NDSWI-log," equation (2) below). The relative success of NDSWI-linear and NDSWI-log in assessing surface water cover and depth (both surface water depth and water table depth) is presented below and is compared to two additional spectral indices that have also been used to describe plant or surface water status: the Water Band Index (WBI, equation (3) below [*Peñuelas et al.*, 1993]) and the Equivalent Water Thickness index (EWT, equation (4) below [*Roberts et al.*, 1997; *Sims and Gamon*, 2003]). EWT was calculated, using a Beer's law approximation [*Gao and Goetz*, 1995; *Roberts et al.*, 1997; *Sims and Gamon*, 2003], where the impact of surface water on reflectance is determined as the negative slope of the linear regression between the water absorption coefficient spectrum [*Sims and Gamon*, 2003; *Green et al.*, 2006] and the natural log of the reflectance spectrum over a wavelength range of 900–1000 nm. The formulas for calculating NDSWI-linear, NDSWI-log, WBI and EWT are:

$$\text{NDSWI-linear} = (\text{R460} - \text{R1000})/(\text{R460} + \text{R1000}) \quad (1)$$

$$\text{NDSWI-log} = \{\ln(\text{R1000}) - \ln(\text{R460})/\ln(\text{R1000}) + \ln(\text{R460})\} \quad (2)$$

$$\text{WBI} = \text{R900}/\text{R970} \quad [\textit{Peñuelas et al.}, 1993] \quad (3)$$

$$\text{EWT} = -\Delta(\ln \text{R})/\Delta(\text{a}) \quad (4)$$

The 18 July values of EWT, WBI, NDSWI-linear, and NDSWI-log were regressed with surface water cover estimated from digital image analysis as described above (n = 90). For assessing which index was most effective at assessing water table depth and surface water depth, we ran regressions between these indices and water depths from a range of sampling dates and locations within the 2008 sampling year. For example, these indices (equations (1)–(4)) measured for 5 days (18, 23, and 28 July and 4 and 9 August 2008) were first calibrated against corresponding surface water depth measurements for those dates using regression analysis. The two spectral indices that most strongly correlated with surface water cover and surface water depth in the above analyses (equations (1) and (2)) were then applied to the entire growing season by using these calibrations to predict surface water depth and water table depth throughout the 2008 sampling period. These predictions were then tested against independent surface water depth and water table depth measurements and used to make plots illustrating the temporal and spatial dynamics of surface water depth for the treatment areas over the 2008 season. Note that since photographic estimates of percent water cover were only available for one date (18 July), surface water cover could not be independently tested in this way.

[16] Particular attention was paid to assessing the accuracy of the model for estimating surface water depth across time, space, and experimental treatments. Data from alternate sampling dates during the peak of the growing season (18, 23, and 28 July and 4 and 9 August 2008) were combined to derive the final model for seasonal analysis. Seasonal surface water depth trends for each tramline were then modeled and compared to measured surface water depth and water table depth to determine if the model over or underestimated water depths in each of the experimental treatments. Plots combining all treatment dates and positions were derived to assess the spatiotemporal behavior of the model along each tramline and throughout the sampling period. To assist in the interpretation of these plots, microtopographic variation along each tramline was also examined. Data for microtopography were acquired from a 1 m digital elevation model developed for the study area from airborne LiDAR acquired in late August 2006 (Tweedie et al., submitted manuscript, 2010).

2.6. Spectral Mixture Analysis

[17] To further understand the effect of surface water on spectral reflectance, we also applied spectral mixture analysis. In remote sensing, this method is most typically used to "unmix" pixels containing more than one cover type into fractions of their component cover types, or "spectral end members," representing different cover classes [*Adams and Gillespie*, 2006]. In our case, we used the reflectance spectra of the dominant cover types (green vegetation and water) and combined them to simulate various levels of percent water cover by area. To do this, we selected end-member spectra from sites along the tram lines that were either 100% water covered or 100% vegetation covered on 18 July 2008, and created synthetic spectra of various fractions (F) of the two spectral types, ranging from 0% surface water cover (100% vegetation cover) to 100% surface water cover (0% vegetation cover), assuming linear (additive) mixing (equation (5)).

$$\rho_{\text{mixture}} = \text{F}_{\text{veg}}(\rho_{\text{veg}}) + \text{F}_{\text{water}}(\rho_{\text{water}}) \quad (5)$$

In this equation, ρ indicates the spectral reflectance (from 400 to 1000 nm) for the mixture, pure vegetation (veg) or pure water, and F is a coefficient representing the contribution of each cover type (vegetation or water), with the two portions always adding to one. These synthetic mixtures were then compared to actual field spectra of plots having a known surface water cover.

2.7. Scaling Analysis

[18] Two high spatial resolution multispectral satellite images (QuickBird, Digital Globe, Longmont, Colorado, USA) acquired on 2 August 2002 and 27 July 2008, were used to calculate NDSWI for the entire study area for

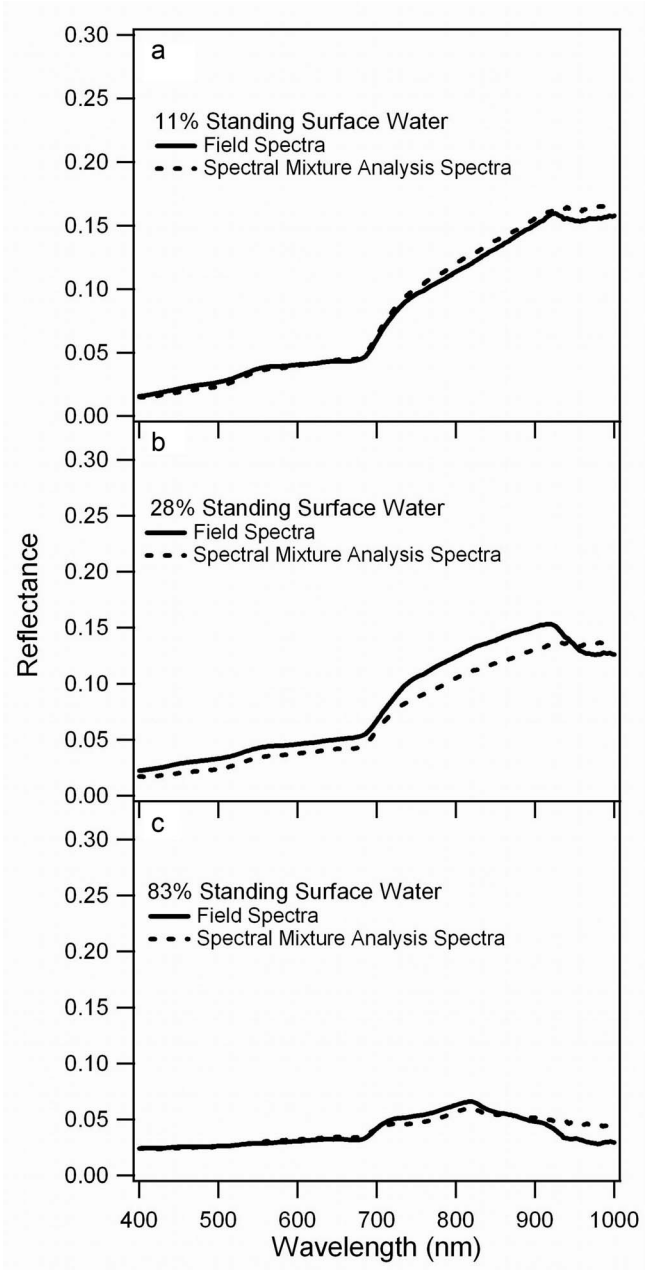

Figure 3. The effect of surface water (expressed as surface water cover) on reflectance spectra. Each field spectrum is compared to a modeled reflectance spectra using spectral mixture analysis for the same percent of standing surface water.

pretreatment (2002) and posttreatment (2008) years. Note that due to frequent cloud cover in this coastal region [*Hope et al.*, 2004], these were the only clear-sky high-resolution Quickbird images we were able to obtain for the experimental period. Radiometrically corrected QuickBird images for these dates were available with four spectral bands: blue (450–520 nm), green (520–600 nm), red (630–690 nm) and near-IR (760–900 nm) at 2.8 m resolution. Using ArcGIS (ESRI, Redlands, California), NDSWI was derived using equation (1) above for both the 2002 and 2008 Quickbird images where R460 and R1000 were substituted with the blue and IR bands of the Quickbird image, respectively. The linear version of the NDSWI equation was used to avoid any problem with band math calculations using the satellite bands. The difference in NDSWI between images (2008 minus 2002) was calculated to visualize and quantify treatment effects for different regions of the basin (flooding, versus drained and control regions; tramline regions versus flux tower regions versus the entire treatment basin).

2.8. Assessment of Experimental Treatment Effects

[19] The tramline transects and idealized flux tower footprints (based on experimental layout), and the inundated lake basin were delineated for each treatment area. For the 2002 and 2008 images, the NDSWI pixel values for the tram and flux tower footprints and treatment basins were extracted for statistical analyses (Systat Software Inc., Chicago, Illinois). To assess differences between the 2002 and 2008 NDSWI coverages for a given sampling area and treatment, t-tests were run. A univariate analysis of variance (ANOVA) was used to assess the difference between treatments within a given year. To determine the difference in the frequency distribution of NDSWI between sampling areas (tramline, flux tower, and treatment basin) within a given experimental treatment and year, a two-sample Kolmogorov-Smirnov test was performed. This nonparametric test assesses whether the tramline footprint area and flux tower footprint area, for example, have a similar NDSWI frequency distribution or whether they are significantly different from one another. This is an important consideration in testing the scaleability of measurements taken in different areas of a particular treatment area. It should be noted that the analyses outlined above do not necessarily imply causation between surface hydrology and the spectral indices analyzed. This is because we cannot fully correct for the effects of covariation between vegetation and surface hydrology on spectral signature, and instead treat NDSWI as a proxy of surface hydrologic state.

3. Results

[20] Spectral reflectance was clearly affected by varying surface water cover within the treatment basin (Figure 3). The least change was observed in the blue spectral region (450–500 nm), and the biggest difference was observed in the near-infrared (>700 nm) with reflectance decreasing markedly with increasing surface water (water table depth, surface water depth, and surface water cover). Synthetic mixtures behaved in a similar manner, and closely matched field spectra. This response to surface water coverage indicated that an index that accounted for the contrasting response to water between the blue and NIR bands could be used as an indicator of surface water. To assess which wavelengths would be optimal for such an index, we correlated several metrics of surface water (water table depth, surface water depth and surface water cover) with reflectance at every 10 nm from 400 to 1000 m for every location where reflectance, water table depth, surface water cover were measured on 18 July 2008 (Figure 4). Regardless of which water metric was used (water table depth, surface water depth, or surface water cover), R^2 values were lowest in

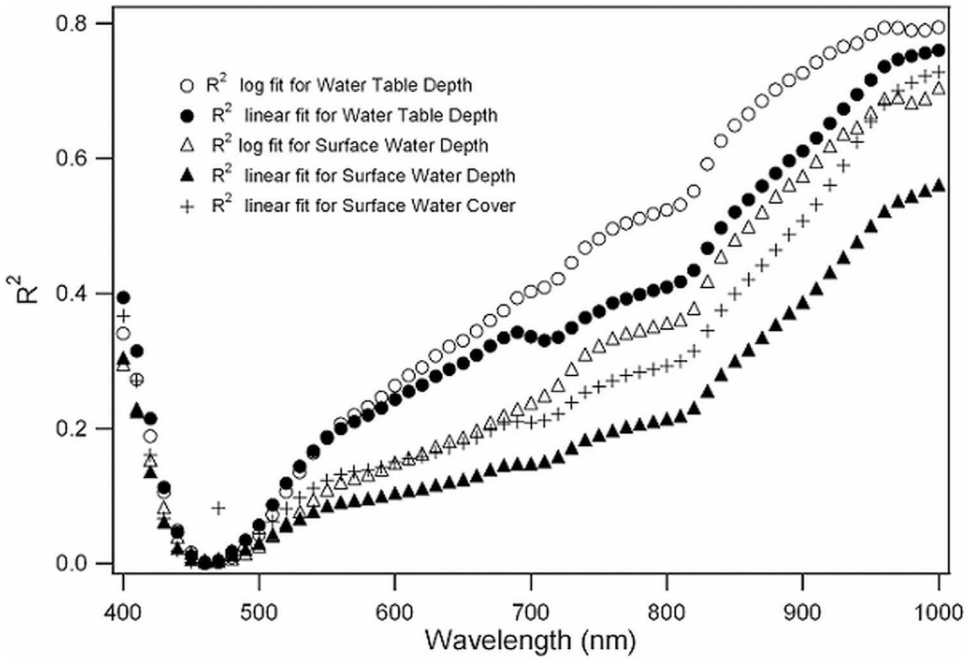

Figure 4. R^2 values for wavelength versus water table depth, surface water depth, and surface water cover. Data for this analysis were collected on 18 July 2008.

the blue (460 nm) and highest in the NIR (approximately 1000 nm), confirming that reflectance in the blue is poorly correlated with surface water, whereas reflectance in the NIR is strongly correlated with surface water. Correlations between reflectance in the NIR and water table depth of surface water cover were greatest for a logarithmic model. R^2 values between reflectance and water table depth were higher than that between reflectance and surface water depth while R^2 values between reflectance and surface water cover were similar to that of reflectance and surface water depth.

[21] Of the indices tested, the best predictor of water table depth was NDSWI-log, closely followed by NDSWI-linear (Table 1). Both NDSWI versions (log and linear) exhibited identical R^2 values with surface water cover (Table 2). All indices showed significant R^2values with water table depth and surface water cover although EWT had a stronger R^2 values with water table depth than WBI and WBI had stronger R^2values with surface water cover than EWT (Tables 1 and 2). Relative to NDSWI linear, NDSWI-log showed slightly higher R^2 values with water table depth throughout most of the sampling period (Figure 5), although the overall differences were very small. Since independent surface water cover measurements were not made over the entire season (just 18 July 2008), we could not evaluate the seasonal dependence of the fits between these indices and surface water cover.

[22] The model for predicting water table depth and surface water cover using NDSWI-log is given in Figure 6. Linear models best described the relationship between NDSWI-log and water table depth. However, when only surface water depth was included, a nonlinear model improved the fit slightly (not shown), and NDSWI tended to saturate at larger water table depth or surface water depth values. When belowground values were examined separately (Figure 6a, open circles) the R^2 value was greatly reduced, but was still significant ($p < 0.001$, Figure 6a). These results demonstrate that the NDSWI-based model's greatest predictive power was for surface water depth (i.e., when the water table was above the surface of the ground). The R^2 value for the linear regression between NDSWI-log and surface water cover was also highly significant (Figure 6b). Modeled results from synthetic mixtures of water and vegetation (Figure 6b, open squares) closely matched the results of the field measurements (Figure 6b, solid circles), providing further support of a strong link between surface water cover and NDSWI-log

Table 1. Results of Regressions Between EWT, WBI, NDSWI-Log, NDSWI-Linear, and Water Table Depth for 18, 23, and 28 July and 4 and 9 August 2008[a]

Indices	Model Equation	R^2 Value	P Value	N Value
EWT	Y = 37.303x – 1.6882	0.55	<0.001	450
WBI	Y = 19.271x – 18.854	0.50	<0.001	450
NDSWI-linear	Y = 31.53x + 22.578	0.71	<0.001	450
NDSWI-log	Y = 57.093x + 20.95	0.75	<0.001	450

[a]Y, water table depth; x, index value. Here R^2 values are calculated from all dates combined.

Table 2. Results of the Regressions Between EWT, WBI, NDSWI-Log, NDSWI-Linear, and Percent Surface Water Cover for 18 July 2008[a]

Indices	Model Equation	R^2 Value	P Value	N Value
EWT	Y = 133.15x + 6.5587	0.71	<0.001	90
WBI	Y = 80.555x + 67.566	0.82	<0.001	90
NDSWI-linear	Y = 108.67x + 88.562	0.89	<0.001	90
NDSWI-log	Y = 188.83x + 81.127	0.89	<0.001	90

[a]Y, percent surface water cover; x, index value. Here R^2 values are calculated from all dates combined.

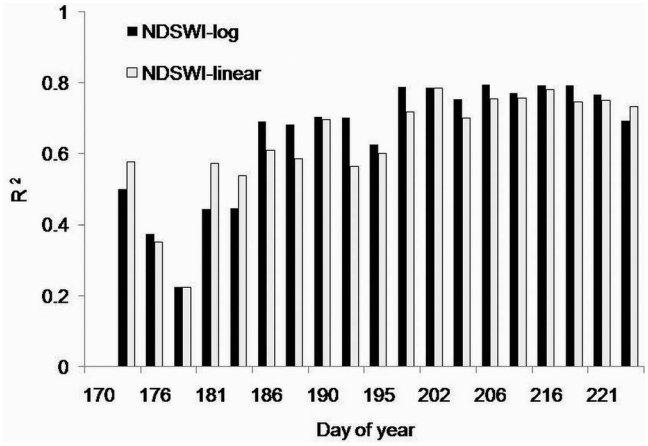

Figure 5. R^2 values for the prediction of water table depth from NDSWI for all tramlines comparing linear and log versions of the index for different dates in 2008.

for this landscape. Surface water cover and surface water depth from 18 July (the date photographic estimates of surface water cover were calculated) were strongly correlated (Figure 7), suggesting that surface water cover, surface water depth, or some combination of the two could be driving this index.

[23] In seasonal analyses, modeled water table depth closely followed measured water table depth for all the tramlines but appeared to be more accurate for the north tramline. Here, water table depth was higher compared to that of the other tramlines, which often had water tables below the ground surface (Figure 8). When the water table depth values were most negative (e.g., between days 190 and 200 in the central and south treatment basins), the index tended to overestimate water table depth when these were below ground (i.e., produce less negative water table depth values, Figures 8b and 8c). The index also had an abberant peak during a snowfall event (day 213) in the central and south basins (Figures 8b and 8c), but not in the flooded north basin (Figure 8a), where surface water prevented snow from accumulating. Direct R^2 values between modeled and measured water table depth for each tramline and for all treatments combined (Figure 9) showed that modeled water table depth tended to overpredict water table depth in the control treatment and underpredict water table depth in the drained treatment. In the flooded treatment, where surface water was present, the model predicted water table depth (i.e., surface water depth) most accurately.

[24] The model developed for water table depth (Figure 6a) depicted the spatiotemporal dynamics of water table depth along each tramline and throughout the sampling period (Figure 10). Measured water table depth and modeled water table depth varied with microtopography (Figure 10, top). Locally high-elevation areas had the lowest water table depth values, and low-elevation areas had the highest water table depth values (green-yellow areas in the water table depth image, Figure 10). In early June, soon after snowmelt (ca. day 170), water table depth was high. As the snow-free period progressed, water table depth decreased throughout each treatment. The horizontal banding in the modeled water table depth around day 210 for the central and south tramlines was caused by a snowfall event, which was also prominent as an anomalous spike in these same treatments shown in Figures 8b and 8c.

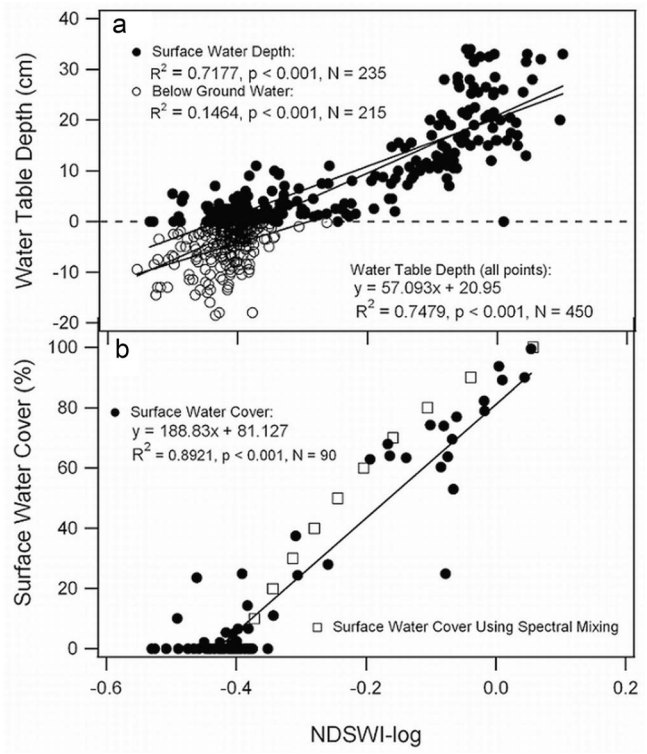

Figure 6. Regressions for (a) water table depth (all points), surface water depth (solid circles), below ground water (open circles), and (b) surface water cover (solid circles) plotted against NDSWI-log, using data from 18, 23, and 28 July and 4 and 9 August 2008. Modeled surface water cover using spectral mixture analysis is also shown (open squares, Figure 6b) and compared against measurements (solid circles).

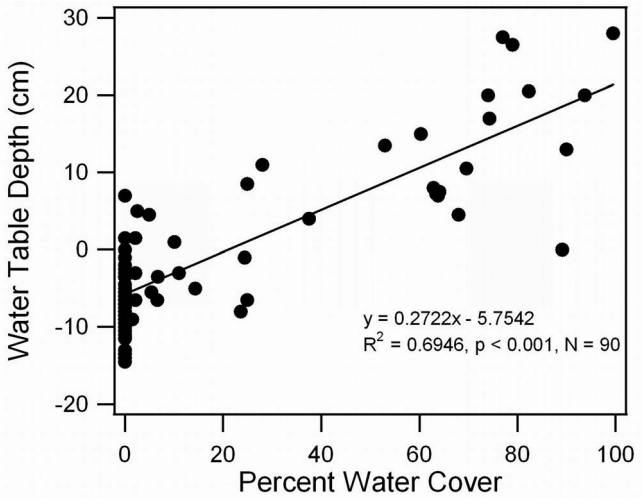

Figure 7. Regression between surface water cover and water table depth for 18 July 2008.

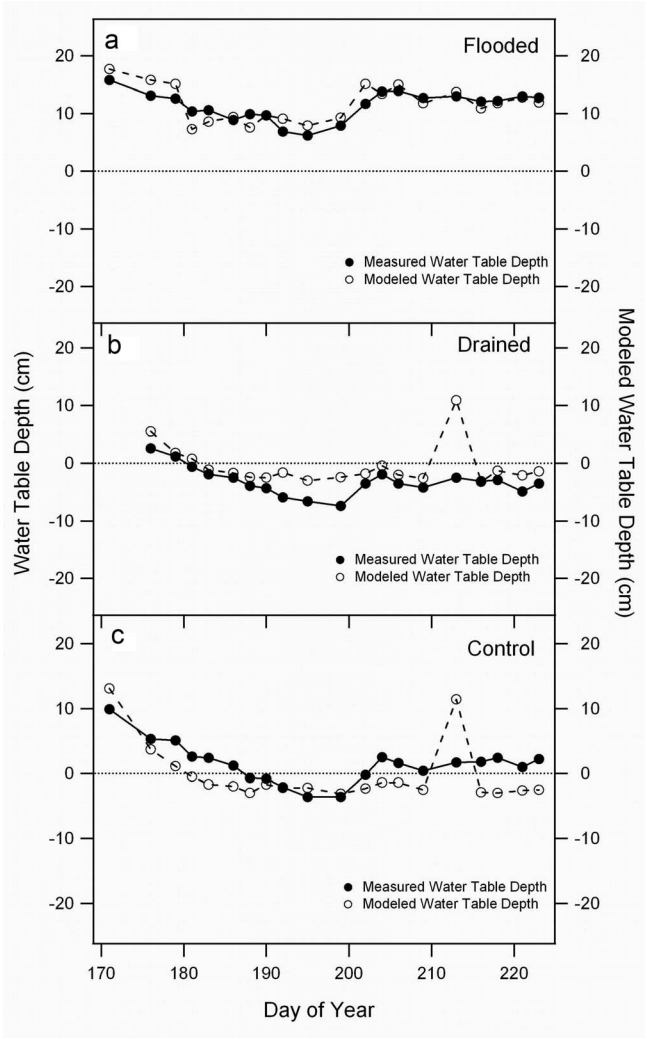

Figure 8. Seasonal patterns of mean measured water table depth along the three tramlines and mean modeled water table depth for each tramline. (a) Flooded (north), (b) drained (central), and (c) control (south) treatments, respectively. The peak in between day 210 and day 215 in the drained and control treatments indicates a snowfall event for that particular day.

[25] NDWSI extrapolated across the experimental area using Quickbird satellite imagery from 2 August 2002 (Figure 11a, pretreatment) 27 July 2008 (Figure 11b, posttreatment) showed spatial and temporal changes in surface water. These changes were particularly evident for the northern basin (flooded treatment). In Figure 11, three sampling areas, the treatment thaw-lake basin, hypothetical flux footprint, and tramline transects, are shown. The most conspicuous difference between these NDSWI extrapolations is an increase in NDSWI (becoming wetter) in the flooded treatment area. Although significant differences between years were recorded in the drained and control treatment areas (Figure 12, asterisks), these are relatively minor compared to the flooding treatment effect illustrated in Figure 11, and is further documented in Figure 12.

[26] Significant differences (t test, $p < 0.05$) were noted between years for all sampling areas and treatments except for the tramline footprint in the drained treatment (see Figure 12, asterisks). Univariate ANOVA showed no significant difference between the tramline footprints in the control and drained treatments for both years (see Figure 12, letters). The tramline footprint in the flooded treatment was significantly different from the tramline footprints in the drained and control treatments for both years (see Figure 12, letters). Kolmogorov-Smirnov tests showed a significant difference between tramline and idealized flux footprints and treatment basins for all years and treatments except for the 2002 flooded treatment, where the tramline was similar to the idealized flux tower footprint and treatment basin (Figure 12, Roman numerals). These results generally highlight a successful flooding treatment in 2008, but revealed little apparent effect in the draining treatment, which yielded no detectable change in NDSWI. These results also indicated substantial variability between sampling areas (tramline, flux footprint area, and treatment basin) in all three treatments (flooded, drained, and control) for both 2002 and 2008. Note that the surface hydrology of the control treatment varied between years for each sampling region, indicating interannual variability in surface hydrology independent of any experimental treatment effect.

4. Discussion

[27] In the Arctic, soil moisture and surface hydrology are important in controlling plant community composition and ecosystem functional processes such as land-atmosphere carbon and water exchange and surface energy balance [*Merbold et al.*, 2009; *Walker et al.*, 2006; *Chapin et al.*, 2005]. Understanding how surface hydrology is changing with climate change could be key to understanding the future state of the Arctic. This study focused on developing a spectral index capable of estimating surface water status that would not be confounded by atmospheric moisture, would be relatively free from instrument errors, and would

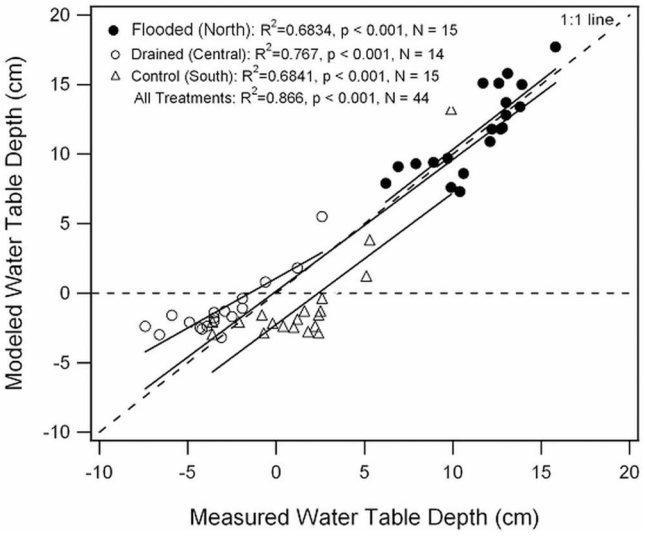

Figure 9. Modeled versus measured mean water table depth for all the three tramlines for the 2008 snow-free period. Measured water table depth data were collected from 21 June to 11 August 2008.

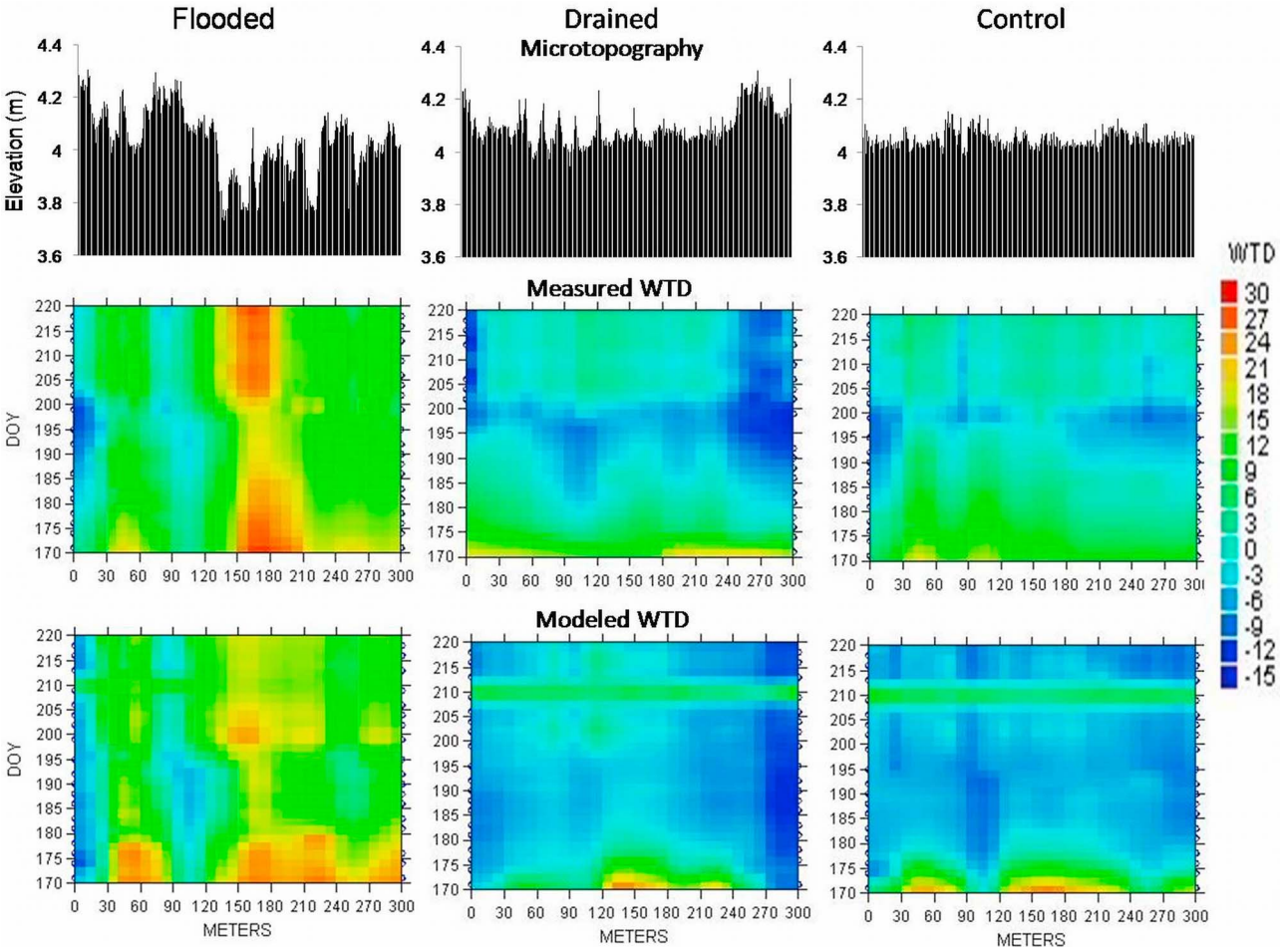

Figure 10. Elevation, modeled water table depth, and measured mean water table depth for all the three tramlines for the 2008 snow-free period. Measured water table depth data were collected from 21 June to 11 August 2008. The water table depth values shown here are in centimeters.

be commonly available from ground-based, airborne or satellite-borne instruments. The Normalized Difference Surface Water Index (NDSWI) was able to accurately estimate surface water cover and surface water depth in an experimental flooding and draining experiment situated in a vegetated thaw-lake basin on the Arctic Coastal Plain of northern Alaska.

[28] Compared to EWT and WBI, two other spectral indices that have been widely used to estimate surface hydrological properties using remote sensing [*Peñuelas et al.*, 1993; *Gao and Goetz*, 1995; *Roberts et al.*, 1997; *Sims and Gamon*, 2003; *Green et al.*, 2006], NDSWI was a better predictor of surface water depth, surface water cover, and water table depth within the study area. We initially expected that EWT could have captured these surface properties better than NDSWI because the calculation of EWT employs more wave bands, and more closely adheres to physical principles of Beer's law. However, both WBI and EWT used wavelengths within the 970 nm water absorption band, a region which is prone to instrument errors with the detector in our instrument [*Sanchez-Azofeifa et al.*, 2009]. It is likely that these factors contributed to the poorer fit with these indices. Additionally, the presence of more than one cover type (vegetation and water, having different scattering properties), may have reduced the efficacy of EWT in this case, since Beer's law assumes minimal scattering. Our instruments and sampling protocols were designed to correct for changing sky conditions [*Gamon et al.*, 2006], but these corrections are often difficult under rapidly varying cloud conditions. Since the 970 nm water band can be affected by varying atmospheric moisture, the often cloudy and misty conditions of the site may have further contributed to the weaker fit with WBI and EWT. One reason why NDSWI may have performed better was that it uses wavelengths that are on the edge of (rather than near the middle of) the 970 nm water band. The slightly better prediction with the log version (versus the linear version) of NDSWI suggests that a Beer's law approximation may actually be a reasonable assumption for modeling surface water depth, since Beer's law predicts an exponential extinction with depth. This becomes problematic for wavelengths affected by varying atmospheric water vapor absorption [*Sims and Gamon*, 2003] and by poor instrument performance (low signal-to-noise and stray light errors).

[29] Electromagnetic radiation in the optical region cannot penetrate deep into opaque surfaces (e.g., soil), which explains why negative water table depth values were not modeled well with NDSWI (low R^2 values for open circles, Figure 6a). When combined with positive water table depth

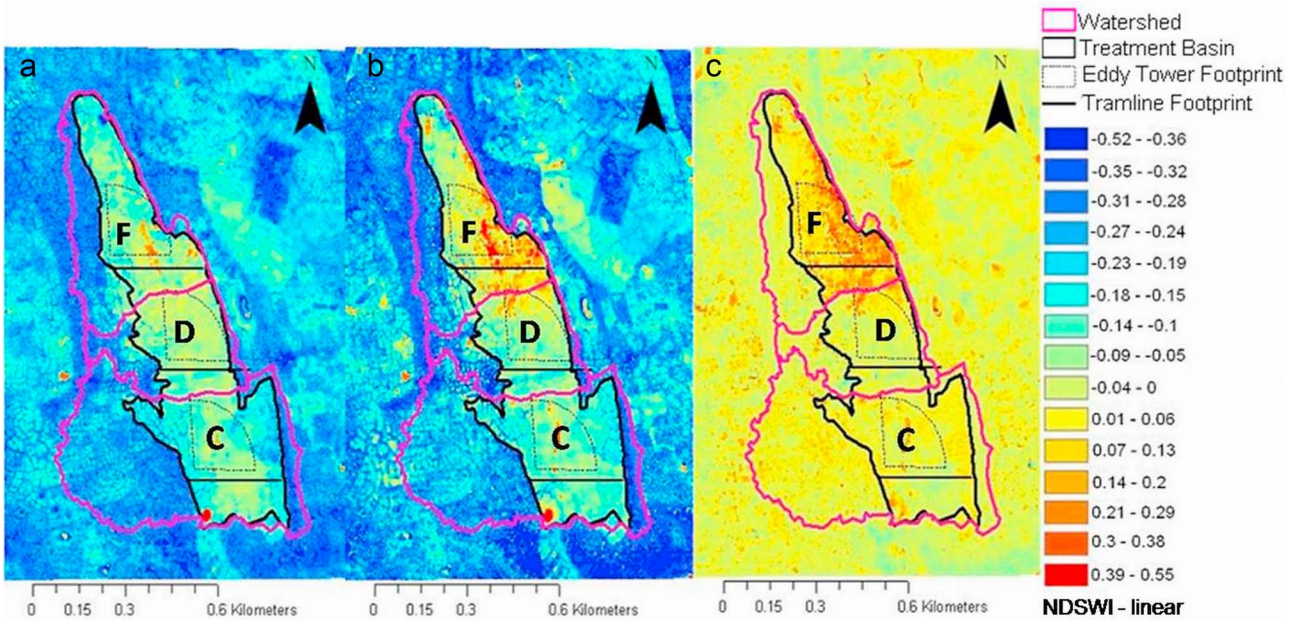

Figure 11. NDSWI-linear values extrapolated across the Biocomplexity experimental area using multispectral Quickbird images for (a) 2002 (pretreatment) and (b) 2008 (posttreatment). (c) The difference of NDSWI-linear values for the 2 treatment years (2008 and 2002). The black lines show the outer boundary of the treatment basin areas: flooded (north), drained (central), and control (south). The letters F, D, and C correspond to the flooded, drained, and control treatment areas, respectively, and the color legend shows the NDSWI values. The sectors indicate hypothetical flux tower sampling footprints according to the original experimental design, with the vertices of the sectors indicating the locations of the flux towers.

values (i.e., standing water above the surface), these negative water table depths did not detract from the accuracy of the NDSWI-derived model. However, the low R^2 values between NDSWI and negative water table depth values indicate that this model is not capable of accurately predicting below-groundwater depth. This weakness explained the poorer fit in the control (south) and drained (central) treatment basins relative to the flooded (north) treatment, which was characterized by positive water table depth values (i.e., aboveground surface water) for the seasonal sampling period (Figures 8 and 9). Thus, we caution that the detection of below ground water is not logically possible using the optical remote sensing techniques we have employed in this study, but note that they work well for visible surface water, whether expressed as surface water cover or as surface water depth (which were strongly correlated with each other, Figure 7). The weak but statistically significant correlation between NDSWI and negative water table depth may have been driven by covariance between water table depth and percent standing water associated with the frequency of local depressions where small amounts of subsurface water may have been visible to the sensor. An NDSWI-log value of approximately −0.4 indicates a water table depth at the ground surface using the model derived in Figure 6 and could be used as a reasonable cutoff for studies wishing to maximize the predictive power of NDSWI in modeling above ground water table depths. Although this study shows a strong potential of NDSWI to be used as an index of surface water depth and surface water cover, we caution that further testing is required to determine the spatiotemporal scalability of NDSWI across multiple sensing platforms, a broader range of land cover types, and regimes of surface hydrology.

[30] For largely pragmatic reasons discussed above, we sought a spectral index that could not be overly confounded by atmospheric moisture and could be calculated from readily available ground-based, airborne or satellite-borne instruments. It appears that NDSWI meets this requirement. Further testing of NDSWI to assess its significance and extrapolation potential in the Arctic and elsewhere will need to address many remote sensing challenges. These include challenges specific to the Arctic, that span multiple spatial scales [*Vanderbilt et al.*, 2007], address spectral variation between sensors, particularly optical and spaceborne sensors [*Ganguly et al.*, 2008], and challenges that are specific to differing surface cover types and hydrological regimes. Because a wide range of NIR wavelengths are sensitive to surface water (high coefficients of determination in Figure 4), this index can be readily adapted to a variety of sensors with wave bands in this region, facilitating its broad use, but also presenting challenges in intercomparison. Additional remote sensing challenges inherent to the Arctic include but are not limited to characterization of diverse and fine-scale landscape heterogeneity [*Stoy et al.*, 2009], frequent cloud cover and high atmospheric moisture [*Hope et al.*, 2004], and characterization of sometimes fine-scale and often short-term biophysical phenomena that are associated with ecosystem structure and function [*Laidler et al.*, 2008; *Vanderbilt et al.*, 2007]. An example of the latter is the occurrence of a midsummer snowfall (day 213 in Figures 8b and 8c) documented in this study. At this time, snow accumulated in the drained and control treatment areas but

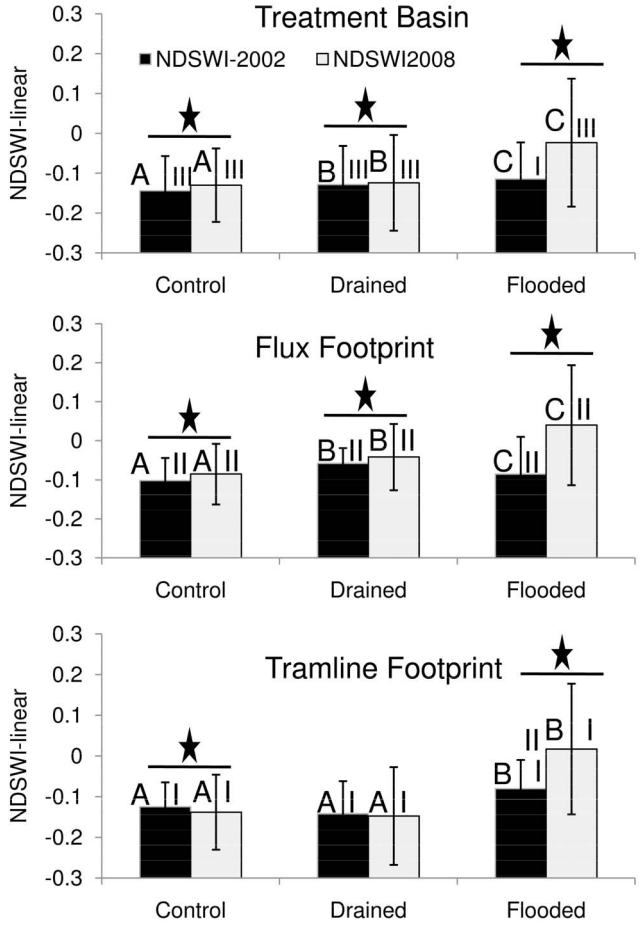

Figure 12. Comparison of average NDSWI-linear mapped to different sampling footprint areas using Quickbird 2002 and 2008 images. Error bars represent one standard deviation. Asterisks indicate a significant difference ($p < 0.05$, t test) between years (2002 and 2008) for a given sampling area (tramline footprint, flux tower footprint, treatment basin) and treatment (flooded, drained, control). Letters A, B, and C indicate a significant difference/similarity ($p < 0.05$, univariate ANOVA) between treatments (flooded, drained, control) in a given year and type of sampling area. Roman numerals indicate a significant difference/similarity ($p < 0.05$, Kolomogorov-Smirnof test) between sampling areas (tramline footprint, flux tower footprint, treatment basin) within a given treatment and year.

not in the flooded treatment area (Figure 8a). The response of NDSWI to this event demonstrated a strong sensitivity to snow, which appears as an anomalously high NDSWI value (Figures 8 and 10).

[31] The capacity of NDSWI to characterize the surface hydrology of the study area enabled us to evaluate the performance of the experimental flooding and draining experiment. Like many other large-scale experimental manipulations in the ecological sciences, our flooding and draining experiment was unreplicated, was a logistic and operational challenge, and displayed a high degree of "natural" variability in land cover and surface hydrology within and between treatment areas (Figures 11 and 12). The integration of various subproject or discipline-based sampling results from this long-term ecosystem experiment is just beginning to be determined and this study has facilitated this process by providing a tool for evaluating the surface hydrological properties of different experimental treatments, time periods and sampling areas (e.g., tram versus flux tower footprint). This study suggests that prior to experimental manipulation (i.e., in 2002), the basin of each experimental treatment had significantly different surface hydrology properties (Figures 11 and 12), as did the flux tower and tramline sampling footprints (Figure 12). There were significant differences between years, indicated by a difference in NDSWI for the control treatment (Figures 11 and 12) and elsewhere throughout the study area outside of the experimental thaw-lake basin (Figure 11). In 2008, flooding appeared to be more effective than draining throughout each treatment basin and within the flux tower and tramline sampling footprints (Figure 12). During the experimental manipulation, further draining of the "drained" basin by pumping water lower than the soil surface (water table depth equal to 0) proved to be logistically difficult, and this may help account for the lack of a clear result of a "drained" treatment effect. Additionally, we caution that our NDSWI-based model cannot readily distinguish between water table depth values of zero and negative values (below ground water), because optical remote sensing methods cannot penetrate far below the soil surface, so a successful drainage treatment may not have been clearly detectable with this method.

[32] A distinct advantage of NDSWI over the other spectral indices tested in this study is that it can be readily adapted to a range of available satellite remote sensing platforms. Considering the importance of surface hydrology on ecosystem processes and properties such as carbon dioxide and methane flux [*Merbold et al.*, 2009; *Wolf et al.*, 2008], surface energy balance [*Chapin et al.*, 2005; *Euskirchen et al.*, 2007], plant phenology and response to warming [*Arft et al.*, 1999; *Walker et al.*, 2006], and geomorphic processes [*Lawrence and Slater*, 2005; *McNamara and Kane*, 2009], the potential for NDSWI to facilitate the advancement of modeling and spatial extrapolation of these processes seems promising. Similar to how satellite-derived NDVI is increasingly being used to model land atmosphere carbon flux, leaf area index, or plant biomass [*Running et al.*, 2004], we believe that, pending further testing and refinement, NDSWI could be applied in a similar manner to improve models of carbon dioxide or methane fluxes, which are highly dependent on surface hydrology [*Merbold et al.*, 2009]. If possible, this could facilitate the development of spatially explicit models that estimate net greenhouse warming potential through the combination of land-atmosphere carbon dioxide and methane flux models. Such development, including ground, air and satellite-based estimates of NDSWI, could be integrated within regional studies or observatories focused on carbon dynamics as recently called for by *McGuire et al.* [2009].

5. Conclusions

[33] This study has addressed a critical need in the Arctic terrestrial sciences: an improved capacity to detect and monitor surface hydrological properties that are associated

with or regulate important ecological processes and phenomena. Our goal was to develop a spectral index from optical remote sensing that could be used to estimate surface water depth, and characterize changes in surface hydrology at multiple spatial and temporal scales. We also sought a method that could be used to assess the impact of a large-scale unreplicated experimental flooding and draining experiment that supported a range of simultaneous multi-disciplinary and multiscale investigations. The Normalized Difference Surface Water Index (NDSWI) out-performed other spectral indices that have been used to estimate similar properties. This index appears to accurately estimate aboveground surface water depth and surface water cover for this landscape, and detected experimental treatment effects at multiple spatial and temporal scales in the experimental manipulation. We caution that while our results describe a vegetated thaw-lake basin on the Arctic Coastal Plain of northern Alaska, further work will be needed to extend this approach beyond the context of this particular study site. We recommend further testing and refinement of NDSWI, and an assessment of its potential use in the development of models that estimate ecological processes and phenomenon that are sensitive to surface hydrology such as land-atmosphere carbon dioxide, methane and water vapor exchange.

[34] **Acknowledgments.** This project was supported by the U.S. National Science Foundation (ASSP-0421588). We are grateful to the Ukpeaġvik Iñupiat Corporation (UIC) for permitting the Biocomplexity experiment on the Barrow Environmental Observatory and the Barrow Arctic Science Consortium and CH2M Hill Polar Services (formerly VECO Polar Services) for logistical support, construction services, and ongoing tramline maintenance. We are grateful to the following for their assistance in the field: Sergio Vargas, Christian Andresen, Irbis Gallegos, Mark Lara, Ryan Cody, Gilda Victorino, Paulo Olivas, and Steven Oberbauer. Vanessa Lougheed and David Johnson in the Department of Biology at UTEP provided statistical advice, and Ryan Cody, Christian Andresen, and Adrian Aguirre provided GIS support. Yufu Cheng, Loren MacKinney, Ann Kelly, and Lekealem Taku assisted with the initial tram assembly. Rob Green and Susan Ustin provided helpful comments on the manuscript.

References

Adams, J. B., and J. R. Gillespie (2006), *Remote Sensing of Landscapes With Spectral Images: A Physical Modeling Approach*, Cambridge Univ. Press, Cambridge, U. K.

Aguirre, A., C. E. Tweedie, J. Brown, and A. Gaylord (2008), Erosion of the Barrow Environmental Observatory coastline 2003–2007, northern Alaska, paper presented at Ninth International Conference on Permafrost, Int. Permafrost Assoc., Fairbanks, Alaska.

Arctic Climate Impact Assessment (2005), *Impacts of a Warming Arctic: Arctic Climate Impact Assessment*, Cambridge Univ. Press, Cambridge, U. K.

Arctic Observing Network (2006), *AON Report: Toward an Integrated Arctic Observing Network*, Natl. Acad. Press, Washington, D. C.

Arft, A. M., et al. (1999), Responses of tundra plants to experimental warming: Meta-analysis of the international tundra experiment, *Ecol. Monogr.*, *69*, 491–511.

Arndal, M. F., L. Illeris, A. Michelsen, K. Albert, M. P. Tamstorf, and B. U. Hansen (2009), Seasonal variation in gross primary production, plant biomass, and carbon nitrogen pools in five high arctic vegetation types, *Arct. Alp. Res.*, *41*, 164–173.

Bockheim, J. G., L. R. Everett, K. M. Hinkel, F. E. Nelson, and J. Brown (1999), Soil organic carbon storage and distribution in arctic tundra, Barrow, Alaska, *Soil Sci. Soc. Am. J.*, *63*, 934–940.

Brando, V. E., J. M. Anstee, M. Wettle, A. G. Dekker, S. R. Phinn, and C. Roelfsema (2009), A physics based retrieval and quality assessment of bathymetry from suboptimal hyperspectral data, *Remote Sens. Environ.*, *113*, 755–770.

Brock, J. C., C. W. Wright, T. D. Clayton, and A. Nayegandhi (2004), Lidar optical rugosity of coral reefs in Biscayne National Park, Florida, *Coral Reefs*, *23*(1), 48–59.

Brock, J. C., C. W. Wright, I. B. Kuffner, R. Hernandez, and P. Thompson (2006), Airborne lidar sensing of massive stony coral colonies on patch reefs in the northern Florida reef tract, *Remote Sens. Environ.*, *104*(1), 31–42.

Brown, J., P. C. Miller, L. L. Tieszen, and F. L. Bunnel (1980), *An Arctic Ecosystem: The Coastal Tundra at Barrow, Alaska*, *US/IBP Synth. Ser.*, vol. 12, 571 pp., Dowden Hutchinson Ross, Stroudsburg, Pa.

Chapin, F. S., et al. (2005), Role of land surface changes in arctic summer warming, *Science*, *310*(5748), 657–660.

Engstrom, R., A. Hope, H. Kwon, and D. Stow (2008), The relationship between soil moisture and NDVI near Barrow, Alaska, *Phys. Geogr.*, *29*(1), 38–53.

Euskirchen, E. S., A. D. Mcguire, and F. S. Chapin (2007), Energy feedbacks of northern high-latitude ecosystems to the climate system due to reduced snow cover during 20th century warming, *Global Change Biol.*, *13*, 2425–2438.

Gamon, J. A., Y. Cheng, H. Claudio, L. MacKinney, and D. A. Sims (2006), A mobile tram system for systematic sampling of ecosystem optical properties, *Remote Sens. Environ.*, *103*(3), 246–254.

Ganguly, S., M. A. Schull, A. Samanta, N. V. Shabanov, C. Milesi, R. R. Nemani, Y. Knyazikhin, and R. B. Myneni (2008), Generating vegetation leaf area index earth system data record from multiple sensors. Part 1: Theory, *Remote Sens. Environ.*, *112*(12), 4333–4343.

Gao, B. C. (1996), NDWI—A normalized difference water index for remote sensing of vegetation liquid water from space, *Remote Sens. Environ.*, *58*(3), 257–266.

Gao, B. C., and A. F. H. Goetz (1995), Retrieval of equivalent water thickness and information related to biochemical components of vegetation canopies from AVIRIS data, *Remote Sens. Environ.*, *52*(3), 155–162.

Green, R. O., T. H. Painter, D. A. Roberts, and J. Dozier (2006), Measuring the expressed abundance of the three phases of water with an imaging spectrometer over melting snow, *Water Resour. Res.*, *42*, W10402, doi:10.1029/2005WR004509.

Hinkel, K. M., W. R. Eisner, J. G. Bockheim, F. E. Nelson, K. M. Peterson, and X. Dai (2003), Spatial extent, age, and carbon stocks in drained thaw lake basins on the Barrow Peninsula, Alaska, *Arct. Antarct. Alp. Res.*, *35*(3), 291–300.

Hinzman, L. D., et al. (2005), Evidence and implications of recent climate change in terrestrial regions of the Arctic, *Clim. Change*, *72*, 251–298.

Hochberg, E. J., M. J. Atkinson, and S. Andréfouët (2003), Spectral reflectance of coral reef bottom-types worldwide and implications for coral reef remote sensing, *Remote Sens. Environ.*, *85*(2), 159–173.

Hope, A. S., K. R. Pence, and D. A. Stow (2004), NDVI from low altitude aircraft and composited NOAA AVHRR data for scaling Arctic ecosystem fluxes, *Int. J. Remote Sens.*, *25*(20), 4237–4250.

Huemmrich, K. F., G. Kinoshita, J. A. Gamon, S. Houston, H. Kwon, and W. C. Oechel (2010), Tundra carbon balance under varying temperature and moisture regimes, *J. Geophys. Res.*, *115*, G00I02, doi:10.1029/2009JG001237.

Illeris, L., T. R. Christensen, and M. Masterpanov (2004), Moisture effects on temperature sensitivity of CO_2 exchange in a subarctic heath ecosystem, *Biogeochemistry*, *70*(3), 315–330.

Intergovernmental Panel on Climate Change (2007), Summary for policymakers, in *Climate Change 2007: The Physical Science Basis. Contribution of Working Group I to the Fourth Assessment Report of the Intergovernmental Panel on Climate Change*, edited by S. Solomon et al., Cambridge Univ. Press, New York.

Irish, J. L., and T. E. White (1998), Coastal engineering applications of high-resolution lidar bathymetry, *Coastal Eng.*, *35*(1–2), 47–71.

Jonasson, S., J. Castro, and A. Michelsen (2004), Litter, warming and plants affect respiration and allocation of soil microbial and plant C, N and P in arctic mesocosms, *Soil Biol. Biochem.*, *36*(7), 1129–1139.

Kasischke, E. S., L. L. Bourgeau-Chavez, A. R. Rober, K. H. Wyatt, J. M. Waddington, and M. R. Turetsky (2009), Effects of soil moisture and water depth on ERS SAR backscatter measurements from an Alaskan wetland complex, *Remote Sens. Environ.*, *113*(9), 1868–1873.

Kimball, J. S., M. Zhao, K. C. McDonald, and S. W. Running (2006), Satellite remote sensing of terrestrial net primary production for the pan-Arctic basin and Alaska, *Mitig. Adapt. Strategies Glob. Change*, *11*(4), 783–804.

Laidler, G. J., M. Paul, P. M. Treitz, and D. M. Atkinson (2008), Remote sensing of arctic vegetation: Relations between the NDVI, spatial resolution and vegetation cover on Boothia Peninsula, Nunavut, *Arctic*, *61*(1), 1–3.

Lawrence, D. M., and A. G. Slater (2005), A projection of severe near-surface permafrost degradation during the 21st century, *Geophys. Res. Lett.*, *32*, L24401, doi:10.1029/2005GL025080.

Legleiter, C. J., and D. A. Roberts (2009), A forward image model for passive optical remote sensing of river bathymetry, *Remote Sens. Environ.*, *113*(5), 1025–1045.

Mazéas, O., J. C. Von Fischer, and R. C. Rhew (2009), Impact of terrestrial carbon input on methane emissions from an Alaskan Arctic lake, *Geophys. Res. Lett.*, *36*, L18501, doi:10.1029/2009GL039861.

McGuire, D. A., F. S. Chapin, J. E. Walsh, and C. Wirth (2006), Integrated regional changes in arctic climate feedbacks: Implications for the global climate system, *Annu. Rev. Environ. Resour.*, *31*, 61–91.

McGuire, D. A., L. G. Anderson, T. R. Christensen, S. Dallimore, L. Guo, D. J. Hayes, M. Heimann, T. D. Lorenson, R. W. Macdonald, and N. Roulet (2009), Sensitivity of the carbon cycle in the Arctic to climate change, *Ecol. Monogr.*, *79*(4), 523–555.

McNamara, J. P., and D. L. Kane (2009), The impact of a shrinking cryosphere on the form of arctic alluvial channels, *Hydrol. Process.*, *23*, 159–168.

Meade, N. G., L. D. Hinzman, and D. L. Kane (1999), Spatial estimation of soil moisture using synthetic aperture radar in Alaska, *Adv. Space Res.*, *24*(7), 935–940.

Merbold, L., W. L. Kutsch, C. Corradi, O. Kolle, C. Rebmann, P. C. Stoy, S. A. Zimov, and E. D. Schulze (2009), Artificial drainage and associated carbon fluxes (CO_2/CH_4) in a tundra ecosystem, *Global Change Biol.*, *15*(11), 2599–2614.

Miller, L. L., M. Allard, K. M. Hinkel, F. E. Nelson, S. I. Outcalt, and R. F. Paetzold (1998), Spatial and temporal patterns of soil moisture and thaw depth at Barrow, Alaska, U.S.A, *Collection Nordicana*, *57*, 731–737.

Oberbauer, S. F., et al. (2007), Tundra CO_2 fluxes in response to experimental warming across latitudinal and moisture gradients, *Ecol. Monogr.*, *77*(2), 221–238.

Olivas, P., S. Oberbauer, C. E. Tweedie, W. Oechel, and A. Kuchy (2010), Responses of CO_2 flux components of Alaskan Coastal Plain tundra to shifts in water table, *J. Geophys. Res.*, *115*, G00I05, doi:10.1029/2009JG001254.

Peñuelas, J., I. Filella, C. Biel, L. Serrano, and R. Savé (1993), The reflectance at the 950–970 nm region as an indicator of plant water status, *Int. J. Remote Sens.*, *14*(10), 1887–1905.

Petrescu, A. M. R., J. Huissteden, M. Jackowicz-Korczynski, A. Yurova, T. R. Christensen, P. M. Crill, K. Bäckstrand, and T. C. Maximov (2008), Modeling CH_4 emissions from arctic wetlands: Effects of hydrological parameterization, *Biogeosciences Discuss.*, *5*, 3195–3227.

Phinn, S., C. Roelfsema, A. Dekker, V. Brando, and J. Anstee (2008), Mapping seagrass species, cover and biomass in shallow waters: An assessment, of satellite multi-spectral and airborne hyper-spectral imaging systems in Moreton Bay (Australia), *Remote Sens. Environ.*, *112*(8), 3413–3425.

Ping, C.-L., G. J. Michaelson, M. T. Jorgenson, J. M. Kimble, H. Epstein, V. E. Romanovsky, and D. A. Walker (2008), High stocks of soil organic carbon in the North American Arctic region, *Nat. Geosci.*, *1*, 615–619.

Post, E., et al. (2009), Ecological dynamics across the Arctic associated with recent climate change, *Science*, *325*(5946), 1355–1358.

Roberts, D. A., R. O. Green, and J. B. Adams (1997), Temporal and spatial patterns in vegetation and atmospheric properties from AVIRIS, *Remote Sens. Environ.*, *62*(3), 223–240.

Running, S. W., R. R. Nemani, F. A. Heinsch, M. Zhao, M. Reeves, and H. Hashimoto (2004), A continuous satellite-derived measure of global terrestrial primary production, *BioScience*, *54*(6), 547–560.

Sanchez-Azofeifa, G. A., K. Castro, S. J. Wright, J. A. Gamon, B. Rivard, M. Kalacska, and S. Schnitzer (2009), Differences in leaf traits, leaf internal structure, and spectral reflectance between two communities of lianas and trees: Implications for remote sensing in tropical environments, *Remote Sens. Environ.*, *113*(10), 2076–2088.

Serrano, L., S. L. Ustin, D. A. Roberts, J. A. Gamon, and J. Peñuelas (2000), Deriving water content of chaparral vegetation from AVIRIS data, *Remote Sens. Environ.*, *74*(3), 570–581.

Shiklomanov, N., D. Streletsky, F. Nelson, R. Hollister, V. E. Romanovsky, C. E. Tweedie, and J. Brown (2010), Decadal variations of active layer thickness in moisture controlled landscapes, Barrow, Alaska, *J. Geophys. Res.*, *115*, G00I04, doi:10.1029/2009JG001248.

Sims, D. A., and J. A. Gamon (2003), Estimation of vegetation water content and photosynthetic tissue area from spectral reflectance: A comparison of indices based on liquid water and chlorophyll absorption features, *Remote Sens. Environ.*, *84*(4), 526–537.

Sitch, S., A. D. McGuire, J. Kimball, N. Gedney, J. Gamon, R. Engstrom, A. Wolf, Q. Zhuang, J. Clein, and K. C. McDonald (2007), Assessing the carbon balance of circumpolar arctic tundra using remote sensing and process modeling, *Ecol. Appl.*, *17*(1), 213–234.

Smith, L. C. (1997), Satellite remote sensing of river inundation area, stage, and discharge: A review, *Hydrol. Process.*, *11*, 1427–1429.

Smith, L. C., Y. Sheng, G. M. MacDonald, and L. D. Hinzman (2005), Disappearing arctic lakes, *Science*, *308*(5727), 1429, doi:10.1126/science.1108142.

Storlazzi, C. D., J. B. Logan, and M. E. Field (2003), Quantitative morphology of a fringing reef tract from high-resolution laser bathymetry: Southern Molokai, Hawaii, *Geol. Soc. Am. Bull.*, *115*, 1344–1355.

Stoy, P. C., M. Williams, L. Spadavecchia, R. A. Bell, A. Prieto-Blanco, J. G. Evans, and M. T. Van Wijk (2009), Using information theory to determine optimum pixel size and shape for ecological studies: Aggregating land surface characteristics in arctic ecosystems, *Ecosystems*, *12*(4), 574–589.

Tarnocai, C., J. G. Canadell, E. A. G. Schuur, P. Kuhry, G. Mazhitova, and S. Zimov (2009), Soil organic carbon pools in the northern circumpolar permafrost region, *Global Biogeochem. Cycles*, *23*, GB2023, doi:10.1029/2008GB003327.

Ustin, S. L., D. A. Roberts, J. Pinzon, S. Jacquemoud, M. Gardner, G. Scheer, C. M. Castaneda, and A. Palacios-Orueta (1998), Estimating canopy water content of chaparral shrubs using optical methods, *Remote Sens. Environ.*, *65*(3), 280–291.

Vanderbilt, V. C., S. Khanna, and S. L. Ustin (2007), Impact of pixel size on mapping surface water in subsolar imagery, *Remote Sens. Environ.*, *109*(1), 1–9.

Walker, M. D., et al. (2006), Plant community responses to experimental warming across the tundra biome, *Proc. Natl. Acad. Sci. U. S. A.*, *103*(5), 1342–1346.

Wedding, L. M., A. M. Friedlander, M. McGranaghan, R. S. Yost, and M. E. Monaco (2008), Using bathymetric lidar to define nearshore benthic habitat complexity: Implications for management of reef fish assemblages in Hawaii, *Remote Sens. Environ.*, *112*(11), 4159–4165.

Wolf, A., E. Blyth, R. Harding, D. Jacob, E. Keup-Thiel, H. Goettel, and T. Callaghan (2008), Sensitivity of an ecosystem model to hydrology and temperature, *Clim. Change*, *87*(1–2), 75–89.

Zona, D., W. C. Oechel, K. M. Peterson, R. J. Clements, U. K. T. Paw, and S. L. Ustin (2009), Characterization of the carbon fluxes of a vegetated drained lake basin chronosequence on the Alaskan Arctic Coastal Plain, *Global Change Biol.*, *16*(6), 1870–1882.

J. A. Gamon, Department of Earth and Atmospheric Sciences, University of Alberta, 1–26 Earth Sciences Bldg., Edmonton, AB T6G 2E3, Canada. (gamon@ualberta.ca)

S. Goswami and C. E. Tweedie, Environmental Science and Engineering Program, University of Texas at El Paso, El Paso, TX 79968, USA.

Appendix 2:

Towards Near-Real Time Data Property Specification and Verification for Arctic Hyperspectral Sensor Data

Irbis Gallegos, Santonu Goswani,
Ann Q. Gates, and Craig E. Tweedie
The University of Texas at El Paso
El Paso, USA
Email: {irbisg, sgoswami2}@miners.utep.edu
{agates, ctweedie}@ utep.edu

John Gamon
University of Alberta
Edmonton, Canada
Email: gamon@ ualberta.ca

***Abstract*—Environmental scientists, especially those conducting studies in remote areas such as the Arctic, can benefit from assessing data quality from autonomous sensors in near-real time. The Data Assessment Run-Time (DART) framework was developed to allow environmental scientists to specify and verify data properties associated with autonomous sensors. Data properties are logical statements about data values associated with sensors and their relationship with other sensor output or properties derived from historical data. The properties can be verified at near-real time, i.e., as the data are being collected in the field, or through post-processing routines after the data has been collected. This paper describes a case study that evaluates the specification of data properties associated with hyperspectral sensor data and how the DART framework was used to verify these data in both near-real time and through post-processing.**

***Index Terms*—Data Quality; information quality; data assessment; sensor data assessment; near-real time data assessment.**

I. Introduction

Environmental scientists commonly conduct ground-based hyperspectral remote sensing studies to monitor surface properties when satellites cannot (e.g., when cloud cover prevails) and to formulate mathematical relationships between surface optical properties and environmental phenomenon. Robotic tram systems have been shown to be useful to conduct such ground-based research [1]. Robotic tram systems typically consist of a tramline that is placed over an area of interest upon which a robotic cart is programmed to collect a range of environmental data using sensors that are activated at selected points along the tramline [2].

Most robotic tramlines operate semi- autonomously and require careful attention to sensor calibration. Environmental conditions such as rain or fog, sun angle, and extreme cold and wind can affect the quality of data. At predefined increments of time or after the robotic cart has travelled a particular distance, the operator generally assesses the quality of the data by physically accessing the cart and visually inspecting the spectrometer that plots the data as they are collected. The operators use their experience-based knowledge and intuition to determine if the collection process is operating as expected. If an anomaly or an unexpected value(s) in the data is suspected, the operator either restarts the measurement process, or persists with data collection and corrects data during post-processing.

Data assessment conducted manually for the tram system presents many challenges particularly under extreme environmental conditions, or when large volumes of data are being collected. In some cases, a scientist can spend an entire day collecting data in the field, being uncertain about the quality of data collection, only to discover later that bad data was collected due to faulty equipment, for example. The scientist then repeats data collection, thus losing time and perhaps most importantly, the chance to document rare environmental events or conditions.

Another concern is that data inspection is dependent on the scientists mental model. Indeed, the data inspection process is subject to the operators experience with the instrumentation and ecosystem in which they are operating as well as his or her intuition. There is a potential danger of rejecting data based on a faulty mental model.

To address the data assessment challenges associated with the verification of hyperspectral data collected using robotic tram systems, the Data Assessment Run-Time (DART) Monitoring Framework was developed. In particular, DART was used to interface with a wireless data stream from a robotic tram system established as a component of the Barrow Biocomplexity flooding and draining experiment [2]. DART applies principles from software engineering techniques, in particular run-time verification and formal methods. DART is intended to detect deviations from an ideal set of data for a particular season (referred to as the representative data set hereafter) that is derived from expert knowledge and historical data. The deviations identify points of interest in the data due to environmental variability or instrument malfunctioning. Section 2 provides the background for the work, Section 3 provides a description of the DART framework, and Section 4 describes the case study. The paper ends with discussion of related and future work in Sections 5 and 6, respectively.

978-1-61284-968-3/11/$26.00 ©2011 IEEE

II. Background

A. Run-time Monitoring

For critical software systems, software assurance mechanisms, such as model checkers and run-time monitoring systems, can be used to check that the software is functioning as expected with respect to a set of properties. A model checker [3] is a formal technique for verifying finite-state concurrent systems and relies on building a finite model of a system and an algorithm that automatically traverses the system model to verify if a desired property (or a set of properties) holds in the model. Run-time monitoring allows practitioners to observe the behavior of a system and determine if it is consistent with a given specification [4]. A run-time monitor takes an executing software system and a specification of software properties and checks that the execution meets the properties. In most run-time monitoring frameworks, the applications code is instrumented. Code representing the property, for example, is injected into the source code, with checks at the points of interest. Usually, the application to be monitored has to be recompiled to include the checks, and monitoring is performed at the code level to ensure that the code is behaving as intended. Delgado et al. [5] have compiled a taxonomy of run-time monitoring frameworks.

B. Hyperspectral Data

Spectral data can be obtained using a dual-detector field portable spectrometer [6]. Radiance (radiation from the target) and irradiance (radiation from the sky) are collected simultaneously, thereby permitting correction of surface reflectance under varying sky conditions [1]. The two detectors are cross-calibrated using a white panel with 99% reflectance [7] at the beginning and at the end of a tramline. The Unispec-DC has a nominal range of operation between 303 nanometers (nm) and 1148 nm in 256 contiguous bands with a spectral resolution of approximately 3 nm and a full-width-half maximum of approximately 10 nm. The optimal range of this detector (range with reasonable signal-to-noise) is approximately 400-1000 nm.

III. Data Assessment Run-time Monitoring Framework

A. Tool Overview

The Data Assessment Run-time (DART) Monitoring framework allows environmental scientists using the tram system to specify and then verify data properties as data are streamed wirelessly from the tram system. DART works similarly to a software engineering run-time monitoring system with minor adaptations to accommodate for data processing. For the DART framework, a data property is a logical statement about data values associated with hyperspectral sensor readings. With DART, a user specifies a set of data properties of interest, which document the data quality summary. DART is intended to detect deviations from an ideal set of data that is derived from expert knowledge and historical data, i.e., the representative data set.

DART can operate in near-real time mode and post-collection mode. Near-real time mode allows scientists to verify the data at near-real time as the data are wirelessly streamed from the tram cart to a computer. In near-real time mode, DART is given a path to a run-time folder, and DART continually checks data stored as new files in the folder, i.e., files sent by a spectrometer. Post-collection mode is used to verify data that has already been collected and stored.

The system takes as input three files: 1) a Run-time Data File (obtained from a run-time folder) that contains the raw data and metadata collected by the spectrometer on the tram cart at a given interval in time or position along the tramline; 2) an expert-validated Representative Data Set File (stored in the Representative Data Set Repository) that contains averaged historical data from the previous season; and 3) an expert-validated Property Specification File (stored in the Specification Repository) that contains the properties to be verified. The Representative Data Set Repository stores seasonal hyperspectral reflectance files, where a representative data set file contains averages of hyperspectral reflectance data considered representative of the data for a particular time of the season. A representative data set is used to compare its values to the data being collected by the tram system. In particular, the property specifications specify threshold values for the difference between the actual readings and the values of the representative data set. Specifications are described in XML files and are divided accordingly to the quality thresholds expected for each week of the season of interest.

The DART framework generates two outputs for every processed Run-time Data File, an Assessment Log File and an Assessment Visual Representation. The Assessment Log File contains the metadata associated with the spectrometer used to collect the data, a local data assessment value for each range of interest in the data, and a global data assessment value derived from local data assessment values from individual ranges. The Assessment Visual Summary is a graphical representation of the assessment results associated to the collected spectral readings.

B. DART Subsystems

A prototype version of DART was developed. The system is composed of six modules: the file parsers, the metadata handler, the run-time data reflectance calculator, the monitor, the specification mapper, and the output generator. The dataflow diagram in Figure 1 depicts the system.

The file parsers module extracts the metadata and raw sensor data from the Run-time Data File, the sensor data from the Representative Data Set File, and property specifications from the Property Specifications File. The metadata handler module uses the metadata about the run-time field data extracted by the file parsers to create a metadata summary to be associated to the corresponding Data Quality Log File. The run-time data reflectance calculator module calculates a reflectance value for each of the 256 spectral wavelength bands recorded by the spectrometer in the Run-time Data File. The module calculates the reflectance value by dividing the radiance value by the

irradiance value and associating the resulting reflectance value to the corresponding wavelength.

The specification mapper module maps the data property specifications extracted from the Property Specification File into a specification code template that is applied by the monitor module to the calculated reflectance data. The property specifications define the upper and lower wavelength limits to the intervals of interest in the data spectrum, and the maximum threshold value, which are determined from scientists expertise and data values expectations for which the normalized sensor data can differ from the ideal seasonal data.

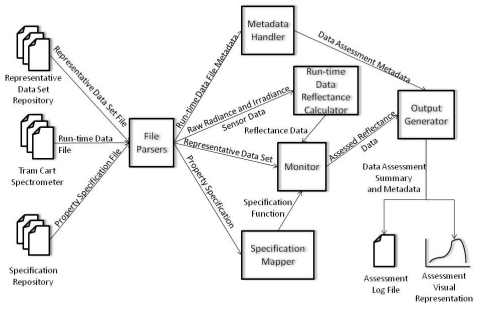

Fig. 1. Flow of data for the Data Assesment Run-time (DART) framework. Rectangles in gray represent modules in the system.

The monitor module calculates the deviation of the normalized sensor data from the representative seasonal sensor data and assigns a data assessment value depending on how distant the deviation is from the specified threshold. The data assessment value for individual readings are used to determine the local data assessment for the predefined ranges in the spectra, and the local data assessment values are used to determine the global data assessment value for the Run-time Data File being processed.

The output generator module uses the results of the monitor module and the metadata handler module to create a quality log file for every processed Run-time Data File and creates a plot of the reflectance values calculated by the run-time data reflectance calculator module. Both artifacts are used to present the data assessment results in DARTs graphical user interface.

The scientists use DARTs graphical user interface to specify the locations of the various file folders, as well as to determine the type of data assessment to be performed, e.g., near-real time or post-processing. Once the Run-time Data File is processed, the interface shows the data assessment flags associated with each wavelength value, the metadata summary, the data assessment summary for the file, and the spectra of the data.

C. DART Quality Assesment Algorithm.

DART performs the data assessment by assigning data assessment flags to individual reflectance values, ranges of interests, and Run-time Data Files. For individual reflectance values, DART determines the deviation of the reflectance value from the ideal seasonal data values. Given a set of predefined thresholds provided by the user, DART compares the reflectance deviations to such thresholds and classifies the severity of the deviation. For every wavelength value in a specific range, the absolute difference (AD) between the derived reflectance value and the representative seasonal value is calculated and compared to a predefined threshold (T); if AD is less than or equal to T, the derived reflectance value is not considered a deviation. If the AD deviates from T, the assessment flag changes accordingly (Table 1).

Flag	Condition	Description
00D	AD $\leq$ T	No deviations found
01D	T $<$ AD $\leq$ T+0.1	Small deviation found.
02D	T+0.1 $<$ AD $\leq$ T+0.2	Medium deviation found.
03D	AD $>$ 0.2	Large deviation found.

TABLE I
TOLERANCE RANGES USED IN DART TO ASSESS HYPER-SPECTRAL DATA GIVEN AN ABSOLUTE DIFFERENCE (AD) BETWEEN A CALCULATED REFLECTANCE VALUE, A REPRESENTATIVE VALUE, AND A DATA ASSESMENT THRESHOLD (T)

For ranges of interest, a count of occurrences of the four types of data assessment flags in individual reflectance values is maintained. The range assessment flag is calculated by identifying the data flag with the largest count within the range. Similarly, the Run-time Data File data flag is that of the range assessment flag with the largest count.

IV. CASE STUDY

A case study was conducted in collaboration with the System Ecology Laboratory at The University of Texas at El Paso and the University of Alberta to evaluate the use of DART in assessing data collected by tram systems located on the Barrow Environmental Observatory near Barrow, Alaska. The tramline infrastructure for this site was a robotic tram system similar to that described by Gamon and others [1]. The three 300 meter-long tramlines were located in treatments in a large-scale hydrological manipulation experiment [2].

The tram cart setup was modified to include a laptop on which DART was executed. The laptop was remotely accessed through a wireless connection. The new setup was used to assess the data at near-real time for three runs on the same date to show the feasibility of the approach; however, due to limited wireless connectivity in the field, the remainder of the 2008 seasonal data was assessed using DARTs post-processing mode.

A. Representative Data Sets

Representative data sets for the 2008 season were created using historical data gathered in 2007. A series of representative data sets, which initially were selected based on the time of the season, were used to compare the representative values to the data being collected by the tram system. The representative data sets included average weekly reflectance data constructed from 2007 post-processed data for the three

tramlines. This resulted in 27 representative data sets - nine per tramline, and one for every week of the 2007 season.

B. Data Property Specifications

The expert and the technical person created 13 specification files containing expected threshold values for different times of the season and delimiters to define ranges of scientific interest in the spectra. The specification files contained properties defined for three ranges of scientific interest within the optimal range in the spectra (i.e., 400-1000 nm) and two noise ranges outside the optimal range, and the initial thresholds used to evaluate the raw data against the ideal data. The thresholds and the delimiter selections were based on the scientists knowledge acquired over time.

C. Results

A total of 81 days of data were processed using DART, for a total of 24,690 spectral files, and 7,407,000 spectral readings for the 2008 season. Six additional days were unprocessed because the measurements were taken with a different spectrometer than the one used to create the seasonally representative data sets; thus, even though the specifications could be reused for these measurements, representative data sets for the new spectrometer were unavailable.

Figures 2-4 depict the results of using DART for data quality assessment. The x-axis presents the day of year when measurements were taken, and the y-axis presents the occurrences of each type of data quality assessment flags. Table II presents the 2008 data assessment generated by DART.

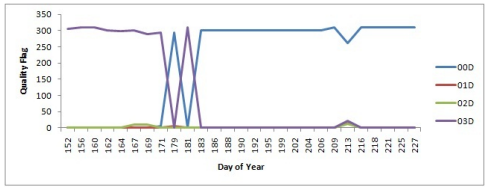

Fig. 2.

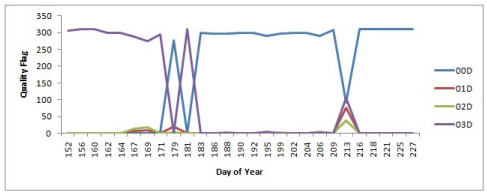

Fig. 3.

D. Discussion

1) General Findings: The hyperspectral data at the beginning of the season was expected to contain large deviations due to prevalent snow and melting snow. DART correctly identified the expected largely deviated (03D) data during this period - a transition period from June 18 (Day 169) to June 30 (Day 181), and the expected no deviations (00D) for the rest of the season for the North and Central tramlines. Technical problems appear to have influenced data obtained from the South tramline data throughout the season.

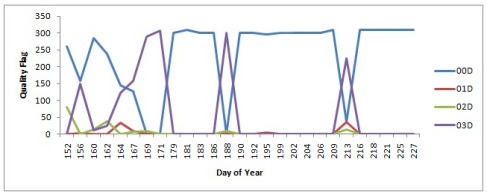

Fig. 4.

Tramline	00D	01D	02D	03D
North	5422	20	32	2742
Central	5204	121	84	2808
South	6412	86	171	1588

TABLE II
TRAM DATA ASSESMENT RESULTS FOR THE 2008 SEASON.

DART data assesment results distribution for North tramline for the 2008 season. Table I defines the values of the data assesment flags.

DART data assesment results distribution for Central tramline for the 2008 season. Table I defines the values of the data assesment flags.

DART data assesment results distribution for South tramline for the 2008 season. Table I defines the values of the data assesment flags.

2) Specific Findings: In July 7, 2008 (Day 188), The North and Central tramlines were flagged as no deviations (298 files flagged as 00D) in each tramline, while the South tramline data were flagged as large deviations (03D). Metadata showed that the par meter equipment used by scientists in the South tramline to calibrate the spectrometer was dysfunctional and, thus, the integration time had to be changed to 25 milliseconds, which might have influenced the sensor reading.

On July 25, 2008 (Day 206), while data was being collected from the Central tramline, a heavy rain event occurred. It was captured by DART, which reported 291 00D files, two 01D files, five 02D, and two 03D files. The North and South tramlines reported 300 00D files, indicating an event that was unique to the Central tramline. Snow fall also occurred in August 1, 2008 (Day 213). The event was captured by the tramlines by showing a mixture of data quality assessment measurements. The North tramline reported 262 00D files, 14 01D files, 12 02D files, and 23 03D files. The Central tramline reported 91 00D files, 75 01D files, 39 02D files, and 105 03D files. The South tramline reported 35 00D files, 36 01D files, 14 02D files, and 225 03D files. Even though DART did not identify the snow event as more than an event of interest, cross checking the results with climate data identified this environmental phenomenon.

3) Scientific Data Properties: The case study identified two types of properties: data properties and instrument properties. Data properties specify expected values and relationships related to field data readings i.e., noise ranges, and data values outside the specified thresholds for spectral ranges. Instrument properties specify expected instrument behavior and relationships by defining examining attributes and instrument functions based on reading (e.g., low voltage, bad fiber optic, and loose connections). The case study also showed that software engineering run-time verification techniques can be adapted to be used as data assessment techniques.

V. Related Work

Other tools used to perform data assessment on sensor data exist, although not specifically for tram data. This section describes some of this work.

The EQWin Data Manager [8] is a commercial database application to manage data types, sampled from the field on a discrete basis. . Input data is validated against built-in and user-defined validation criteria such as: coding checks, valid numeric values checks, and quality assessment/ quality control checks. EQWin is platform dependent and does not support real-time assessment or reusable data properties.

The UWEDAT [9] data management and monitoring system is used to screen ambient air quality data. UWEDAT uses a centralized host and a threshold service to screen user-defined limits and thresholds values of data sent from station computers. UWEDAT does not support reusable data properties and is based on Web services orchestrated from a central host; thus, no information redundancy is supported, which may lead to data being lost during the transfer process.

The Data Quality Health and Status (DQHS) [10] system is a data assessment Web that uses a set of algorithms to determine the percentage of data falling within specified thresholds. Results of automated checks are displayed in color-coded tables, plots and data assessment reports. DHQS does not support reusable data properties and relies on algorithms and pre-defined quality intervals that are not transparent to the scientist.

VI. Future Work

Future work will address DART limitations, including providing the ability to characterize representative data sets based on environmental variability, threshold selection, and identification of instrument malfunction. In particular, a systematic way to address the uncertainty associated with selecting data assessment thresholds will be defined. Standard deviations calculated from historical ecosystem data being studied will be used to supplement expert provided thresholds. Anomaly detection will be constructed to characterize and model meteorological events and equipment malfunction that will have degrees of truth associated to them. In addition, automated storage of the quality assessment summary with the raw data will be created to allow scientists to identify and remove bad data from a query or calculations.

VII. Conclusion

Scientists use robotic tram systems to collect hyperspectral data and are uncertain about the quality of the data being collected. The DART framework uses an adaptation of software engineering techniques to allow scientists to specify and verify data properties at near real-time as data is collected by the robotic tram system or at the post-processing stage. A case study showed how DART can help scientists identify anomalies in data and data assessment properties and procedures used by scientists working with the tram system.

Acknowledgement

This work was supported by US National Science Foundation (NSF) grants ASSP-0421588, HRD 0734825, and CNS1042341. Any opinions, findings, conclusions, or recommendations expressed in this material are those of the authors and do not necessarily reflect the views of NSF. We thank the Barrow Arctic Science Consortium for logistics support and the Ukpeagvik Inupiat Corp. for access to their lands. We also thank Baljeet Malhotra for his valuable comments.

References

[1] Gamon, J., Cheng, Y., Claudio, H., MacKinney, L., Sims, D.A., *A Mobile Tram System for Systematic Sampling of Ecosystem Optical Properties*. In Remote Sensing of Environment, 103. 2006, pp. 246-254.

[2] Goswami, S., Gamon, J., Tweedie, C.E., *Surface Hydrology of an Arctic Ecosystem: Multi-scale Analysis of a Flooding and Draining Experiment Using Spectral Reflectance*. In Journal of Geophysical Research. Vol. 116, 2011.

[3] Holtzmann, G., *The Spin Model Checker*. In IEEE Transactions on SE, 23(5). 1997, pp. 279-295.

[4] Peters, D., *Automated Testing of Real-Time Systems*. Technical Report, Memorial University of Newfoundland., 1999.

[5] Delgado, N., Gates, A., Roach, S.,]emphA Taxonomy and Catalog of Runtime Software-Fault Monitoring Tools. In IEEE Transactions in Software Engineering, Vol. 30, 2004, pp.859-872.

[6] Unispec DC, PP Systems, Amesbury, MA, USA. http://www.ppsystems.com/unispec_spectral_analysis_systems.htm.

[7] Spectralon, Labsphere, North Sutton, NH, USA. http://www.labsphere.com/productdetail.aspx?id=226

[8] GemTeck Environmental Software Ltd. EQWin Data Manager Ver 6.0. http://www.gemteck.com/

[9] Schimak, G., *Environmental data management and monitoring system UWEDAT(c)*. In Environmental Modelling & Software, Volume 18, Issue 6, Applying Computer Research to Environmental Problems, July 2003, pp. 573-580.

[10] Atmospheric Radiation Measurement. Data Quality Health and Status (DQHS) system. http://www.arm.gov/data/data_quality.

Biographical Sketch

Santonu Goswami was born and brought up in the beautiful state of Assam in the North Eastern part of India. He did all his schooling from Assam and completed a M.Sc. degree in Physics from Gauhati University, Assam before coming to the United States in 2003 for higher studies. He completed an MS program in Physics at University of Texas at El Paso and worked with a cohort of twenty high school teachers from local school districts in El Paso, TX who were going through a master of arts in science teaching program. Using qualitative and quantitative education research tools i.e. surveys, journals, participant observations; his research investigated how the self-efficacy of the in-service teachers towards science teaching changed during the course of the program. After this, Santonu went to work as a middle school math teacher for one year 20004-2005 in El Paso ISD to have a firsthand experience with students from US Schools. He finished his masters thesis in fall 2005.

In spring 2006, Santonu joined the PhD program in Environmental Science and Engineering at UTEP and joined the Systems Ecology Lab under Dr. Craig Tweedie and started his field research in the summer of the same year in Barrow, Alaska. My PhD dissertation research was supervised by Dr. Craig E. Tweedie from UTEP and Dr. John A. Gamon from University of Alberta, Edmonton, Canada.

From his dissertation work, Santonu have so far published one first author paper titled "Surface hydrology of an arctic ecosystem: multi-scale analysis of a flooding and draining experiment using spectral reflectance" in 2011 in Journal of Geophysical Research – Biogeosciences (doi:10.1029/2010JG001346). He has also co-authored a paper titled “Towards Near-Real Time Data Property Specification and Verification for Arctic Hyperspectral Sensor

Data" in the Proceedings of North American Fuzzy Information Processing Society Coneference in 2011 (doi: 10.1109/NAFIPS.2011.5752047) with research colleague Irbis Gallegos from Computer Science at UTEP. \

As part of my field research, Santonu has successfully managed world's largest spectral data collection infrastructure located within the Barrow Environmental Observatory (BEO) in the Arctic for three years. During this time, he has extensively worked with field spectrometers for collecting surface reflectance data using ground-based robotic tram system and airborne platforms in the Arctic. I was also part of an expedition to the Antarctic Peninsula in Dec 2007 – Jan 2008 as part of an International Polar Year (IPY) educational grant i.e. IPY-ROAM (www.ipyroam.org) and worked as part of the terrestrial ecology group member.

So far, Santonu has disseminated his research findings through presentations in several national and international conferences and meetings. He has also actively participated in education and outreach activities through presentations in local El Paso Schools, students in Barrow, Alaska and to the community in general in El Paso, TX and Barrow, Alaska. Santonu is also a member of the bureau of Arctic Speakers in Arctic Research Consortium of US (ARCUS) and hope to educate schools students and community in general in US and beyond through this program soon. I have also been actively involved with international network i.e. Association for Polar Early Career Scientists (APECS).